Sheffield Hallam University

Planar waveguide enzyme sensors coated with nanocomposite membranes for water pollution monitoring.

HARON, Saharudin.

Available from Sheffield Hallam University Research Archive (SHURA) at:

http://shura.shu.ac.uk/19756/

Published version

Copyright and re-use policy

Fines are charged at 50p per hour

0 2 MAR 2006

REFERENCE

ProQuest Number: 10697058

uest

ProQuest 10697058

PLANAR WAVEGUIDE ENZYME SENSORS COATED WITH NANOCOMPOSITE MEMBRANES FOR WATER POLLUTION MONITORING

SAHARUDIN HARON

A thesis submitted in partial fulfilment of the requirements of

Sheffield Hallam University

for the degree of Doctor of Philosophy

May 2005

Declaration

I hereby declare that this thesis submitted for the degree of PhD is the result of my own research and that this thesis has not been submitted for a higher degree to any other university or institution.

Signed

Saharudin Haron

To my wife and my parents
whose love and support have made this possible.

ABSTRACT

Attenuated total reflection (ATR) of light in a SiO_2/Si_3N_4 planar waveguide was successfully exploited with a view to developing a highly sensitive enzyme sensor for monitoring typically agricultural and industrial water pollutants. The Si_3N_4 surface of the waveguide sensing window was coated with nanocomposite polyelectrolyte self-assembled (PESA) membranes containing cyclotetrachromotropylene (CTCT) indicator and enzymes. The reaction of three enzymes namely urease, acetylcholine esterase or butyrylcholine esterase was accompanied by changes in pH, varying the absorption coefficient of the CTCT indicator.

An experimental set-up of a single channel enzyme sensor was constructed to investigate the capability of the planar waveguide to register small changes in the light absorption of the PESA membrane. It was found that due to the multiple reflections phenomena, the sensitivity of a planar waveguide was higher than that for traditional absorption spectroscopy and previously reported waveguiding structures by at least three orders of magnitude. The respective enzyme reactions as well as their inhibition with toxic agents such as cadmium and lead ions were studied by *in-situ* monitoring the changes in output intensity of the planar waveguide. The results were remarkable, since traces of the above pollutants were detected with concentrations as low as to 1 ppb.

The work was also extended to design and implement a laboratory scale enzyme sensor array. A multi-channel reaction cell and light guiding system were designed for this purpose. The analysis of the experimental results demonstrated that the multi-channel enzyme sensor was able to produce adequate responses to the presence of different pollutants of industrial (cadmium, lead and nickel) and agricultural (imidacloprid, paraoxon and DVDP) origin, in the concentration range from 1 ppb to 1000 ppb. The distinct pattern of sensor responses was analysed by the implementation of artificial neural network algorithm. Despite a rather small amount of experimental data, the trained neural networks were able to classify and quantify the pollutants with an acceptable average error of 6.24 %.

ACKNOWLEDGEMENTS

First, I would to thank Universiti Teknologi Malaysia for the award of the scholarship. Without their financial support, it would have been difficult for me to study abroad.

Special appreciations and thanks to my director of studies Prof. Asim K. Ray for introducing me to the world of biosensing. It has been exciting to be a part of the ever-growing research activities in medical and environmental science. I am deeply indebted to Prof. Ray for his advice, encouragement, assistance and support during these years.

I would like to express my sincere thanks to my supervisors, Dr. Alexei Nabok and Dr. Aseel Hassan for their guidance and advice. Dr. Nabok has been a solid support and an extraordinary source of inspiration throughout these years. I thank him for his excellent supervision and discussion of various aspects of science, experimental procedures and the results obtained.

I am grateful to Prof. Yu. M. Shirshov of the Institute of Semiconductor Physics, National Academy of Sciences of Ukraine for providing the planar waveguide devices. My special thanks to Prof. N. F. Starodub of Institute of Biochemistry, National Academy of Sciences of Ukraine for fruitful discussion during his frequent visit to Sheffield Hallam University.

I would also like to thank all technical staff of the School of Engineering, especially Mr. Ken Duty from the Electronic Department, Mr. Roger Tingle from the Mechanical Department and Mr. Tony Earnshaw from the Chemical Department for their special help.

I would like to take this opportunity to thank all my fellow Ph.D. colleagues for sharing in the pain and the pleasure. Alistair, Alan, Malik, Abbas and Anna deserve credit.

Finally, I would like to express my deepest gratitude to my family. To my wife, Haily, thank you so much, for your firm support and love. Without you, this could not have been possible. Your patience and understanding can never be repaid. To my parents, Haron and Noraini, and my sons, Arif and Imran, your love and encouragement have been the most influential forces in my life. Thank you so much for the constant faith you have shown me.

CONTENTS

LIST OF PUBLICATIONS

Journal Publications

1. *Planar silicon nitride waveguide for biosensing*, published in the IEE Proceedings on Nanobiotechnology, Volume 150, pp. 25-30.

2. *Registration of heavy metal ions and pesticides with ATR planar waveguide enzyme sensors*, published in the Applied Surface Science, Volume 238, pp. 423-428.

Conference Publications

1. *Silicon planar waveguide coated with polyelectrolyte thin film for water pollution monitoring*, presented at the Postgraduate Research Conference in Electronics, Photonics, Communications & Networks, and Computing Science (PREP) Conference, 14-16 April 2003, Peter Chalk Centre, University of Exeter, Exeter, UK.

2. *Optical biosensing transducer based on silicon waveguide structure coated with polyelectrolyte nanolayers*, presented at First SPIE International Symposium on Microtechnologies for the New Millennium, 19-21 May 2003, Maspalomas, Gran Canaria, Canary Islands, Spain.

3. *Optical enzyme sensors based upon silicon planar waveguide coated with composite polyelectrolyte film*, presented at First APHYS-2003 International Meeting on Applied Physics, 15-18 October 2003, Badajoz, Spain.

4. *Planar waveguide sensor array with composite enzyme/chromophore /polyelectrolyte coating for water pollution monitoring*, presented at IX European Conference on Organised Films (ECOF 2004), 22-25 July 2004, Palacio de Congresos Conde Ansúrez, Valladolid, Spain.

LIST OF FIGURES

LIST OF TABLES

CHAPTER 1

INTRODUCTION

1.1 Water Pollution and Environmental Legislation

Recently, pollution of water resources with chemical contaminants has become one of the crucial ecological problems. The increasing manufacture, use and disposal of agricultural and industrial chemicals, particularly pesticides and heavy metal ions, are causing worldwide pollution. These toxic agents do not remain where they originate (see Figure 1.1). They can be transported to different locations in a number of different ways. Some compounds can evaporate and drift away by winds before precipitating as rainfall. A study from Switzerland revealed that much of the rain in Europe contains high levels of dissolved pesticides, and that it would be illegal to supply this water for drinking purposes. Almost 4 μg/l of 2,4-dinitrophenol was found in one sample of rainwater [Pearce and Mackenzie, 1999].

In addition, runoff from agricultural and urban areas into drainage pipes and sewers also contributes to significant pollution of surface and ground water. For instance, a field conditions study in Hungary revealed the presence of 154 μg/l of atrazine, 89.1 μg/l of acetochlor, 47.4 μg/l of propisochlor, and 0.139 μg/l of chlorpyrifos in runoff water [Konda and Pásztor, 2001]. While in Japan, 53 pesticides ranged from 3 ng/l to 8.2 μg/l were found in waters collected from the Shinano River. The presence of pesticides in the river water correlates with the time of pesticide application in the rice fields near the river [Tanabe et al, 2001].

^ Regional Transport

r

rjrv
y
Deposition

Precipitation

Evaporation

Spray Dntt

\Wind Erosion ^

iWaste
Runoff ^ Water

Runoff

i

X

Seepage   Groundwater   Seepage

Discharge to Stream
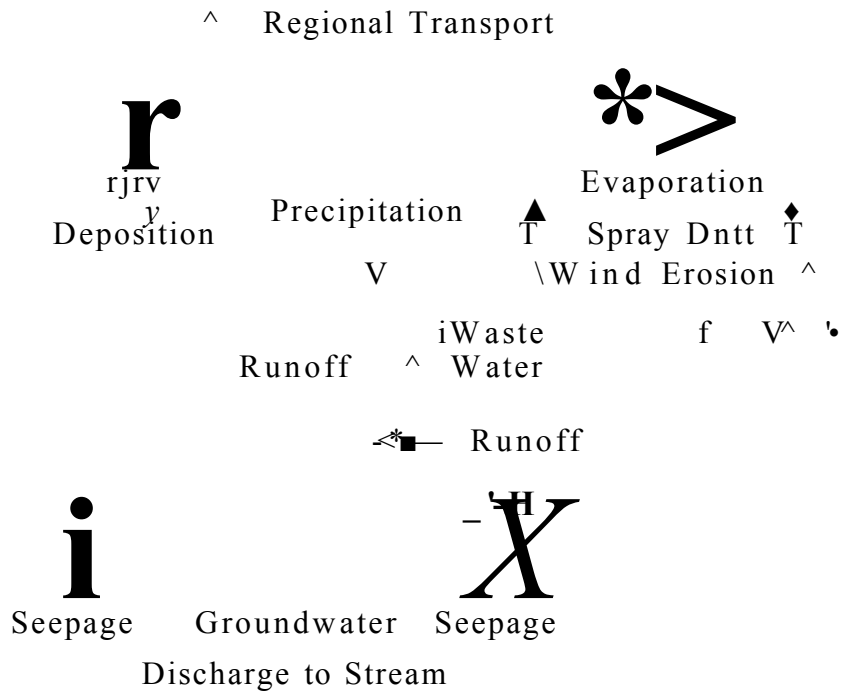
Figure 1.1. Illustration of pollutant transportation [adapted from http://europa.eu.int/comm/environment/youth/index_en.html. Last accessed on 27 October 2002].

Pollutants can be deposited on sediments, where they can be attached to particulates, such as plankton, or absorbed by aquatic organisms. It has been reported that a large area along a 35 km stretch of the southwest coast of Spain, near the joint mouth of the polluted Tinto and Odiel Rivers, contains sediments with high concentrations of metals, such as 2.5 mg/kg of cadmium and 197 mg/kg of lead [Morillo et al, 2003]. These heavy metals can spread easily into the Atlantic Ocean under changing environmental conditions. Since water resources are interconnected, pollution at one point can spread widely, even globally.

International environmental legislation has been implemented as a precautionary measure to ensure the progressive reduction of pollution of water resources, as well as to enhance the protection and improvement of the aquatic environment. Regulatory frameworks, such as the World Health Organisation (WHO) guidelines values, US Environmental Protection Agency (EPA) maximum contaminants levels, EU drinking water directive (98/83/EC), EU dangerous substances directive (76/464/EC), and EU groundwater directive (80/68/EC), demand that contamination of natural water resources should not exceed a certain threshold level. Some of the guidelines are not only based on human health criteria, but are also set at the limit of current ability to detect pollutants in water. For instance, the maximum permitted concentration for any individual pesticide given in the EU drinking water directive is 0.1 μg/l which corresponds to one-tenth of a part per billion (ppb) [Council Directive 98/83/EC, 1998] (See Table 1.1).

3

Table 1.1. Guidelines for some chemical parameters in the EU drinking water directive (98/83/EC) [Council Directive 98/83/EC, 1998, *The quality of water intended for human consumption*, Official Journal of the European Communities, L330, pp. 32-54.]

Compound	Parametric value	Unit
Arsenic	10	µg/l
Benzene	1.0	µg/l
Boron	1.0	mg/l
Bromate	10	µg/l
Cadmium	5.0	µg/l
Chromium	50	µg/l
Copper	2.0	mg/l
Cyanide	50	µg/l
1,2-dichloroethane	3.0	µg/l
Lead	10	µg/l
Mercury	1	µg/l
Nickel	20	µg/l
Pesticides	0.1	µg/l

1.2 Analytical Devices for Water Analysis

The extensive legislation described above, clearly indicates the need for reliable environmental monitoring methods, which are fast, portable, sensitive and cost effective. Conventional analytical methods, such as gas chromatography (GC), high performance liquid chromatography (HPLC), and inductive by coupled plasma mass spectrometry (ICPMS), are very sensitive and reliable [Steen et al, 1997; Saleh et al, 2001; Angelino and Gennaro, 1997]. However, they suffer from the disadvantages of high costs, time consumption, the need for highly trained technicians, and the fact that they are mostly laboratory based [Rodriguez-Mozaz et al, 2004; Andreescu et al, 2002]. E.g., in many cases, time consuming and difficult preparation procedures, such as liquid–liquid extraction and solid-phase extraction, are applied off-line before the HPLC measurements [Bovanova and Brandsteterova, 2000]. Therefore, an alternative technique is needed to simplify the environmental analysis.

Several sensing systems are already available, such as ion sensitive sensors based on sensitive polymer films [Cobben et al, 1992; Mlika et al, 1996; Ali et al, 2002], and fibre optic chemical sensors consisting of immobilised indicator dyes [Vaughan and Narayanaswamy et al, 1998; Malcik et al, 1998; Mahendra et al, 2003]. They are portable and can monitor specific compounds or ions in complex samples, on a real-time basis. Chemical receptors (the sensitive polymer films and indicator dyes), however, are very selective to particular chemical compounds. As a consequence, the synthesis of specific receptors is required for every toxic agent. This fact has also restricted the application of these chemical sensors as a multi-analyte detector.

1.3   Biosensors for Monitoring Water Contaminants

An alternative approach is the use of biosensors for pollutants monitoring. The biological base of biosensors makes them ideal for toxicological measurements, which are suited for health and safety applications [Bernabei et al, 1993; Galassi et al, 1993; Farre and Barcelo, 2003]. They are generally defined as analytical devices, incorporating bioreceptors, e.g. biological sensing elements (such as enzymes, antibodies or microorganisms) integrated within a physicochemical transducer, such as electrochemical, optical or piezoelectric transducers [Rogers and Williams, 1995]. Specific interactions between the target analyte and recognition sites within the bioreceptor produce a physicochemical change, which is detected and can be measured by the transducer by transforming it into an electrical signal, as illustrated in Figure 1.2.

In general, biosensors for water pollution monitoring can be separated into two main classes [Scheller and Schubert, 1992]:

1) Affinity biosensors, where target analytes are specifically bound to bioreceptors and a signal is produced as a result of the binding process (no conversion of the analyte takes place).

2) Catalytic biosensors where target analytes are specifically bound to bioreceptors, the conversion of the analyte takes place, and a signal is produced as a result of a catalytic reaction.
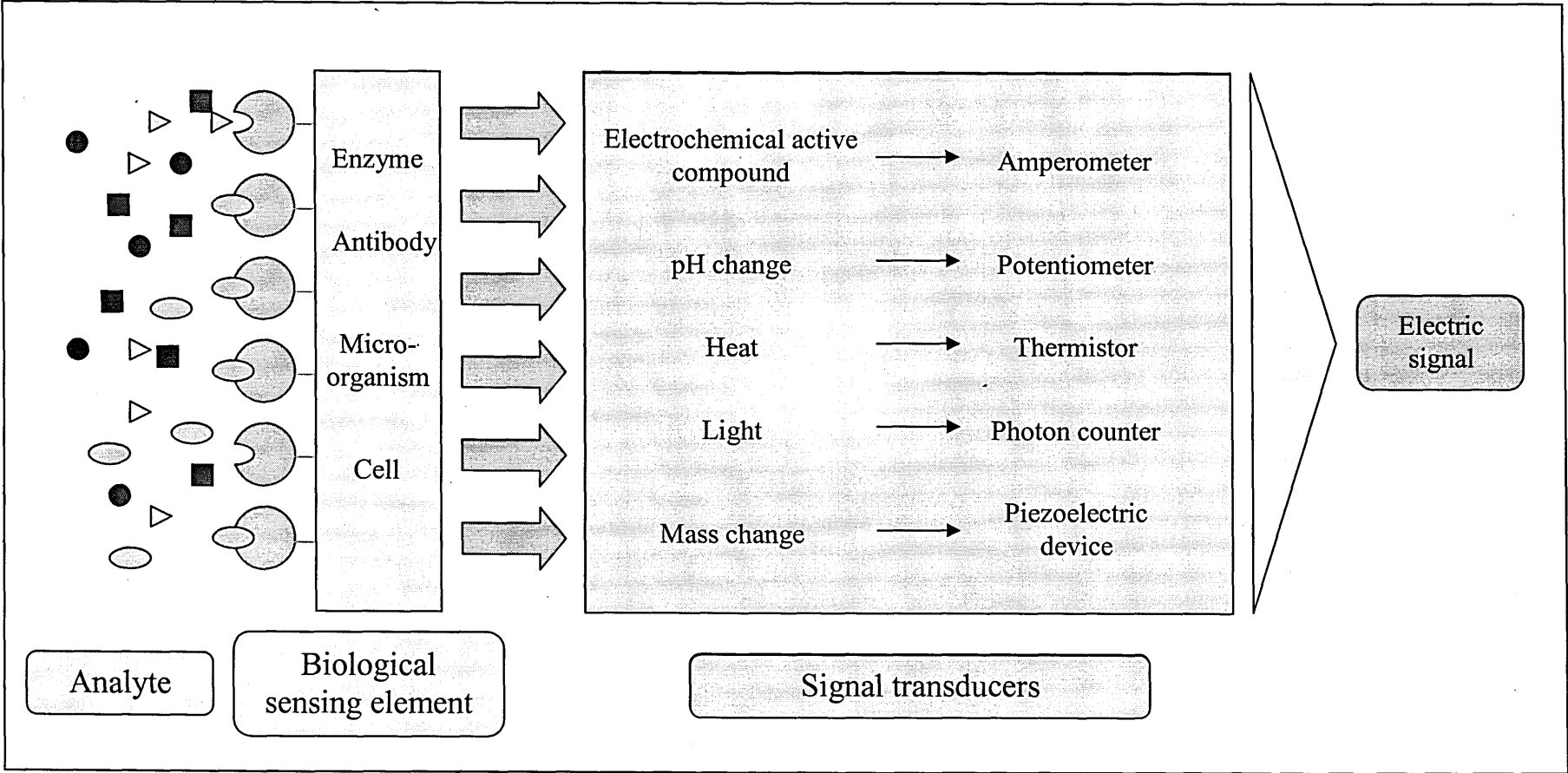
Figure 1.2. Illustration of the principle of Biosensors [adapted from http://www.jaist.ac.jp/~yokoyama/biosensor.html. Last accessed on 2 November 2003].

The affinity biosensors for water analysis (commonly known as immunosensors), typically use antibodies as the bioreceptors integrated with optical transducers which utilize evanescent waves in optical fibers or planar waveguides. The antibodies are combined with respective antigens (the target analyte) to give an exclusive antibody-antigen complex. This binding process can then be detected by variations of the output light intensity after multiple interactions with the sensing film within the evanescent field volume of the waveguides.

Different optical techniques based on this sensing principle are described in Chapter 2. They show a superior performance, where proteins and pesticides can be detected in a wide concentration range from 10^{-15} M up to 10^{-8} M. However, these optical immunosensors have certain limitations. The selective binding of the antibodies with antigens has resulted in the requirement to design specific antibodies for the detection of every pollutant. For example, 2,4-dichlorophenoxyacetic acid (2,4-D) antibodies and simazine antibodies were used for the detection of the pesticide 2,4-D and simazine in water [Klotz et al, 1998]. Therefore, the affinity biosensors are very specific and more suitable for single analyte detection.

In contrast, the catalytic biosensors are more versatile. These biosensors normally use enzymes as the bioreceptors, and are based on the enzyme inhibition mechanism for the pollutants detection. It is possible to implement enzyme sensors for multi-analyte detection due to a diversity of pollutants that inhibit a number of enzymes in a different ways. For example, it has been demonstrated that a general discrimination between pesticides and heavy metal ions in a sample solution is possible due to selective inhibition of butyrylcholine esterase by pesticides and urease by heavy metals ions [Starodub et al, 1999; Arkhypova et al, 2001]. The type of pesticides or heavy metal

ions can then be determined by comparing the inhibition level of urease or butyrylcholine esterase, respectively. Those studies revealed that the array of enzyme-inhibition based biosensors containing different enzymes could be a solution for the simultaneous determination of various pollutants.

During the last two decades, electrochemical enzyme sensors with amperometric [Zhylyak et al, 1995; Palchetti et al, 1997] and potentiometric [Jeanty and Marty, 1998; Shi et al, 1997] transducers, have been extensively studied for water pollution monitoring. They were successfully tested on a number of pesticides and heavy metal ions, such as paraoxon [Zhang et al, 2001], dichlorvos [Andreescu et al, 2002] and silver ions (Ag^{2+}) [Soldatkin et al, 2000]. Figure 1.3 shows the limit of detection and the determination range of several electrochemical biosensors for pesticides registration. Despite high sensitivity to some pollutants (in ppb level), they usually have a narrow detection range of two orders of magnitude concentration. For example, Cremisini et al [1995] found a linear detection range from 1.4 ppb (5×10^{-7} M) to 14 ppb (5×10^{-8} M) for paraoxon with a low detection limit of 1.3 ppb (4.7×10^{-9} M).

A similar situation was observed for the determination of pesticides and heavy metal ions using optical enzyme sensors [Andres and Narayanaswamy, 1997; Preininger and Wolfbeis, 1996; Nabok et al, 2000]. A higher detection limit was found by using an optical enzyme sensor, as compared to those of electrochemical biosensors. For instance, Andres and Narayanaswamy [1997] found a linear detection range for paraoxon as 5×10^{-7} M to 5×10^{-6} M with a low detection limit of 1.1×10^{-7} M, calculated at 10 % of inhibition. These optical enzyme sensors have limited sensitivity because they rely on a single act of light reflection (or transmission) through the sample solution, which permits a short interaction of light with the sample medium.

9
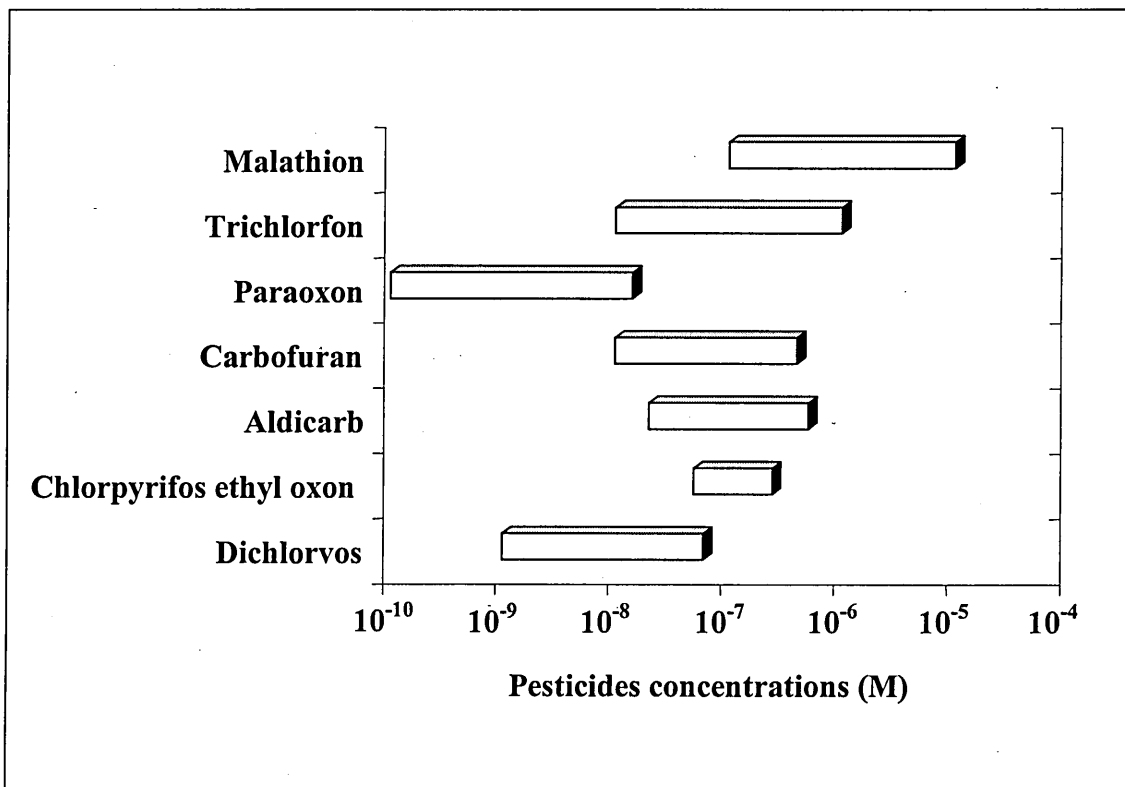
Figure 1.3. The sensitivity of electrochemical biosensors for pesticides registration.

1.4   Hypotheses of the Research

The use of enzymes as the bioreceptor in the optical evanescence wave biosensor, may offer the possibility of multiple analyte detection, while retaining high sensitivity of the biosensor. The determination of pollutants using enzymes inhibition shows certain advantages: first, a large number of environmental pollutants that can inhibit enzymes, and secondly, low pollutant concentrations needed to affect the enzymes activity, which can be easily detected using evanescence field transducers.

Several waveguiding structures have been tried for optical evanescent wave transducers development, but silicon dioxide/silicon nitride (SiO_2/Si_3N_4) waveguides were demonstrated to have the highest evanescent field volume due to a large difference in refractive indices between the core and cladding layers. During the last decade, the research in planar optical waveguide sensors was mostly based upon fluorescence and interferometric principles [Lukosz et al, 1997; Nabok et al, 2000] (see Chapter 2.2). Although they show high sensitivity, most of these sensors are quite complex in terms of their fabrication and operation. In addition, they have only been exploited as immunosensors using antibodies as the bioreceptors.

In this study, the potential usage of a SiO_2/Si_3N_4 planar waveguides as enzyme sensors is investigated by utilising a simple transducing principle of the attenuation of the light intensity during multiple reflections in the waveguide. A nanocomposite membrane containing both an organic indicator namely, Cyclotetrachromotropylene (CTCT) and enzymes, such as Urease or Acetylcholine Esterase (AChE), produced using a polyelectrolyte self-assembly (PESA) technique, is integrated with the planar

waveguide transducer, so that the biochemical reactions accompanied by changes in pH can be registered with the optical measurements.

Recently, the PESA method proved to be a versatile immobilisation technique for proteins [Lvov et al, 1995]. It provides a unique opportunity to incorporate other electrically charged macromolecules, such as enzymes and chromophores into the polymer matrix [Ariga et al, 1997; Cooper et al, 1995; Nabok et al, 1999]. In addition, the PESA method is low cost and environmentally friendly. Therefore, it is expected that the combination of a highly sensitive optical technique and a superior immobilisation method may improve the functionality of an optical enzyme sensor for water pollution monitoring.

1.5 Aims and Objectives of the Research

The aim of this research is to develop an optical enzyme sensor for in-situ monitoring of heavy metal ions and pesticides in water. This enzyme sensor is expected to have a high degree of sensitivity and can be used directly in liquid environments to measure individual toxic agents, by exploiting the combination of a PESA immobilisation method and a multiple reflection of light in the SiO_2/Si_3N_4 planar waveguide as the optical transducing technique.

The following objectives are specified for this research work:

1. To research and produce a literature review into different enzyme sensors and optical techniques.

2. To form composite films containing several enzymes and organic indicators by means of polyelectrolyte self-assembly techniques.

3. To construct an experimental set-up for a single channel planar waveguide sensor.

4. To study the sensitivity of the planar waveguide sensor in comparison to the UV-visible spectroscopy method.

5. To investigate the response of composite PESA films to different pollutants using the effect of the attenuation of light intensity propagated through the planar waveguide.

6. To develop an enzyme sensor array set-up, which consists of a flow cell with a number of reaction channels.

7. To design a pattern recognition algorithm to enable the identification and quantification of specific pollutants.

CHAPTER 2

LITERATURE REVIEW AND THEORETICAL

BACKGROUND

2.1   Enzyme Sensors for Water Pollution Monitoring

Biosensors for environmental applications have employed a wide range of biochemical recognition systems, utilising a number of bioreceptors such as bacteria [Philp et al, 2003], fungal cell [Baronian, 2004; Reiss et al, 1998], enzyme [Marty et al, 1993; Davis et al, 1995; Kok and Hasirci, 2004], antibodies [Gonzalez-Martinez et al, 2001; Rodriguez-Mozaz et al, 2004] and plant tissue [Mazzei et al, 1995; Liawruangrath et al, 2001]. Among these, enzyme sensors have recently become the target of intense research and development, and have proven to be both fast and highly selective [Karube and Nomura, 2000]. There is now a wide selection of enzymes commercially available, and the capability of enzyme sensors to operate in diverse media, such as aqueous solutions [Bisenberger et al, 1995], organic solvents [Campanella et al, 1998] and air [Hämmerle et al, 1996] has been demonstrated. Several types of enzyme sensors developed for pesticide and heavy metal ions detection in aqueous solutions are discussed in the following sections.

14

2.1.1 Enzyme sensor for pesticides detection

The majority of pesticides used are inhibitors for cholinesterase enzymes. Thus, biosensors based on the inhibition of enzyme cholinesterase such as acetylcholine esterase (AChE) or butyrylcholine esterase (BChE) are frequently proposed for use in pesticide detection. This biosensor is usually based on amperometric approaches, which is responding to the enzymatic hydrolysis of acetylthiocholine chloride to thiocholine. The latter is electrochemically active and can be oxidized at 410 mV (versus the Ag/AgCl reference electrode) to disulphide compound according to the following equation [Marty et al, 1993, 1995; Jeanty and Marty, 1998]:

$$\text{acetylthiocholine} + \text{water} \xrightarrow{\text{AChE}} \text{thiocholine} + \text{acetic acid} \qquad (2.1)$$

$$2 \text{ thiocholine} \xrightarrow[\text{+ 410 mV}]{\text{anodic oxidation}} \text{dithio-bis-choline} + 2H^+ + 2e^- \qquad (2.2)$$
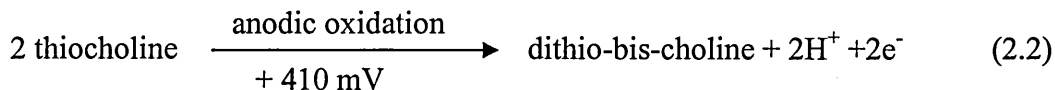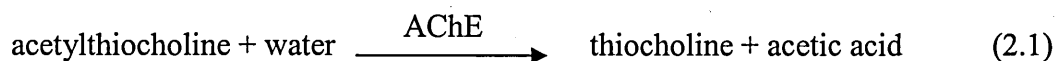
This electrochemical oxidation of thiocholine was performed at 100 mV versus the Ag/AgCl reference electrode by applying an organic mediator, namely 7,7,8,8-tetracyanoquinonedimethane (TCNQ) on the working electrode [Andreescu et al, 2002; Bonnet et al, 2003; Schulze et al. 2002]. The current change due to the participation of electrons in this electrochemical process was proportional to the amount of oxidized thiocholine. This oxidation was correlated to the enzyme AChE activity. Then, the pesticide concentrations were determined by measuring the difference in AChE activity before and after the inhibition process. These amperometric biosensors had low detection limits for several pesticides, such as carbofuran and paraoxon at 0.1 ppb [Marty et al 1993], and dichlorvos and chlorpyrifos ethyl oxon at 1 ppb [Andreescu et al 2002].

In addition to a single enzyme system, AChE was coupled with the enzyme choline oxidase (ChO) to form another type of amperometric biosensor with dual enzyme system [Kok et al, 2002; Zhang et al, 2001; Palchetti et al, 1997]. In this amperometric biosensor, the enzyme substratum, namely acetylcholine chloride, was hydrolysed by AChE to acetic acid and choline. Then ChO converted choline to betaine and hydrogen peroxide on consuming oxygen according to the following equation [Zhang et al, 2001]:

$$\text{acetylcholine chloride} + \text{water} \xrightarrow{\text{AChE}} \text{choline} + \text{acetic acid} \qquad (2.3)$$

$$\text{choline} + \text{oxygen} \xrightarrow{\text{choline oxidase}} \text{betaine} + \text{hyrdogen peroxide} \qquad (2.4)$$
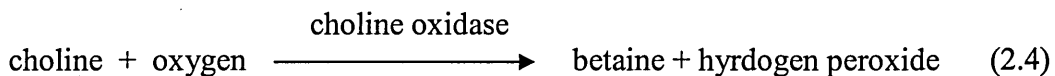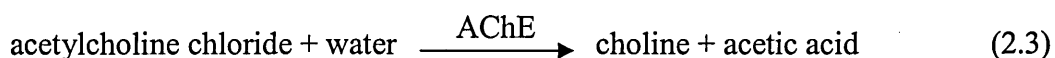
The hydrogen peroxide produced was oxidized at 600 or 700 mV versus the Ag/AgCl reference electrode, and the generated current signal was found to be proportional to the amount of active AChE. These amperometric biosensors were also found to be highly sensitive to pesticides, such as carbofuran with a detection limit of 2 μg/l (2 ppb) [Palchetti et al, 1997], aldicarb with a detection limit of 11.7 ppb [Kok et al, 2002] and paraoxon with a detection limit of 1.3 ppb [Cremisini et al, 1995] and 10 ppb [Zhang et al, 2001].

Potentiometric approaches for monitoring pesticides concentration based on the inactivation of cholineterase enzyme were also reported [Ristori et al, 1996; Ivanov et al, 2000]. Most of these potentiometric biosensors determined the AChE or BChE activity by measuring the pH changes during the hydrolysis of acetyl or butyrylcholine to yield choline and acetic or butyric acid, which can easily be done using a pH electrode or ion selective field effect transistors (ISFET). They were simple in design

and operation. However, the sensitivity of these cholinesterase potentiometric biosensors was low. E.g., the detection limit for the pesticide malathion [Ristori et al, 1996] and trichlorfon [Ivanov et al, 2000] was about 0.1 mg/l (100 ppb) and 0.01 mg/l (10 ppb), respectively.

Several attempts to increase the sensitivity of cholinesterase potentiometric biosensors were made. Campanella et al [1996] constructed two solid-state biosensors with the enzyme BChE as a bioreceptor and either graphite electrode or ISFET as the potentiometric transducer. Both transducers were coated with a H_3O^+ ion selective polymeric membrane sensitive to pH and containing tridodecylamine as an exchanger. BChE was immobilized either in a nylon membrane or in a polyazetidine prepolymer. The biosensors showed high sensitivity to paraoxon with the detection limit of 1 μg/l (1 ppb) and 3 μg/l (3 ppb) using a graphite electrode and an ISFET transducer, respectively. Nevertheless, both sensors have narrow determination range from 2.5 to 82 μg/l.

Recently, Lee et al [2002] developed a potentiometric flow injection-type AChE-biosensor used for the determination of ten phosphorus pesticides. The sensor system consisted of the reactor made with porous glass, and the detector based on a tubular H^+-selective membrane electrode. AChE was immobilized by cross-linking with glutaraldehyde in 0.05 M phosphate buffer, pH 7. The sensitivity of the sensor was enhanced by converting phosphorus pesticides to their oxidized forms (stronger inhibitors) as shown in Table 2.1. The low detection limit of the sensor was increased from 10^{-7} M before oxidation, to 2×10^{-10} M after oxidation of pesticides. Despite the high sensitivity, this sensor is too complicated, because of the pretreatment of pesticides required prior to measurements.

Table 2.1. Comparison of the percent inhibition of the sensor enzyme by organophosphorus pesticides before and after oxidation [Lee et al, 2002].

Pesticides	Before oxidation		After oxidation	
	Inhibition %	Reactivation %	Inhibition %	Reactivation %
Parathion	17	100	77	97
Fenitrothion	7.7	104	31	89
Fenthion	8.5	107	19	83
Chlorpyrifos	3.9	100	69	80
Diazinon	13	107	73	95
EPN	5.6	100	80	109
Dichlofenthion	11	100	75	80
Parathion-methyl	11	100	48	93
Bromophos-ethyl	7.4	93	12	92
Bromophos-methyl	8.7	92	20	88

Other types of cholinesterase biosensors using optical transducers were also reported [Andres and Narayanaswamy, 1997; Choi et al, 1998; Doong and Tsai, 2001]. Most of these biosensors utilized the fibre-optic device as the light waveguide and used either pH-sensitive fluorescence or organic dye as the light indicator. E.g., Andres and Narayanaswamy [1997] described a fibre-optic pesticide biosensor based on covalently immobilized AChE on preactivated isothiocyanate glass mixed with the thymol blue indicator bound on the aminopropyl glass. The liberated acetic acid during the hydrolysis of acetylcholine chloride caused a local decrease in pH and the resulting colour change of thymol blue indicator was detected, thereby leading to the increase in the reflected light intensity at 600 nm. The introduction of pesticides in the flow cell reduced the sensor response linearly in the concentration ranges 5×10^{-8} to 5×10^{-7} M for carbofuron and 5×10^{-7} to 5×10^{-6} M for paraoxon. The detection limits, calculated at 10 % inhibition, were 1.5×10^{-8} M (3.1 ppb) and 1.1×10^{-7} M (24.7 ppb) for carbofuron and paraoxon, respectively.

An AChE fibre-optic biosensor using litmus dye indicator was reported [Choi et al, 1998]. Instead of being immobilised in the sensor reaction cell, the litmus dye was dissolved in the potassium phosphate buffer and mixed with the enzyme substratum, acetylthiocholine iodide, using a peristaltic pump before it flowed to the reaction cell. The AChE was immobilised by the electrostatic adsorption on a support polymer viologen, which was transfered on a glass slide by the Langmuir-Blodgett (LB) technique. Decreases in pH value due to the formation of acetic acid from hydrolysis of acetylthiocholine iodide by AChE, caused the original blue colour of the litmus dye to change to red, which caused an increase in the absorption spectra at 633 nm. When the pesticide was introduced, a difference in decrease of the absorption occurred due to the inhibition of AChE, which was the proportional to pesticide concentration. The sensor showed a narrow detection range of paraoxon that was about 0.2 to 2.0 ppm.

Doong and Tsai [2001] proposed an AChE fibre-optic biosensor with a better sensitivity to paraoxon. This sensor consisted of pH-sensitive fluorescent indicator encapsulated together with enzyme AChE in a sol-gel network on a glass cap, which could be fixed on an optical fibre, and then integrated with a flow through reaction the cell for continuous monitoring. Nine fluorescent indicators were tested, and FITC-dextran was found to be the most suitable indicator due to the advantages of high sensitivity, low leaching rate and low toxicity to AChE. The fluorescence colour of FITC-dextran was blue in alkaline solutions and became colourless as the pH decreased to 2. Therefore, the enzymatic activity of AChE, resulting in pH change, was given in terms of the decrease of the fluorescence light intensity. The ability of the sensor to detect the organophosphorus pesticides was investigated with 0.54 μM (152 ppb) of paraoxon. A 30 % inhibition of the sensor response was obtained after the paraoxon was introduced into the system.

A different type sensing scheme of fibre-optic biosensors for simple and direct detection of organophosphorus pesticide (paraoxon) was described by Choi et al [2001]. This fibre-optic biosensor employed the colourless enzyme substratum, o-nitrophenyl acetate, which was converted into a yellow product o-nitrophenol in the presence of AChE. The AChE was immobilised using a similar method proposed by Choi et al [1998]. In the absence of the pesticide, o-nitrophenyl acetate was completely hydrolysed, while in the presence of the pesticide the amount of yellow product was reduced. This change of absorbance at 400 nm by o-nitrophenol production was related to the amount of phosphorus pesticide, and thus the enzyme reaction was not affected by the pH. This type of sensor deviated from the indirect detection method (from measuring the absorbance change of a pH-sensitive dye due to the formation of an acidic product), which was widely used by other optical AChE-biosensors. However, the detection range of the sensor was about 0.2 to 2 ppm, which was similar to the range obtained from optical enzyme sensor described by Choi et al [1998].

2.1.2   Enzyme sensor for heavy metal ions detection

In the case of heavy metal ions determination, the enzyme urease was commonly used as the bioreceptor. Zhylyak et al [1995] described a urease biosensor based on amperometric approach for heavy metal ions determination. The biosensor consists of a miniaturized conductance glass cell with a pair of reference and gold electrodes. The reference electrodes were coated with bovine serum albumin (BSA), and the gold electrodes were coated with a biological sensitive membrane, formed by crosslinking urease with BSA in saturated glutaraldehyde vapour. A low noise differential amplifier measured the differential signal between the pair of sensitive gold and reference

electrodes. The urease inhibition by heavy metal ions resulted in reduction of the conductivity changes produced by the catalysed hydrolysis of urea. Six heavy metal ions were tested and their toxicity towards urease was found in the following decreasing order: $Hg^{2+} > Cu^{2+} > Cd^{2+} > Co^{2+} > Pb^{2+} > Sr^{2+}$. The linear dynamic range of the sensor for heavy metal ions analysis was in the range of part per million and was presented as in Table 2.2. Complete reactivation of immobilized urease using 10 mM of ethylene diamine tetra acetic acid (EDTA) in 15 minutes, gave a possibility to re-use the biosensor for up to 10 measurements with the relative standard deviation of a sensor response of not more than 5 %.

Table 2.2. The linear dynamic range of the conductometric biosensor for heavy metal ions analysis [Zhylyak et al, 1995].

Metal ions	Hg^{2+}	Cu^{2+}	Cd^{2+}	Co^{2+}	Pb^{2+}	Sr^{2+}
Linear dynamic range (μM)	1-50	2-100	5-200	10-500	20-5000	100-5000

A urease biosensor based on ISFET as a potentiometric transducer for heavy metal ions detection has also been reported [Soldatkin et al, 2000; Hamlaoui et al, 2002]. The influence of two different immobilisation techniques of urease on ISFET (consist a Si_3N_4 pH-sensitive layer) has been studied by Soldatkin et al [2000]. They found that covering the deposited urease on the gate surface of ISFET with a charged polymer layer increased the sensor stability and sensitivity to urea since the enzyme molecules were not cross-linked and in a free configuration. They also found that the sensor sensitivity towards the selected heavy metal ions was improved by using a negatively charged polymer (Nafion) due to the accumulation of the positively charged

metal ions in the enzymatic layer. On the other hand, covering the enzyme with a positively charged polymer (Poly 4-vinylpyridine-co-styrene) prevented the diffusion of heavy metal ions because of the electrostatic repulsion effects between positively charged groups of the polymer and the ions. Table 2.3 shows the detection limits for the tested metal ions by the urease biosensor with a Nafion membrane.

Table 2.3. The detection limits for the heavy metal ions by the urease ISFET biosensor with a Nafion membrane [Soldatkin et al, 2000].

Metal ions	Ag^{2+}	Cu^{2+}	Ni^{2+}
Detection limits (μM)	0.035	2	70

A different sensing scheme of urease ISFET biosensor based on a NH_4^+-sensitive zeolite membrane was described by Hamlaoui et al [2002]. Rather than detecting the hydrogen ions, this ISFET biosensor detected the ammonium ions that were produced during urease enzymatic reactions. The ammonium sensitive membrane was formed by depositing a mixture of siloprene (a silicon rubber polymer diluted in tetrahydrofuran solvent) and zeolite on the ISFET surface. The ammonium sensitive membrane was then covered by the layer of enzyme urease, which was cross-linked with BSA and glycerol solution in the presence of saturated glutaraldehyde vapour. This ISFET biosensor was tested with mercury ions (Hg^{2+}) and showed high sensitivity where the detection limit obtained was less than 5×10^{-2} μM.

Another urease biosensor that used ammonium sensitive membrane incorporated with a disposable cuvette system was proposed by Preininger and Wolfbeis [1996]. The sensing scheme of this biosensor was based on the change of light absorption by the

ammonium sensitive membrane due to the urease enzymatic reaction in a disposable polystyrene cuvette. The sensitive membrane was fixed onto one of the cuvette walls. The full activity of enzyme urease was measured by the addition of 0.4 ml of 1 M urea solution into the cuvette containing a mixture of 2.9 ml maleate buffer and 0.2 ml urease solution. The inhibition effect of heavy metal ions was measured by mixing 0.1 ml of selected heavy metal solution with 2.8 ml maleate buffer and 0.2 ml urease solution, before the addition of urea solution. The efficiency of inhibition was found not to be affected by the incubation time. In spite of utilizing the non-immobilized enzyme urease, the detection limits for most of the tested heavy metal ions were still above 1 ppm as shown in Table 2.4.

Table 2.4. The linear dynamic range of the potentiometric biosensor for heavy metal ions analysis [Preininger and Wolfbeis 1996].

Heavy metal	LOD (ppm)	Linear range (ppm)	I_{50} (ppm)
Ag^+	0.02	0.02-0.2	0.13
Hg^{2+}	0.07	0.07-1	0.65
Cu^{2+}	0.25	0.4-0.7	0.55
Ni^{2+}	3	3-15	7
Co^{2+}	10	10-30	30
Cd^{2+}	20	20-200	95
Fe^{3+}	30	30-60	50
Zn^{2+}	50	50-70	85
Pb^{2+}	100	100-350	210

LOD – limit of detection
I_{50} – concentration of metal ions at 50 % inhibition level

Registration of heavy metal ions based on the absorbance change of a light indicator was also described by Nabok et al [2000]. Here, a pH-sensitive dye Cyclotetrachromotropylene (CTCT) was used. A composite film consisting of enzyme urease and CTCT was deposited on a glass slide using polyelectrolyte self-assembly (PESA) to form a sensitive element of the sensor. The films obtained were characterised with UV-visible absorption spectroscopy. The lowest concentration of detected metal ion was 10^{-4} M (100 ppm). The spectral changes were not very significant for low concentrations of metal ions but the principle of optical registration of enzyme reaction by combining the enzyme urease and CTCT in the same membrane using PESA method was demonstrated.

2.1.3 Multi-enzyme sensor arrays

Biosensors based on enzyme inhibition are typically demonstrated using compounds of a few specific chemical classes. Recent reports show these enzyme sensors to be inhibited by compounds from diverse chemical classes [Mulchandani el al, 1998]. Based on this phenomenon, multi-enzyme sensor arrays have been proposed to screen various common environmental pollutants. Schmid and co-workers [Bachmann and Schmid, 1999; Bachmann et al, 2000] described a sensitive screen-printed amperometric multienzyme biosensor for the determination of the pesticides paraoxon and carbofuran mixtures. The multi-enzyme sensor used different types of native, recombinant and mutant AChE as the bioreceptors, which were immobilized by screen-printing on a four-electrode thick film transducer as illustrated in Figure 2.1. The immobilized AChE hydrolyzed acetylthiocholine chloride to produce thiocholine, and this reaction was determined by thiocholine oxidation at 100 mV versus Ag/AgCl

printed electrode. The change of output current measured by a four-channel potentiostat was correlated to the AChE activity.
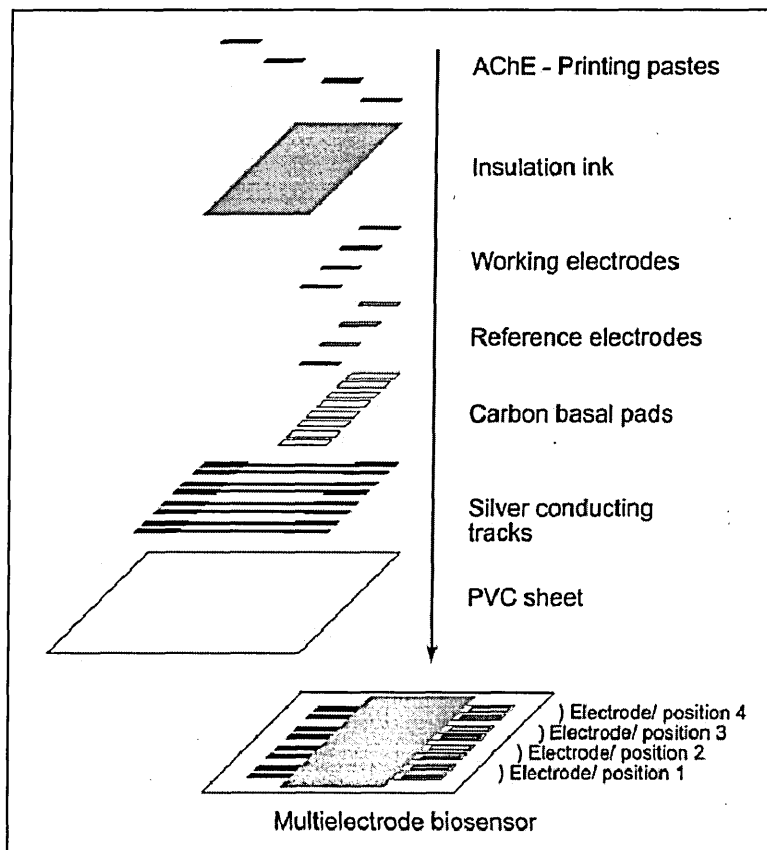
Figure 2.1. Schematic view of multielectrode biosensor assembly by screen-printing [Bachmann and Schmid, 1999].

The sensitivity of the multi-enzyme sensor towards pesticide was analysed using individual and binary mixtures of paraoxon and carbofuran in a concentration range of 0 to 20 µg/l [Bachmann and Schmid, 1999]. It was found that the biosensor was able to detect both pesticides in very low concentration down to 0.2 µg/l. However, the relationship between concentration and inhibition observed for binary mixtures was not linear where each enzyme electrode displayed individual inhibition patterns, depending on the type and concentration of the pesticide analysed. Consequently, artificial neural network data processing was used to discriminate the two tested pesticides. After 10 network training runs, the optimised neural network was able to discriminate 50

25

samples with different concentrations of the pesticides. The average errors of prediction were 0.9 µg/l and 1.4 µg/l for paraoxon and carbofuran, respectively [Bachmann and Schmid, 1999].

Arkhypova et al [2001] proposed an enzyme sensor array based on the combination of a potentiometric ISFET transducer with three types of biologically active membranes consisting enzyme urease, AChE and BChE. The active membranes were formed by cross-linking of 5 % (w/v) enzyme with 5 % (w/v) bovine albumin and 10 % (w/v) glycerol in the presence of saturated glutaraldehyde vapour. It was found that the inhibition of cholinesterase enzyme by pesticides and toxic ions depended on pollutants concentration in different ways and to different extents, while urease is not inhibited by tested pesticides but has considerable inhibition by mercury ions (see Table 2.5) [Arkhypova et al, 2001].

Table 2.5. Level of inhibition (%) of enzymes by different toxic substances [Arkhypova et al, 2001].

	Urease	BChE	AChE
10 µM trichlorfon	0	50	5
50 µM trichlorfon	0	70	25
1 mM trichlorfon	0	100	85
100 µM carbofuran	0	100	50
10 µM Ag$^+$	0	3	25
50 µM Ag$^+$	10	7	70
10 µM Hg^{2+}	15	3	10
50 µM Hg^{2+}	40	7	70
Mixture No.1	20	100	30
Mixture No.3	95	100	90
Mixture No.4	100	100	100
Mixture No.2	30	100	35

Mixture No. 1: 10 µM Ag$^+$ + 10 µM Hg^{2+} + 10 µM trichlorfon + 10 µM carbofuran.
Mixture No. 3: 50 µM Ag$^+$ + 20 µM Hg^{2+} + 50 µM trichlorfon + 20 µM carbofuran
Mixture No. 4: 50 µM Ag$^+$ + 50 µM Hg^{2+} + 50 µM trichlorfon + 50 µM carbofuran
Mixture No. 2: unknown mixture

Starodub and co-workers [Starodub et al, 1999; Kukla et al, 1999] described a multi-enzyme electrochemical sensor based on electrolyte-insulator-semiconductor (EIS) structures consisting of five channels with an integrated flow–injection system (Figure 2.2). Four channels contained enzymatic membranes and one channel served as a reference. Each channel consisted of a pH-sensitive multilayer $Si–SiO_2–Si_3N_4$ structure, an electrolyte and a metallic electrode. The operating principle of each sensor channel was based on the measurement of high-frequency C-V curves for the above-mentioned multilayer structure. The changes of this parameter with time served as a response of the sensor channel during enzyme reactions.
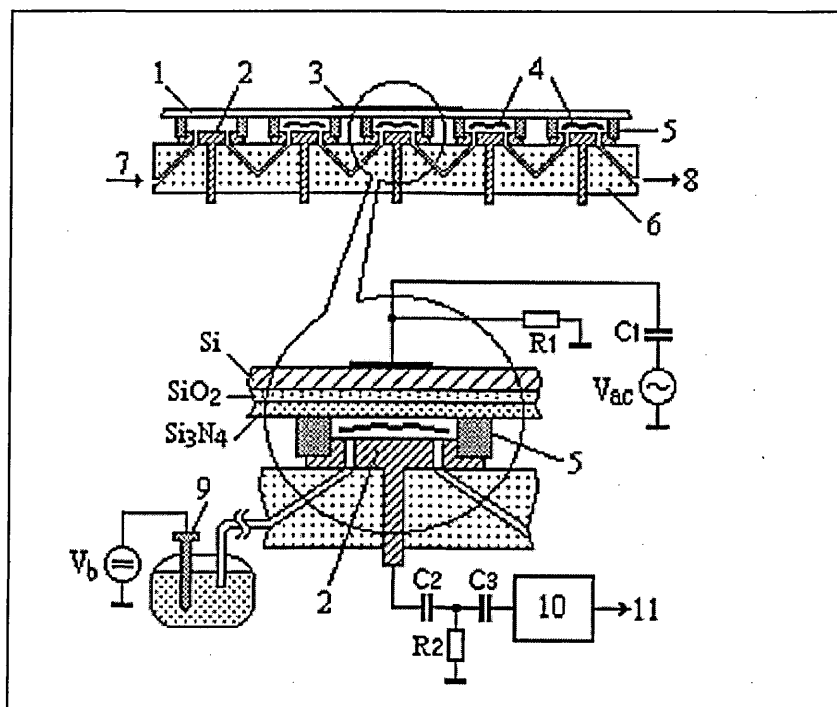
Figure 2.2. Schematic view of the 5-channel EIS enzyme sensor: (1) sensitive $Si–SiO_2–Si_3N_4$ structure, (2) steel contrary electrode, (3) Al contact to Si, (4) enzymatic membranes, (5) rubber sealing, (6) organic glass support, (7) flow input, (8) flow output; (9) reference electrode, (10) C/V converter, (11) connection to PC [Kukla et al, 1999].

The enzyme membranes were prepared by deposition of 10% enzyme solutions on the nitrocellulose membrane-carriers. Enzymes urease, AChE, BChE and glucose oxidase (GOD) were used for the pesticides and heavy metal ions detection. The registration procedure was as follows. At first, the responses of enzymatic reactions for pure substratum or their mixtures of known concentrations were measured. Then model pesticide or metal salt solution without substratum was added into the system and held there for approximately 15 minutes. After this, the responses of the sensor channels under similar conditions were recorded again. The residual enzyme activity was estimated from the response drop compared with its initial value. This value of activity was used for the determination of pollutant concentrations. The concentrations of pesticides and heavy metal ions, which were detected by this sensor, were within the range of 10^{-4} to 10^{-7} M.

2.2 Planar Optical Waveguides for Biosensing

Optical biosensors offer many advantages over the existing sensor types due to their capability of remote and multiple sensing [Lukosz, 1995]. They are also immune to electric interference and easy to miniaturise for the development of an integrated, portable and flexible sensor [Kunz, 1997]. In addition, the sensitivity of miniature integrated optical sensors has been improved by exploiting the principle of multiple reflections of the light beam in fibre optics and planar optical waveguides. In order to make full use of this principle, the biological sensing elements are immobilised on the top surface rather than on the end (or edge) of the waveguide. In the case of fibre optics, it involves difficult preparation processes, where the cladding layer needs to be removed from the core layer. Furthermore, the exposed glass core is very fragile and, susceptible to chemical degradation and fouling in most sensing environments [DeGrandpre and Burgess, 1988]. Thus, the planar waveguide is more preferable for the application of this technique due to the convenience in forming such a configuration. Moreover, it is very durable and easy to fabricate using a variety of materials and methods.

In general, planar optical waveguides can be formed from thin dielectric films (0.095 – 10 μm) or thicker internal reflection elements (0.8 – 1.5 mm). Thin planar waveguides are usually supported by a rigid substrate of low refractive index such as silicon oxynitride (SiON) and silicon nitride (Si_3N_4) deposited on quartz or silicon dioxide (SiO_2). Thick planar waveguides are more durable than thin planar waveguides, however, the propagating light makes discrete contacts with the waveguide interface [Choquette et al, 1992], and its sensitivity is primarily limited by the number of reflections (from 10 to 100) [DeGrandpre et al, 1990]. In contrast, light guided by a thin planar waveguide makes a continuous energy distribution along the path of propagation.

In addition, a thin film planar waveguide with approximately 1 μm thickness can have thousands of reflections per centimeter [DeGrandpre et al, 1990]. This phenomena is explained further in the next section, which describes the theoretical aspects of the multiple internal reflection principle.

2.2.1 Multiple internal reflections principle

Generally, an optical waveguide is made from a dense dielectric medium surrounded by a less dense medium. As shown in Figure 2.3, light waves travelling in an optically denser medium (refractive index, n_1) of the waveguide may be transmitted or reflected, when they strike the less dense medium with a refractive index, n_2. In this case, the transmitted angle is obviously greater than the incidence angle. A critical angle occurs when the transmitted angle reaches 90°, and can be determined by the ratio of the refractive indices;

$$\theta_c = \sin^{-1}\left(\frac{n_2}{n_1}\right) \qquad (2.5)$$

When the incidence angle θ_i exceeds θ_c then the wave is only reflected together with the existence of an evanescent wave that travels on the medium interface. It is assumed that the incident and reflected waves are plane waves. This phenomenon is called total internal reflection (TIR). It leads to the propagation of light waves in a dielectric medium surrounded by a medium of smaller refractive index [Kasap, 2001]. Figure 2.4 illustrated the multiple internal reflection of light in a ray optic perspective [Plowman et al, 1998].

Transmitted
light

Evanescent
wav? ,

$0_i = 0$, critical'
angle

$\setminus$ $> 0C_;$
Total internal
reflection (TIR)

Incident
light

Reflected
light

(a)   (b)   (c)
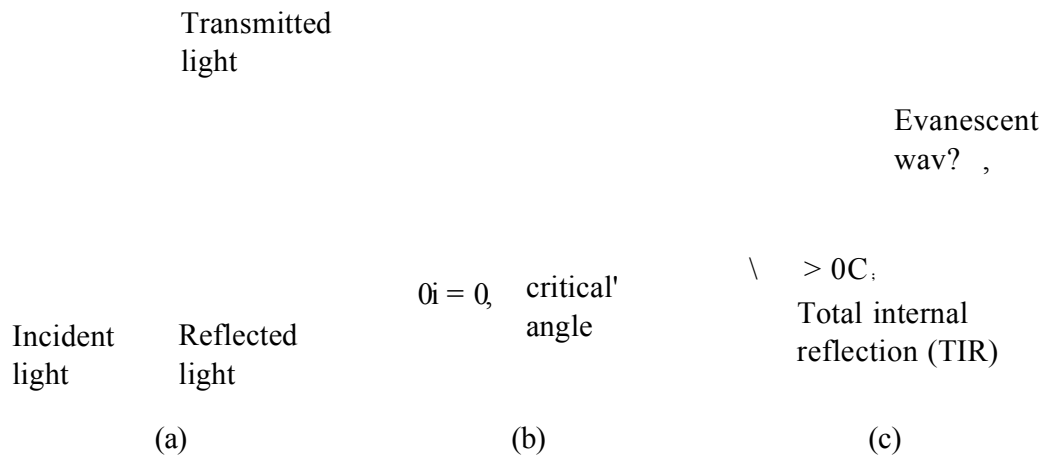
Figure 2.3. The effect of increasing the incident angle to the light wave travelling in a more dense medium and strikes a less dense medium (plane waves are assumed) [Kasap, 2001].

$Lf = (Ie/10df$ $_U^y$

Figure 2.4. A ray optic perspective of multiple internal reflections in a planar optical waveguide, with a part of the dense medium surface covered with a thin absorbing material (figure was modified from Plowman et al [1998]).

Apparently, the evanescent wave is established by the spreading of the incident intensity at the interface for each reflection. The evanescent wave interfacial intensity (I_e) per unit incident intensity (I_i) is given by [Saavedra and Reichert, 1990],

$$\frac{I_e}{I_i} = \frac{n_2 4\cos\theta_i}{n_1[1-(n_2/n_1)^2]} \qquad (2.6)$$

This evanescent wave is used to interact with an absorbing material that replaces the rarer medium, based upon the material thickness and absorptivity. The field of the evanescent wave (E) is largest at the interface (I_e) and decays exponentially, as it penetrates further with distance (y) into the less dense medium;

$$E = I_e \exp(-y/d_p) \qquad (2.7)$$

The depth of penetration, d_p, at which the evanescent field has decayed exponentially from its initial value is given by the equation;

$$d_p = \frac{\lambda/n_1}{2\pi\left[\sin^2\theta_i - (n_2/n_1)^2\right]^{1/2}} \qquad (2.8)$$

It is obvious from the above equation, by decreasing θ_i closer to the critical angle, the evanescent field will penetrate more deeply into the rarer medium, and hence more light energy becomes available for interaction with the external medium. The depth of penetration is also proportional to the light wavelength, λ, and it is greater at longer wavelength. However, large penetration depth will cause large lateral shift of the reflected beam at the interface. The lateral shift, Δz, known as Goos-Hänchen shift depends on the angle of incidence and the penetration depth;

32

$$\Delta z \approx 2d_{\mathrm{p}} \tan\theta_{\mathrm{i}} \qquad\qquad (2.9)$$

Large lateral shift may cause considerable impact on the distance between each reflection, which will affect the number of reflections, N at the interface of the waveguide, given by

$$N = \frac{L}{2(d\tan\theta_i + \Delta z)} \qquad\qquad (2.10)$$

where L and d are the length and the thickness of the waveguide, respectively. Clearly from equation (2.10), a decrease in the thickness of the waveguide will reduce the distance between reflections and hence increase the number of the reflection. A close gap between the reflection points may produce a continuous evanescent energy distribution along the path of propagation.

However, not all light waves that have an angle of incidence greater than the critical angle will be propagated in the dense medium. This is because the light wave will interfere with itself as it travels through the waveguide. In order to propagate successfully, the light wave must not interfere destructively, and only certain reflection angles give rise to the constructive interference, which means only certain waves can exist in the waveguide. These constructive interference waves are called guided modes and designated by an integer $m = 0, 1, 2\ldots$ The number of guided modes is dependent upon the light wavelength, waveguide thickness and refractive index, and can be estimated with the formula [Kasap, 2001],

$$M = \text{Int}\left(\frac{2d(n_1^2 - n_2^2)^{1/2}}{\lambda}\right) + 1 \qquad (2.11)$$

where Int (x) is the integer function which drops the decimal fraction of x. A general waveguide condition for guided waves is given in the form,

$$\frac{2\pi n_1 d}{\lambda}\cos\theta_m - \phi_m = m\pi \qquad (2.12)$$

where ϕ_m and θ_m are the phase change and the incident angle at the interface for the specific guided mode, respectively. The phase change ϕ_m of the transverce electric field wave is written in the form,

$$\phi_m = 2\tan^{-1}\left(\frac{\sqrt{\sin^2\theta_m - \left(\frac{n_2}{n_1}\right)^2}}{\cos\theta_m}\right) \qquad (2.13)$$

Thus, if the waveguide thickness, refractive index ratio and the light wavelength are known, the value for ϕ_m and θ_m can be ascertained by the self-consistent solution of equation (2.12) and (2.13). Then all calculations using previous equations must be based on the guided modes that needed to replace θ_i with θ_m. For instance, in the case of silicon oxynitride (SiON) waveguide [Walker et al, 1993] with the thickness of 1.416 μm, the refractive index ratio of water to SiON, $n_2/n_1 = 0.875$, and the wavelength of excitation, $\lambda = 514.5$ nm, the self-consistent solution of equations (2.12) and (2.13) give the values of 84.32° and 128.63° for θ_m and ϕ_m, respectively, for the single mode

propagation ($m = 0$). Therefore, the number of reflections, N in the waveguide calculated from equations (2.10) is equal to 303 reflections per centimeter.

Normally, light can propagate through the waveguide without significant attenuation, since both mediums are transparent in the visible range. However, if a sensitive thin film has a non-zero absorption coefficient deposited on the dense medium, optical loss will occur each time reflection takes place at the interface between the medium and the sensing film. In this case, the attenuation of the transmitted intensity, I_{out} (output light intensity) will normally occur according to the Beer-Lambert law,

$$I_{out} = I_{in} \exp(-A N) \qquad\qquad (2.14)$$

where I_{in} is the input light intensity, and A is the fractional absorption from each encounter with the sensing film, given by

$$A = 1 - \exp(-\alpha\delta) \qquad\qquad (2.15)$$

where α and δ are the absorption coefficient of the film and the interaction length per reflection, respectively. For a very thin film, the term $\alpha\delta$ is very small and Beer-Lambert approximation of $\exp(-\alpha\delta) \approx 1 - \alpha\delta$ can be applied to equation (2.14) and (2.15), yielding

$$I_{out} = I_{in} \exp(-\alpha\delta N) \qquad\qquad (2.16)$$

The interaction length, δ is calculated from the expression [Plowman et al, 1998],

$$\delta \approx L_f = \frac{I_e}{I_i} d_f \qquad (2.17)$$

where L_f is the evanescent path length related to the thickness of the thin film, d_f. By substituting I_e/I_i from equation (2.6) into equation (2.17), the interaction length can be expressed by

$$\delta \approx \frac{4 n_f d_f \cos\theta_m}{n_1 [1 - (n_f/n_1)^2]} \qquad (2.18)$$

where n_f is the refractive index of the thin film and θ_m is the incidence angle at the guided mode m.

Equation (2.16) shows that multiple internal reflections in a planar waveguide can provide an extremely sensitive tool for registration of small changes in optical absorption in the thin film. For example, a monolayer of copper phthalocyanine (CuPc) molecules ($d_f \approx 1.5$ nm and $\alpha \approx 10^7$ m^{-1}) exhibits a large attenuation of $I_{out}/I_{in} = \exp(-300)$ [Ray and Nabok, 2002]. Preliminary experiments have shown that deposition of two monolayers of CuPc molecules reduced the output light intensity from the waveguide down to a noise level. It is therefore anticipated that a high degree of sensitivity can be achieved in monitoring different chemical and bio-chemical reactions with a planar optical waveguide.

The optical techniques that most frequently use the multiple internal reflections principle are attenuated total reflection (ATR), total internal reflection fluorescence (TIRF) and planar interferometry. The applications of different types of planar optical waveguides for biosensing based on the above optical techniques are reviewed in the following sections.

2.2.2 Planar waveguide as an attenuated total reflection (ATR) transducer

In an ATR transducer, the presence of optically absorbing material on the waveguide interface can be monitored as light energy absorbed from the evanescent wave of the internally reflected light beam. As expressed by equation (2.16) and (2.17), the optical losses at each reflection are proportional to the absorption coefficient and thickness of the deposited sensing film. The changes of the film properties parallel to the attenuation of the transmitted light provide a simple and effective tool in monitoring different bio-chemical reactions or protein deposition on the waveguide surface.

E.g., an ATR immunosensor, which utilised thick multiple internal reflection elements to monitor immunoreactions of haemoglobin with rabbit anti-haemoglobin antibodies, was reported (Figure 2.5) [Sutherland and Dahne, 1987]. The rabbit antibodies were covalently immobilised on the surface of a quartz microscopic slide and then reacted with different concentrations of haemoglobin. Light at 410 nm was coupled into the quartz slide via a quartz prism, and the incidence angle of the light was varied by rotating the mirrors. The attenuation of the reflected light was measured using a photomultiplier tube. Specific binding of 10 mg/ml of haemoglobin with the rabbit antibodies was clearly detected by the ATR immunosensor.

The application of an ATR transducer for monitoring the adsorption of bovine serum albumin (BSA) to the surface of a polymer waveguide was also reported [Walker et al, 1993]. The thin film polymer waveguide was prepared by depositing a mixture of two types of polymer, namely hydroxyethyl methacrylate (HEMA) and ethyl methacrylate (EMA), on a quartz slide substrate using a spin coating technique. The spun cast polymer films were macroscopically smooth and optically clear to be suitable
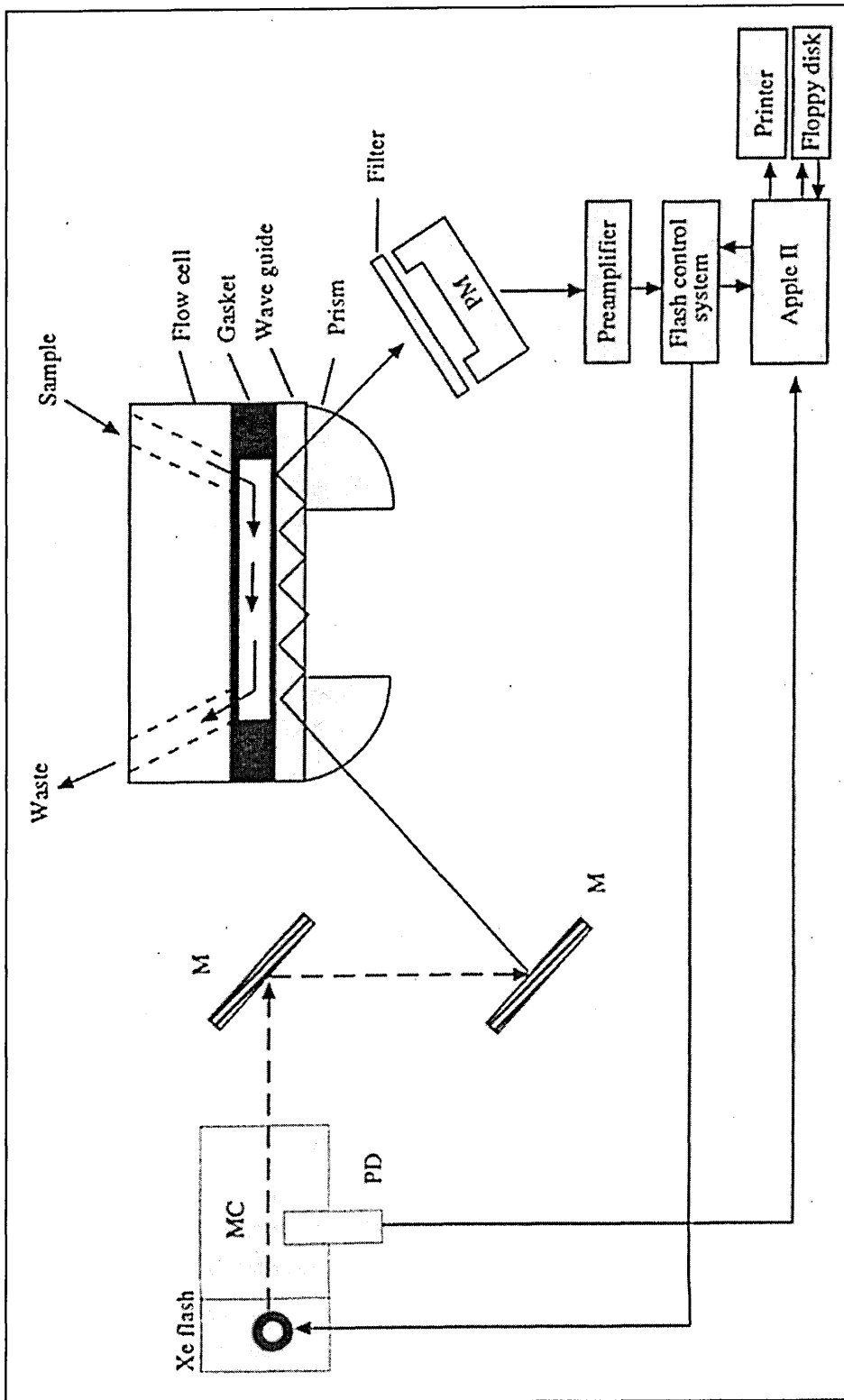
Figure 2.5. Diagram of instrumental layout used for measuring immunoassays with a multiple-internal reflection plate. PM, photomultiplier tube; PD, photodiode; MC, monochromator; M, mirrors [Sutherland and Dahne, 1987].

to perform as a waveguide. The thickness of the polymer waveguide varied within 0.93 µm to 2.80 µm, depending on the mixture composition of HEMA and EMA. The polymer waveguides were assembled into a flow cell, and were placed in parallel with a liquid-nitrogen-cooled charged couple device (CCD) camera. An argon laser beam at 488 nm wavelength was coupled into the waveguide through a high index prism configured into the flow cell housing. The attenuation of light intensity due to the adsorption of chromorephore-labeled BSA on the polymer film, was measured by directly imaging the waveguide streak using the CCD camera. The measurements range of BSA surface densities was 34 to 757 ng/cm^2, with standard deviations ranging from 1 to 9 ng/cm^2. However, this report did not mention the total amount of concentration of the adsorbed BSA on the waveguide surface.

Recently, Kovacs et al [2003] described an ATR enzyme sensor based on a microscopic glass waveguide (76 x 26 x 1 mm dimensions) coated with an ammonium ion selective membrane and a urease enzyme layer for urea concentration measurements. Figure 2.6 shows the cross-section of the coated waveguide and the instrumental set-up of the ATR enzyme sensor. The flow-through cell consisted of a coated microscopic glass waveguide placed in between two 40 x 55 x 15 mm plexiglass blocks, with the upper block drilled through, having two holes for inserting the solution in- and out-flow tubes. A reaction cell of 30 µl in volume was formed by placing a 100 µm thick teflon sheet with a 36 mm long and 8 mm wide channel in between the coated glass slide and the upper block. Two uncoated tips of the waveguide reaching out at both sides of the plexiglas block, were attached to 3 x 5 mm of 750-line/mm transparent polyacetate diffraction grating for light in and out coupling.
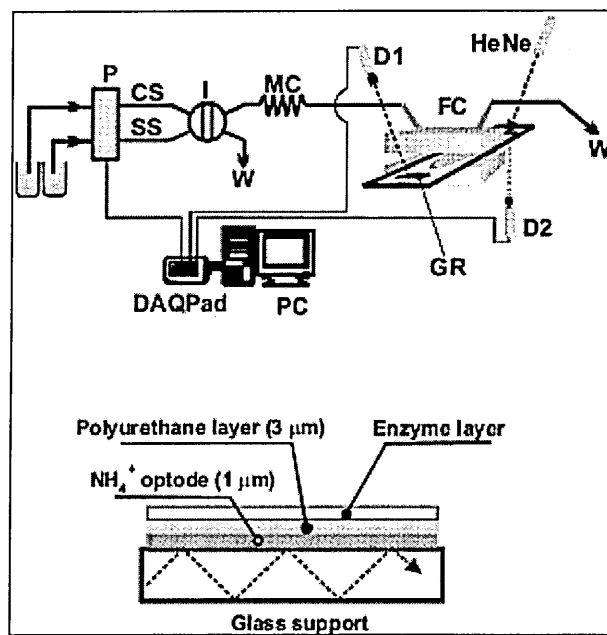
Figure 2.6. Schematic drawing of the instrument setup and cross-section of the coated planar waveguide used for optical urea sensor. P—pump, CS—carrier stream, SS—sample stream, I—injector, W—waste, MC—mixing coil, FC—flow-through cell, HeNe laser source, D1, D2—planar silicon detectors, GR—optical grating [Kovacs et al, 2003].

About 11-13 reflections of HeNe laser at 633 nm wavelength were counted on the sensing membrane interface after focusing the beam to the in-coupling grating. The resultant beam was detected using a photodiode placed above the out-coupling grating. When a sample solution containing urea was injected into the reaction cell, a urease enzymatic reaction occurred and produced ammonium ions, which could diffuse to reach the ammonium sensitive membrane. The ammonium ions were then selectively complexed by the nonactin component of the sensitive membrane. Simultaneously the other active component of the membrane, namely chromoionophore Nile blue derivative became deprotonated in order to keep the membrane electrically neutral. During this

process, the colour of the indicator changed from blue to red. Thus, the concentration of urea can be registered by the level of deprotonation of the indicator. Experimental results showed that the ATR sensor could successfully register different urea concentrations in the dynamic range from 7×10^{-5} M to 8×10^{-3} M.

The above examples demonstrate that the ATR technique is well suited for different biosensing applications. It provides a direct measurement of the analyte with a simple preparation of the waveguide and experimental setup. However, the ATR transducer needs further improvement as its sensitivity is substantially lower than other optical techniques such as TIRF that are reviewed in the next section.

2.2.3 Planar waveguide as a total internal reflection fluorescence (TIRF) transducer

A TIRF transducer is constructed by placing a fluorescent material in contact with the reflecting surface of a planar waveguide. The evanescent energy generated from the propagating light will not only be absorbed as in the case of ATR technique, but will also be partly be re-emitted as fluorescent light. The intensity of the emitted fluorescence was measured for quantification of the studied analyte. Literature shows that different structures of planar waveguide have been used for the development of TIRF biosensors.

For instance, a reusable TIRF immunosensor based on a silver ion (Ag^+)-exchanged waveguiding layer, for clinical analyte theophylline was developed by Choquette et al [1992]. The Ag^+ waveguiding layer was fabricated using an ion

diffusion process, by immersing a glass substrate in a molten solution of 10 mol % silver nitrate ($AgNO_3$) and 90 mol % sodium nitrate ($NaNO_3$), at 280 °C for 15 min to 4 hours. The diffusion depth of silver ion in the glass substrate was calculated to be approximately 6 μm. Fluorescence experiments were performed by monitoring the competitive binding reaction of modified liposomes and theophylline with the covalently immobilized mouse anti-theophylline IgG layer on the surface of the waveguiding layer. Sensor response to theophylline concentration was determined by measuring the fluorescence emission of the specifically bound liposome fraction caused by the evanescent and scattering components of the propagating Argon ion laser at 488 nm in the waveguide. The fluorescence emission was measured through the waveguide substrate by a rectangular (0.8 mm x 9.7 mm) fused-silica fibre bundle of a fluorometer. The TIRF immunosensor responded well to variations of theophylline concentration in the range from 2.0×10^{-5} to 2.0×10^{-10} M even after 15 sequential measurements, with signal degradation less than 10 %.

A more sensitive TIRF immunosensor used to detect analyte in femtomolar concentrations (less than 1 part per trillion) on a SiON planar waveguide was described by Plowman et al [1996]. The planar waveguide was produced by depositing a 1.3 μm thick SiON layer on the surface of a 4-inch diameter quartz wafer using the PECVD process. The SiON coated wafer was masked, etched and cleaved to have a 23 mm x 69 mm rectangular waveguide with two 1 mm x 65 mm parallel strips or channels of SiON film. The planar waveguide was attached to a flow cell with a dual channel formed by two rounded rectangular grooves sealed with two silicone rubber O-ring gaskets. A small coupling prism measuring 4 mm wide and 10 mm high was placed on the SiON waveguiding layer in each flow channel. Figure 2.7 illustrates the measurement configuration of this dual channel TIRF immunosensor. A HeNe laser used to excite the
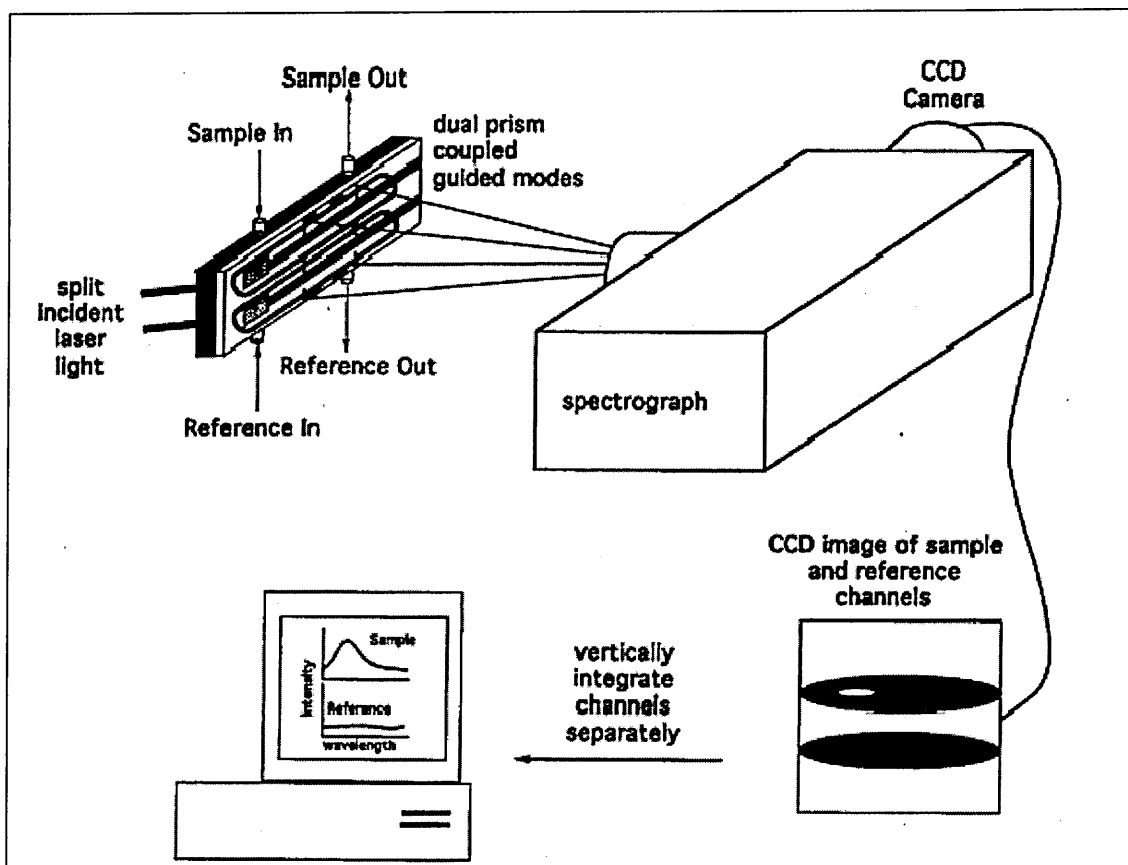
Figure 2.7. Schematic illustration of measurement configuration of dual channel TIRF immunosensor [Plowman et al, 1996].

reference and sample signals, was split into dual beams and passed through a small hole of the flow cell before continuing through a prism coupled into the SiON channels of the waveguide. The guided mode was imaged through the quartz plate by back-collection with a CCD camera. The TIRF immunosensors showed very high sensitivity when tested with low concentration of ligand-receptor systems. Binding of 3 x 10^{-15} to 10^{-8} M murine monoclonal anti-fluorescein labelled with cyanine dye to immobilized avidin was observed.

Plowman et al [1999] has also demonstrated a TIRF immunosensor for multiple analyte detection based on the SiON planar waveguide, which consists of a SiON

waveguiding layer deposited by the PECVD process on 2 cm width quartz substrate. Figure 2.8 shows the schematic representation of the multiple analyte immunosensor. The 3 mm-sized channel array were formed by three capture polyclonal antibodies, namely anti goat-IgG, anti human-IgG and anti rabbit-IgG which were physically adsorbed on the surface of the SiON waveguiding layer. The two sections of the antibody-free SiON surface were coated with a passivating and preserving solution of porcine serum albumin to block non-specific sites. A Diode laser at 635 nm was coupled via grating diffraction to establish a continuous streak of light at the waveguide
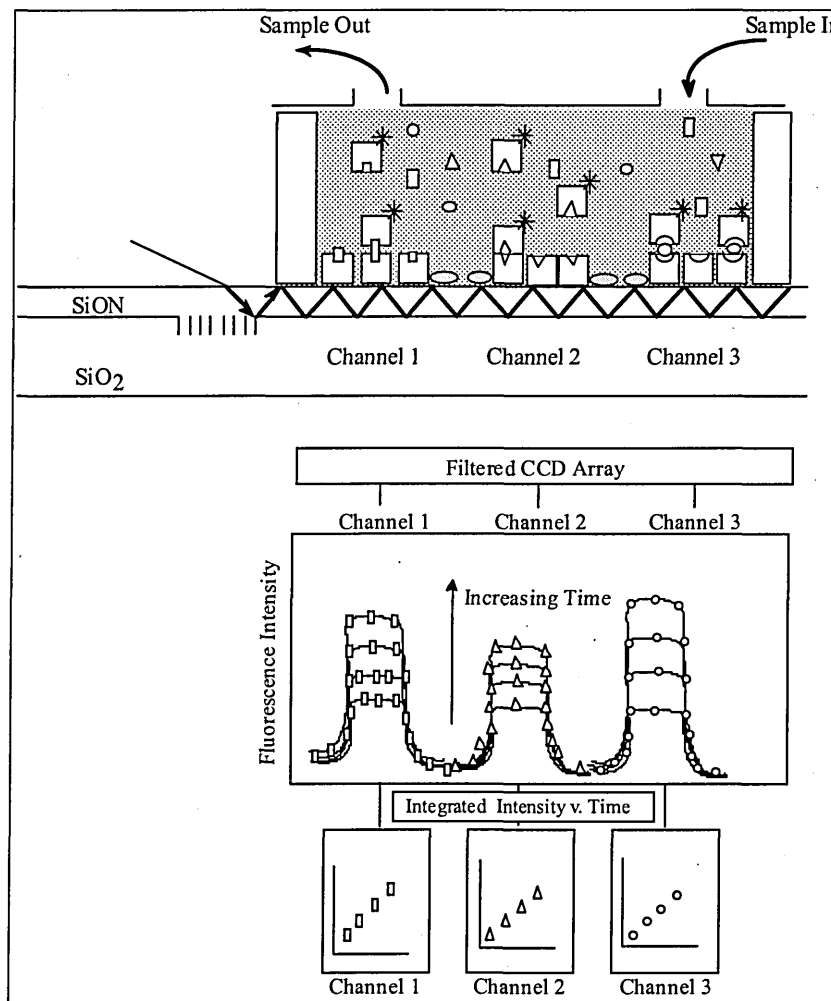
Figure 2.8. Schematic representation of a multiple analyte immunosensor performed on a grating coupled SiON planar waveguide [Plowman et al, 1999].

interface. Fluorescence excitation was measured using a spatially binned CCD camera placed at the bottom of the quartz waveguide. Experiment results for immunoreactions of the immobilised antibodies with low concentration (3×10^{-11} to 10^{-7} M) of specific antigens (goat-IgG, human-IgG and rabbit-IgG) labelled with cyanine dye were registered.

TIRF sensor with microarrays sensing cells, which enable parallel ultra-sensitive nucleic acid analysis, was demonstrated by Duveneck et al [2002]. The transducer structure consisted of a 150 nm thick Ta_2O_5 waveguiding layer with a refractive index of 2.092, which was deposited on a planar glass substrate. Two different sizes of plastic structure consisting of a number of flow cell arrays were placed on top of the waveguiding layer to form two different format transducers (see Figure 2.9). Each cell was capable of accommodating a sample volume as low as 15 µl within the cell. The cell inlets could be addressed by regular pipette tips, thus, allowing filling of the cells, by means of manual or robotic multipipettors.

A red laser light at 635 nm wavelength was coupled into the waveguide through a glass substrate using 0.5 mm broad relief diffraction gratings located within the flow cells (Figure 2.10). Fluorescence excited in the evanescent field of the waveguide was collected by a CCD camera. Experimental results showed that binding of Cy5-labelled target cytosine-deoxyribonucleic acid (cDNA) with immobilised double-stranded mouse brain cDNA were succesfully registered. This TIRF sensor had higher sensitivity than a conventional confocal fluorescence scanner. Measured signal-to-noise ratios ranging from 5 to 10 for the scanner data and from 300 to 750 for the TIRF sensor results were observed.
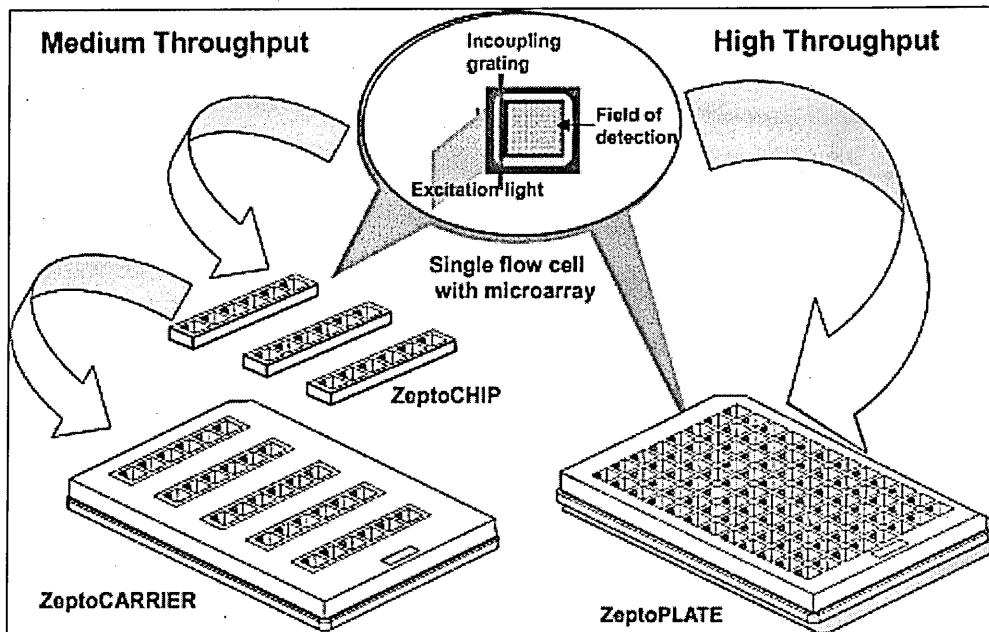
Figure 2.9. TIRF planar waveguide chip formats and flow cell arrangements [Duveneck et al, 2002].
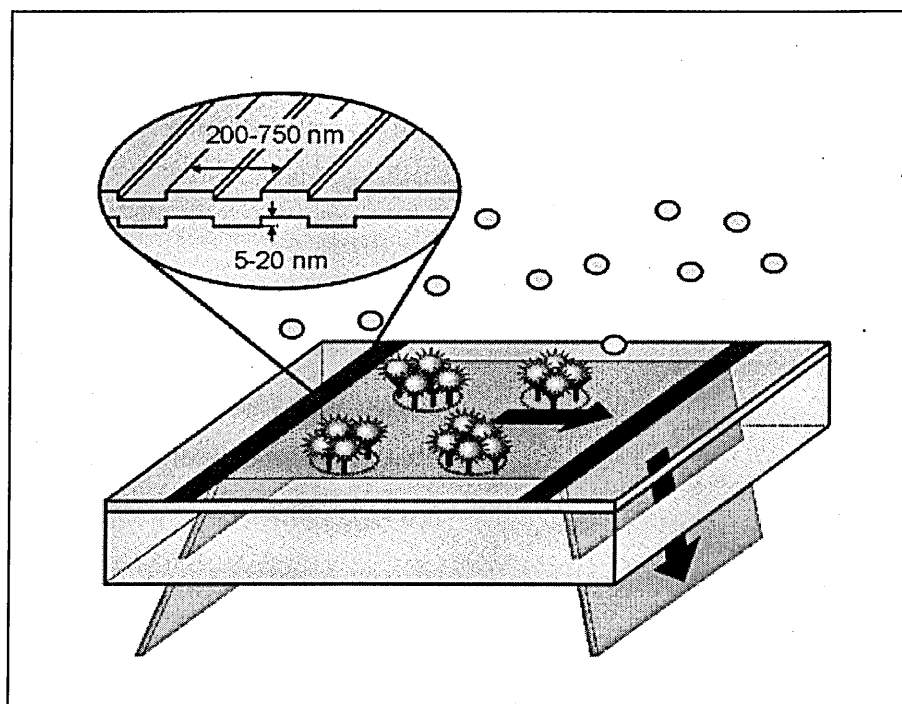
Figure 2.10. Excitation light coupled into Ta_2O_5 waveguides using diffractive relief gratings [Duveneck et al, 2002].

Determination of trace level pesticides using a TIRF immunosensor based on an internal multiple reflection elements were explored by Gaulitz and co-workers (Klotz et al, 1998; Mallat et al, 2001; Barzen et al, 2002). A schematic of the sensor set-up is depicted in Figure 2.11. A bulk optical glass slide (dimensions of 60 mm x 15 mm) with a thickness of 1.5 mm and a refractive index of 1.52 was used as the transducer element. The surface of the glass slide was polished and modified with a layer of aminodextran, which was conjugated with the carboxylic group of pesticide derivatives, to form three sensitive spots of 3 mm in diameter and with 2.5 mm distance in between. The glass slide waveguide was mounted on a flow cell with a flow channel dimension of 1.7 mm width and 0.1 mm depth. Through this flow cell, the sensitive spots were exposed to a premixed solution and bound with any non-blocked anti-pesticide labelled with cyanine dye, to produce fluorescence signals that were inversely correlated to the pesticide concentration.
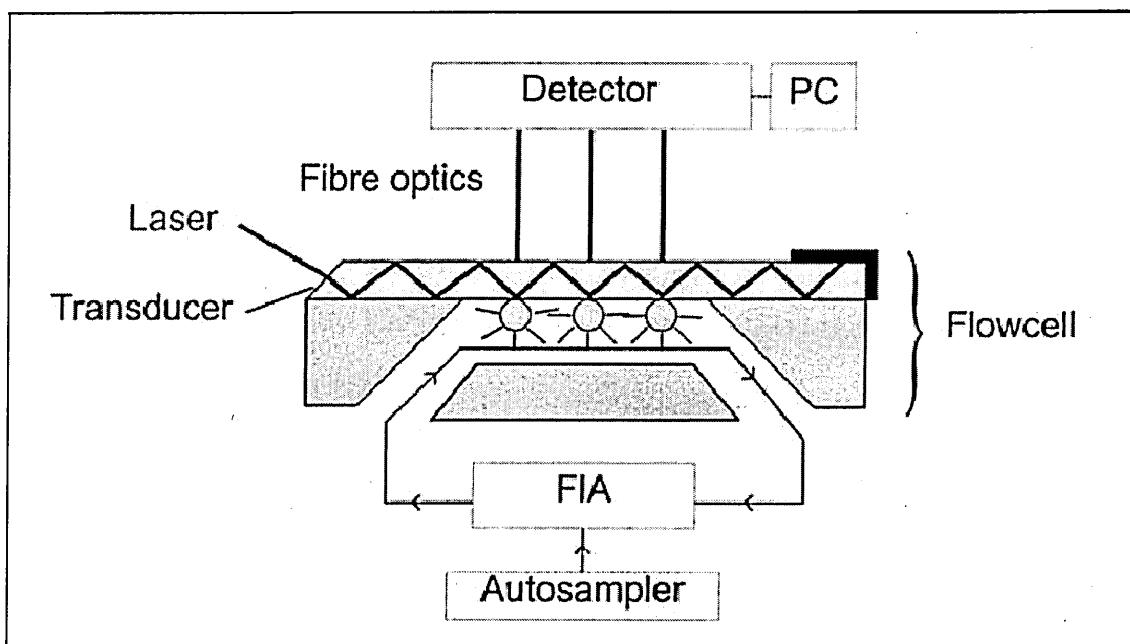
Figure 2.11. TIRF immunosensor based on optical glass slide waveguide [Barzen et al, 2002].

Fluorescence was excited using a modulated laser diode operated at 635 nm coupled into the waveguide through the 45° bevelled waveguide end-face. Fluorescence excitation was collected by high numerical aperture polymer fibres located on the back surface of the waveguide opposite the sensitive spots. The collected light was filtered and detected by photodiodes using lock-in detection. This TIRF immunosensor offers the advantage of performing immunoassays for sets of three pesticides simultaneously in one sample. Two sets of three different analytes (atrazine, alachlor, pentachlorophenol and 2,4-dichlorophenoxyacetic acid, simazine, isoproturon) were detected successfully with no cross-reactivity effects occurred. The lowest detection limit of this sensor was 0.03 µg/l.

The above reviewed studies shows that TIRF technique provides high sensitivity and selectivity for various analyte detection. However, it involves complex preparation prior to the experiment such as the target analyte or the sensing element need to be labelled with fluorescence material.

2.2.4 Planar waveguide as a planar interferometer transducer

Planar interferometry is a slightly different technique but still utilises the multiple reflections, and has been exploited for biosensing. It is based on the change in the propagation velocity of light passing through a planar waveguide. Two variations of the planar interferometer used are the Mach-Zehnder interferometer and the planar polarization interferometer. A Mach-Zehnder interferometer to detect the physical adsorption of proteins and immunoreactions was demonstrated by Heideman et al [1991, 1993, and 1994]. The planar waveguide structure is illustrated in Figure 2.12. It

48

was fabricated on a 3 inch diameter silicon wafer covered with a 1 μm thick thermal growth of SiO_2 substrate layer at 1150 °C. The waveguiding layer of Si_3N_4 with a refractive index of 2.0 and a thickness of 95 nm was deposited using low pressure chemical vapour deposition (LPCVD) at 800 °C. On top of the waveguiding layer, a protective 1.5 μm thick SiO_2 layer with a refractive index of 1.457 was grown using plasma enhanced chemical vapour deposition (PECVD) at 300 °C.
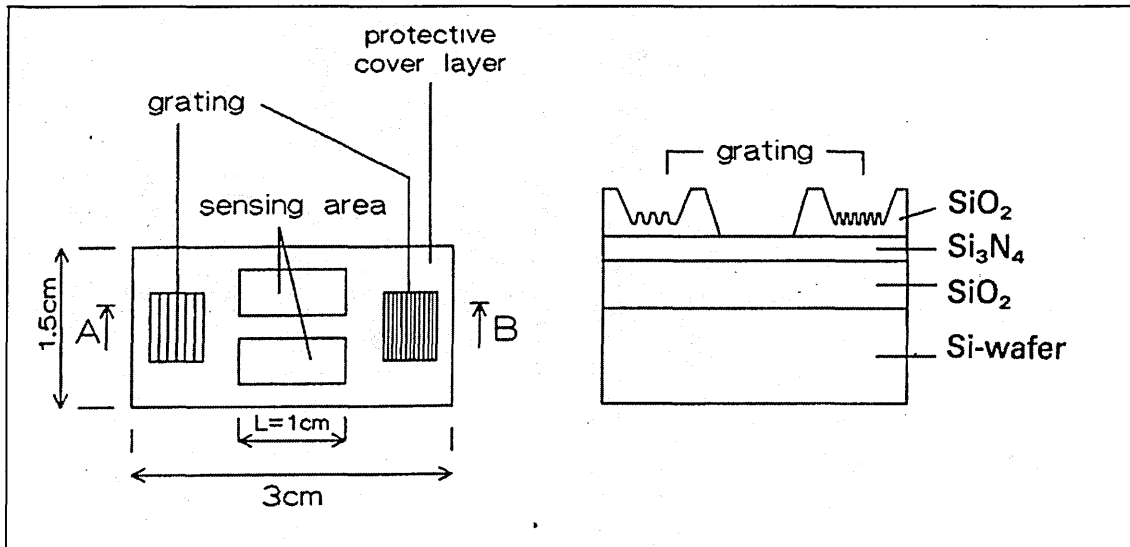
Figure 2.12. Top view and cross-section (through the line A-B) of SiO_2/Si_3N_4 waveguide as a Mach-Zehnder interferometer transducer [Heideman et al, 1994].

Two sensing windows were formed by completely removing the protective layer in two rectangles with a width of 3 mm and a length of 10 mm using standard photolithography on a positive photoresist layer, followed by wet chemical etching with hydrofluoric-ammonium fluoride (HF/NH₄F) solution. The same photolithography and wet chemical etching method was applied to develop two gratings (with a remaining SiO_2 thickness of 500 nm) used to couple light into and out of the waveguide. He-Ne laser light with a wavelength of 633 nm was split into two parallel beams by a cubic beamsplitter before being coupled into the waveguide. Detection of protein adsorption and immunoreactions on the sensing surface was done by measuring the phase change

of the recombine beams. The adsorption of antibody anti-human chorionic gonadotropin (αhCG) with the concentration of 3×10^{-8} M, and protein bovine serum albumin (BSA) with the concentration of 2×10^{-4} M, were successfully determined. Immunoreactions with different concentration of antigen human chorionic gonadotropin (hCG) have also been done. The lowest detectable concentration of bind hCG was 5×10^{-11} M.

A Mach-Zehnder interferometer based on the same SiO_2/Si_3N_4 planar waveguide structure for immunoreactions detection was described by Lechuga et al [1995]. The same fabrication method used by Heidemen et al [1993] was applied to develop SiO_2 and Si_3N_4 waveguiding layers. The only difference was the grating coupler system was replaced by the end-fire coupling through cleaved and polished end faces of the Si_3N_4 planar waveguide. The sensitivity of this interferometer for immunosensing was tested using the antibody/antigen system of antihuman serum albumin/human serum albumin (α-hSA/hSA). Detection of hSA binding with concentration ranging from 1×10^{-11} M to 1×10^{-7} M was achieved.

Another Mach-Zehnder interferometer based on $SiO_2/SiON$ waveguide structure was described by Brosinger et al [1997] (Figure 2.13). The SiO_2 substrate layer with a 2.5 μm thickness was produced by thermal oxidation of a silicon wafer. On top of the substrate layer, a SiON waveguiding layer with a refractive index of 1.55 and a thickness of 350 nm was grown using the PECVD process. The rib of the waveguide was structured by standard lithography and reactive ion etching (RIE) with an etch depth of 55 nm. A reference guided layer was branched off in front of the classical design Y-junction of the Mach-Zehnder interferometer in order to compensate for instabilities in the coupling of the light into the waveguide and fluctuations of the source. The protective layer of SiO_2, with a refractive index of 1.46 and a thickness of

50

2 µm, was deposited by the PECVD process on top of the waveguiding layer. The sensing window of the waveguide with an effective length of 12 mm was formed by the RIE process in the SiO_2 protective layer. TE-polarized light of a He-Ne laser with a wavelength of 633 nm was end-fire coupled into the planar waveguide. The immunosensing capability of the interoferometer was tested using antibody/antigen system of anti 2,4-dichlorophenoxyacetic acid IgG/2,4-dichlorophenoxyacetic acid (anti 2,4-D IgG/2,4-D). Determination of 2,4-D at detection limit of 1 µg/ml was achieved with immunoreactions of 10 µg/ml anti 2,4-D IgG.
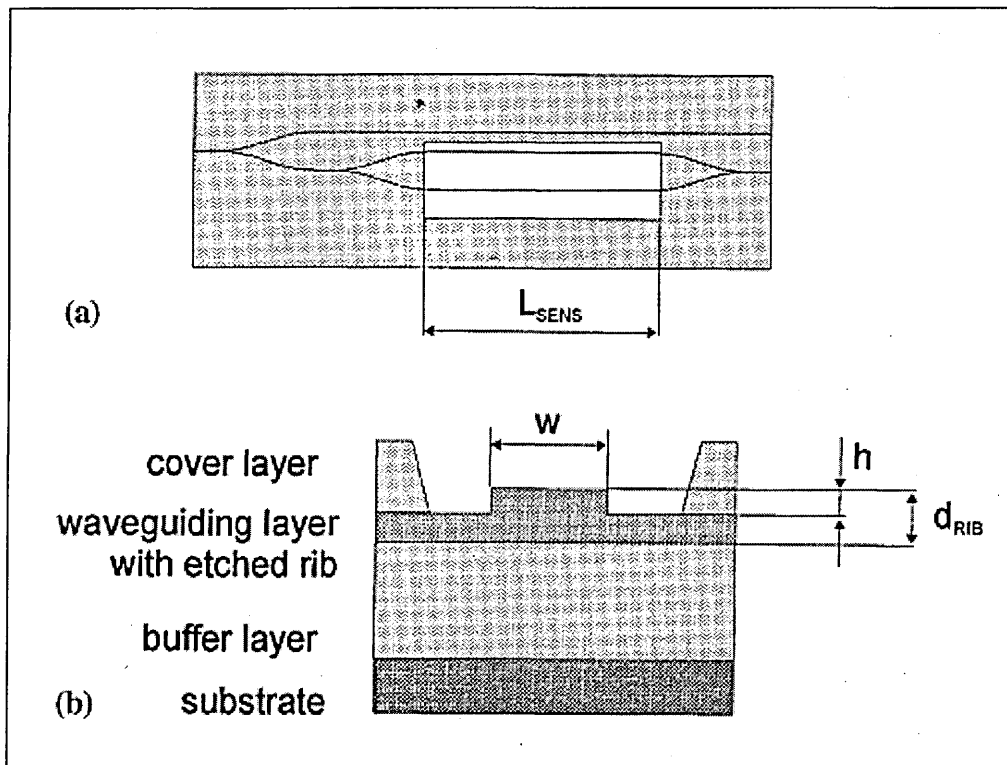
Figure 2.13. SiO_2/SiON waveguide as a Mach-Zehnder interferometer transducer. (a) waveguide layout, L_{sens} = sensitive length of the interferometer; (b) cross section of the waveguide, w = width of the waveguiding rib, h = height of the waveguiding rib, dRIB = thickness of the waveguide under the rib [Brosinger et al, 2002].

The planar Mach-Zehnder interferometer described previously has shown great potential for biosensing applications. However, it has the disadvantage in difficulties of coupling the light into the branches of the waveguide. In addition, microstructuring is required to fabricate the two branches and the Y-junction of the guided layer. In some cases, beam splitters and connectors were necessary to produce two light beams from the same source. Due to this drawback, planar polarization interferometer, which measured the phase difference between the transverse electric (TE_o) and transverse magnetic (TM_o) modes or s- and p-components of the same polarized light, was proposed. The two modes of the polarized light interact differently with the sample on the waveguide sensing surface, which produced a time-dependent phase difference between them. This method makes the light coupling and waveguide fabrication much easier since a wider guided layer is used, and no branches or guided channels are needed.

Stamm and Lukosz had explored such an interferometer based on a SiO_2-TiO_2 waveguide structure as a relative humidity sensor, as a refractometer for liquid samples, and as an affinity- and immunosensor [Stamm and Lukosz, 1993, 1994, 1996; Lukosz et al, 1997]. The SiO_2-TiO_2 waveguiding layer, with a refractive index of 1.75-1.85 and thickness of 140-200 nm, was fabricated by the sol-gel process (at 500 °C and 850 °C) on a 3.6 μm thick SiO_2 substrate layer, which was thermally grown on a 500 μm thick silicon wafer. The waveguiding layer was covered with a 2 μm thick evaporated SiO_2 protective layer to prevent any perturbation of the light beam by a flow cell, which was pressed against the protective layer above the sensing windows.

Polarized light at a wavelength of 632.8 nm was end-coupled into the waveguide and interacted with the sample over a sensitive length of 12-32 mm. The out-

coupled light was interfered with an additional phase change by a half-wave and quarter-wave plate, and was split into four channels using two Wollaston prisms (see Figure 2.14). Time-dependent phase difference of TE_o and TM_o modes were determined from the intensity of the four channels measured by four photodetectors. This polarized interferometer worked well for affinity sensing and immunosensing where an affinity reaction of 0.7 nM biotin with immobilized avidins [Stamm and Lukosz, 1993, 1994] and immunoreactions of 0.33 nM rabbit IgG with immobilized goat anti-rabbit IgG [Stamm and Lukosz, 1996] were clearly detected.
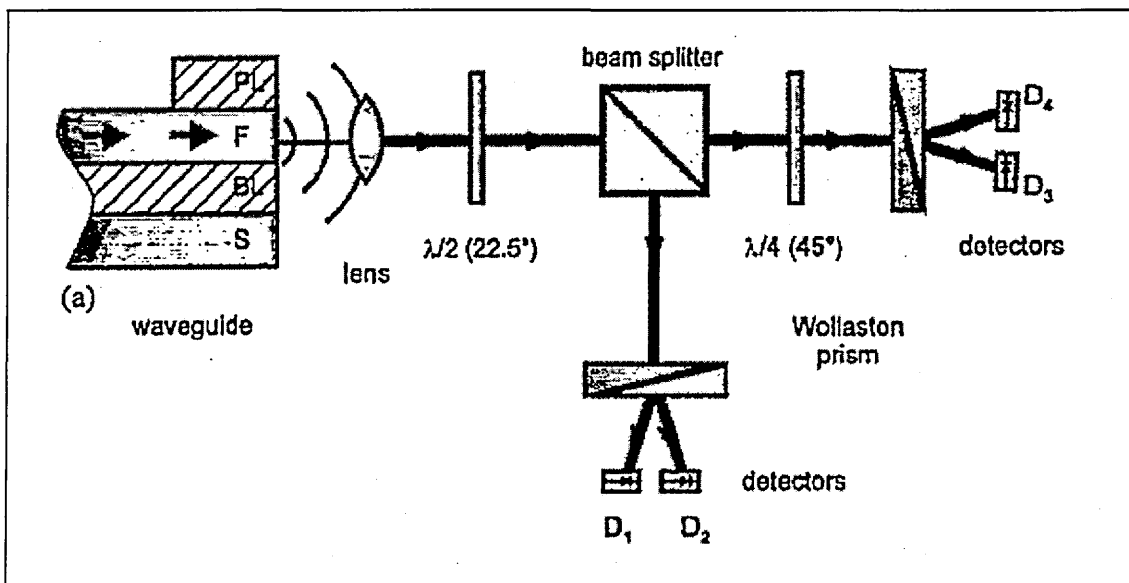
Figure 2.14. Phase measurement methods of a planar polarization interferometer. The outcoupled light is split up into four channels and the phase difference is determined from the intensities measured by detectors D1-D4 [Lukosz et al, 1997].

A polarized interferometer with the same working principle as that used for immunosensing was described by Fattinger et al [1993] and Schlatter et al [1993]. The phase change of the polarized light was measured using the same set-up and method used by Stamm and Lukosz [1993]. However, instead of using Si/SiO_2 as the substrate layer, a planar glass substrate with a refractive index of 1.52 was used as the base of the

waveguide. On top of the glass substrate, an inorganic amorphous TiO_2-SiO_2 waveguiding layer, with a refractive index of 1.8 and a thickness of 230 nm, was fabricated. The waveguiding layer was covered with a 1 μm thick SiO_2 protective layer consists of 12 mm long open area for the interaction of the guided lightwave with the sample. The sensitivity of the interferometer for immunosensing application was tested with different concentrations of anti-human IgG binding to the immobilised human IgG. Detection of very low concentration of anti-human IgG at 0.01 nM was registered.

A polarized interferometer based on Si_3N_4 waveguide structure has also been explored by Shirshov et al [1998, 2001]. The planar waveguide was fabricated on a silicon wafer and has a smaller sensing window of 6 mm length. Figure 2.15 shows the general view of the multilayer waveguide structure and the experimental setup of this interferometer. It consists of a Si_3N_4 waveguiding layer with a thickness of 0.19 μm and refractive index of 2.0, deposited by the LPCVD process on a thermally formed SiO_2 substrate layer with a thickness of 1.2 μm and a refractive index of 1.46. Phosphosilicate glass (PSG) with a thickness of 1.2 μm and a refractive index of 1.51 was used as the protective layer. The waveguide surface area was 10 mm x 12 mm and its edges were cleaved and polished to improve light guiding both in and out without special matching elements (prisms or grating).
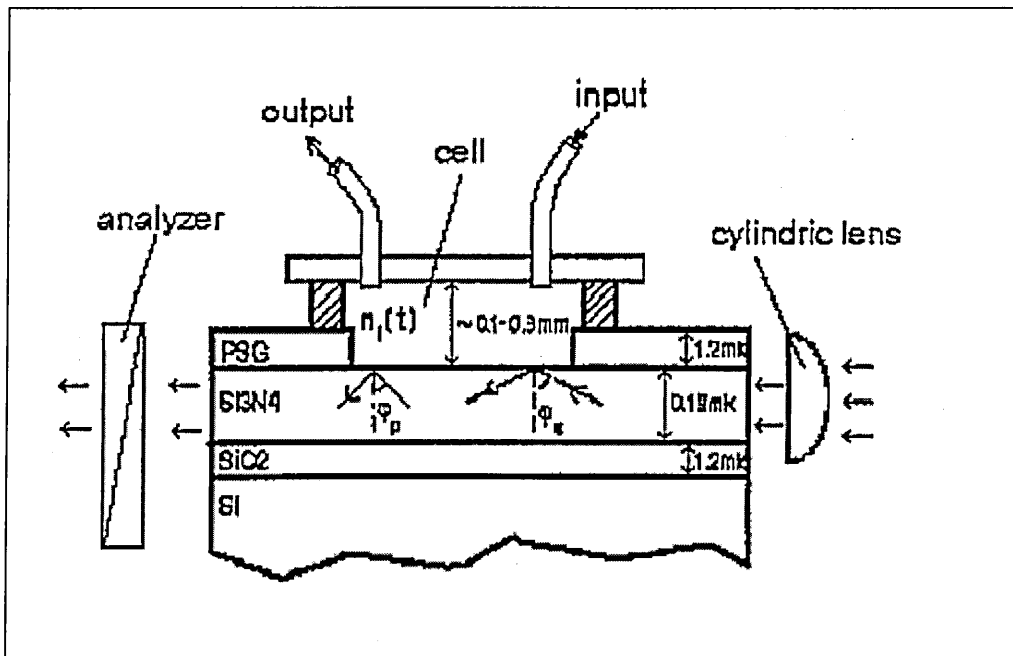
Figure 2.15. A planar polarization interferometer based on SiO_2/Si_3N_4 waveguide structure [Shirshov et al, 1998].

A polarized He-Ne laser beam was focused with a semi-cylindrical lens onto the input face of the waveguide and interacted with the substance studied within the sensing windows. A 0.2 mm thick film serving as a linear polarizer was placed immediately at the light beam output. The output beam was then transmitted to a photomultiplier by a glass optical fibre with an input window of 0.5 mm in diameter, which was pressed against the polarizer at a distance less than 1 mm from the edge of the waveguide. Adsorption studied on the sensing surface shows that proteins such as BSA, mouse anti-IgG and rabbit IgG were strongly held on the Si_3N_4 surface. The polarized interferometer was able to register the response of immunoreactions between mouse IgG and immobilized mouse anti-IgG [Shirshov et al, 1998], and immunoreactions between mouse-antirabbit IgG and immobilized rabbit IgG [Shirshov et al, 2001].

The capability of a polarized interferometer as an immune sensor in comparison to the conventional surface plasmon resonance (SPR) method was also studied by Nabok et al [2000]. A similar device, which was described by Shirshov et al [1998], was used and instead of PSG material, SiO_2 with a thickness of 1.2 μm and a refractive index of 1.46 was used as the covering layer of the waveguide. Different sequences of immobilisation of the immune components (human IgG and human anti-IgG) and their immunoreactions were studied. High sensitivity of the interferometer method in comparison with SPR was observed. A human IgG concentration of 3 ng/ml was registered with the inteferometer while the lowest concentration detected by SPR was 30 ng/ml.

2.3 Polyelectrolyte Self-Assembly Technique for the Formation of Nanocomposite Membranes

The idea of developing a multilayer molecular structure by electrostatic interaction was suggested by Iler [1966], who had constructed multilayer films composed of positively and negatively charged colloidal particles. This pioneering layer-by-layer self-assembly technique was extended to a new preparative method of organised thin films by adsorption of oppositely charged polyelectrolytes. The interest dates back to early 1990s when Gero Decher and coworkers [Decher et al, 1992; Lvov et al, 1993] showed that it was possible to deposit layers of oppositely charged polymers onto substrates with molecular-level control over the resultant multilayer structure. Since then studies on the properties and application of polyelectrolyte multilayers has grown exponentially [Ariga et al, 1997; Decher, 1997; Wu et al, 1998; Onda et al, 1999; Mamedov et al, 2001; Li et al, 2001].

Generally, polyelectrolytes exist in the form of salts, and dissolve in water to dissociate into polymers chains containing ionic groups and counterions. They form as polycations or polyanions solutions, depending upon the charge of the ionic groups. For instance, poly(styrene sulfonate) will form as a polyanions solution due to the presence of a sulfonate group (SO_3^-) in its constituent macromolecules (Figure 2.16). Attraction of different charges between the polycation and polyanion become the driving force for the polymer film formation through the polyelectrolyte self-assembly (PESA) technique [Lvov et al, 1994]. In addition, the electrostatic attraction allows the formation of multilayered films on a substrate surface, simply by sequential dipping of the electrically charged substrate into the polycations and polyanions solutions.

$$O$$

$$SO_3^- \quad Na^+$$

Figure 2.16. Chemical structure of poly(styrene sulfonate).

The four steps basic sequence for the polyelectrolyte layer deposition in the simplest film architectures, (polyanion/polycation)n is illustrated by Figure 2.17. This polyelectrolyte deposition on a glass substrate can be carried out either manually or by an automated device [Okayama et al, 2001]. The process starts by immersing a positively charge glass substrate in a beaker containing a polyanion solution (Step 1). Then it is followed by the rinsing step (Step 2) in deionised water or buffer solution, before dipping the substrate in the polycation solution (Step 3). The important rinsing steps in between two consecutive polyelectrolyte adsorptions are to remove the non-adsorbed (liquid adhering) or weakly adsorbed polymer molecules, which are loosely attached to the preadsorbed polymer layer. The substrate is rinsed again (Step 4), before continuing the dipping sequence in the polyanion solution.

anionic
solution   rinsing   cationic
solution   rinsing

Figure 2.17. A basic sequence of the polyelectrolyte self-assembly technique.

During the first contact of the substrate with the polyanion solution, the substrate surface charge might be sub-compensated, exactly compensated or overcompensated by the electrical charges of the adsorbed polyanion (Figure 2.18) [Decher et al, 1994]. The initial adsorption mechanism of the polyanion chains is relatively fast and may be completed within a few seconds. As shown in Figure 2.19(a), the polyanion chains start to become anchored on the substrate surface due to electrostatic attraction between the polymer ionic groups and the positively charged adsorption sites on the substrate surface. The remaining adsorption sites are filled during the second stage of the process. This involves the adjustment and penetration of other polyanion chains between the anchored ones, and this process requires a longer time, usually up to 20 minutes [Lvov et al, 1993]. The successful deposition of the next polyelectrolyte layer requires that the adsorbed electrical charges overcompensate for the initial electrical charge of the substrate (Figure 2.19(b)).

overcompensation

compensation

sub-compensation
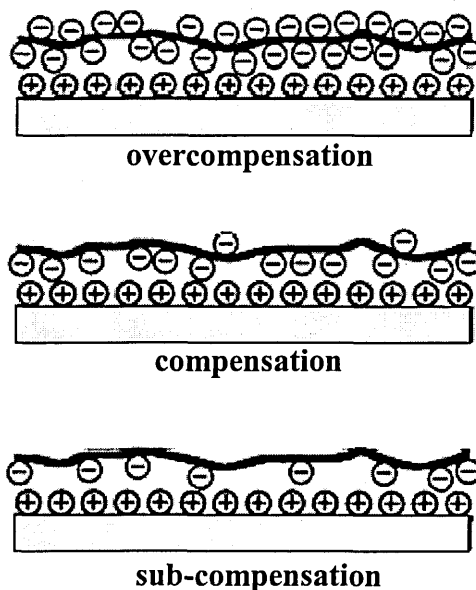
Figure 2.18. Three different types of adsorption of a single polymer layer on a substrate surface [after Decher et al, 1994].
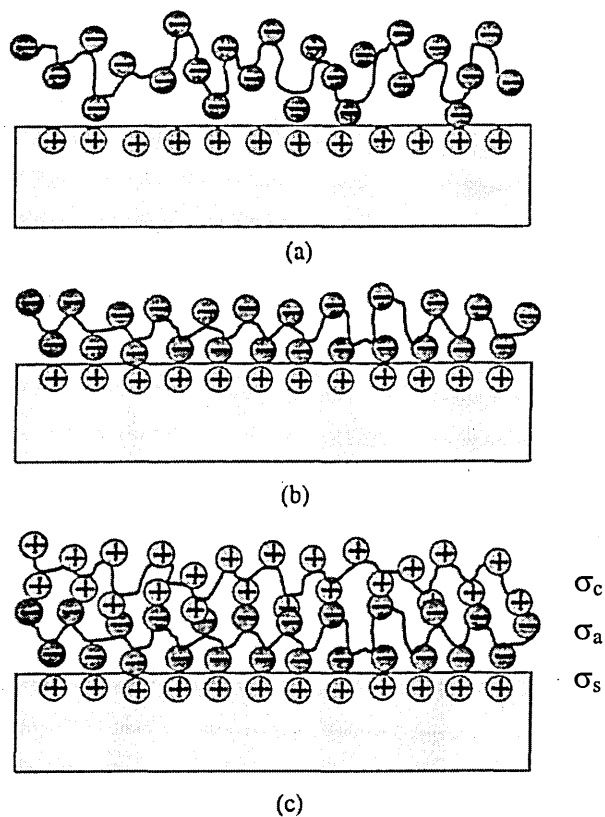
Figure 2.19. Layer-by-layer polyelectrolyte deposition. (a) Anchoring the first polyanion layer on a positively charged surface. (b) Stabilized adsorption of the polyanion layer. (c) Stabilized adsorption of the polycation layer.

Let σ_a^- and σ_s^+ represent the surface charge densities of the polyanion and the substrate, respectively. Generally, the overcompensation condition can be written in the form

$$\sigma_a^- = 2\sigma_s^+ \tag{2.19}$$

In this case, half of σ_a^- is used to compensate for σ_s^+, and the other remaining half of σ_a^- will be available for binding the next polycation layer. Similar processes of anchoring and stabilization occur during adsorption of the polycation layer on top of a polyanion layer. Figure 2.19(c) shows the resulting polyanion/polycation bilayer

regarded as a basic repeated unit of multilayered PESA films. If σ_c^+ denotes the surface charge density of the polycation, the overcompensation of charges in the polyelectrolyte bilayer must satisfy the condition

$$\sigma_c^+ = \sigma_a^- \tag{2.20}$$

The above condition describes the intrinsic type of charge compensation for the existence of multilayers, and can be achieved by using a strongly charged polyelectrolyte pair, such as poly(styrene sulfonate) and poly-2-vinylpyridine [Hoogeveen et al, 1996] during PESA deposition.

Based on the above deposition scheme, the PESA technique is free of some problems typical to other popular wet processes such as conventional spin coating or Langmuir-Blodget (LB) methods, in developing of thin composite films. Spin coating is a very simple and fast technique, which forms ultra thin films by dispercing solutions onto rotating substrates. However, the spin coating technique cannot control the molecular order and the thickness of the films. In the case of the LB technique, ultrathin films are formed by transferring a monolayer of ordered amphilic molecules from the water surface onto a solid substrate. The LB technique has high accuracy in controlling the film thickness; however, it needs special instrumentation called an LB trough with mobile barriers and a Wihelmy balance, to control the surface pressure of the amphiphilic monolayer on the water surface. In addition, the materials suitable for the LB preparation are usually limited to water insoluble with high purity and surfactant-like properties [Ariga et al, 1997].

In contrast, the PESA technique allows the fabrication of well defined layer-by-layer structures of ultrathin films, without requiring complicated and expensive equipment. The adsorption processes are independent of the substrate size and topology. The PESA technique also does not require a very high purity of the solution to have a satisfactory multilayer deposition [Lvov and Decher, 1994]. However, the layers in PESA films are found to be less ordered than those in LB films [Lvov and Decher, 1994]. Nevertheless, the films are chemically and thermally stable [Lvov et al, 1993; Decher et al, 1992] because of strong electrostatic interaction between the polymer layers and the substrate. Furthermore, the PESA technique is not only limited to a large variety of water-soluble polyions, but also can employ other types of charged macromolecules such as organic dyes and proteins, which can be assembled alternately with the oppositely-charged polyions.

Multilayer films composed of polyion/organic dye molecule bilayers were assembled on a quartz slide and quartz crystal microbalance (QCM) using the PESA method by Ariga et al (1997). Prior to the deposition, the substrates were washed with alkaline alcohol solution in an ultrasonic bath to generate anionic charges on their surface. Several organic dyes with different molecular sizes namely congo red (CR), tetraphenylporphine-tetrasulfonic acid (TPPS), acid red 26 (AR26), acid red 27 (AR27), ponceau S and indigo carmine (IC) were used in the experiment. Most of the organic dyes have a negative surface charge from their $SO_3^-Na^+$ groups, and were successfully alternated with polycation poly(diallydimethylammonium chloride) (PDDA).

The in-situ QCM measurement revealed that the dyes adsorbed from their high-concentration solutions, tend to be desorbed in the subsequent step, especially in the case of higher polyion concentrations. For example, a mass decrease was observed for

the TPPS-PDDA film at 10 mM TPPS and 19 mM PDDA. Contamination of polyion solutions might cause formation of ion complexes in the solution, which makes it difficult to conduct multilayer self-assembly by alternate immersions. Constant film growth was observed at lower concentrations, such as for CR/PDDA film at 1.0 mM CR and 1.9 mM PDDA, and for the TPPS-PDDA film at 1.0 mM TPPS and 1.9 mM PDDA. In general, most of the dyes can be assembled alternately with the oppositely charged polyions at the lower concentration.

The thicknesses of dye layer were found in the range of 5 to 34 Å, which were defined by the size, shape and the number of charges in the dye molecule. Obviously, large molecules cause larger film growth than small molecules, such as 12 Å for CR (MW 697) and 9 Å for IC (MW 466) which have an identical shape and number of charges. Difference in the number of charges may also affect the layer growth of the dye, as in the case of AR26 and AR27, which have an identical size and shape. The third sulfonate (SO_3^-) group at the left side in the AR27 produced a different mode of interaction with the polycation surface that gave a larger film growth (10 Å) than the AR26 layer (7 Å). This estimation of the thickness of the absorbed dye, such as for CR/PDDA bilayer (22 Å), coincides with the ellipsometric data of a related layer of CR/poly(L-lysine) reported by Cooper et al (1995).

Cooper et al (1995) studied the formation of multilayer films by alternately assembling the cationic polypeptide poly(L-lysine) with rod-shaped CR dye or plate-shape copper phthalocyanine tetrasulfonic acid sodium salt (CPTA), on a glass slide substrate. The films were characterised with different optical techniques such as UV-visible absorption spectra and ellisopmetry. Low concentration of poly(L-lysine) about 2 mg/mL and organic dye about 1 mg/ml (1.43 mM for CR and 1.085 mM for CPTA)

were used for the deposition. Varying the concentration of the dye (0.1, 0.5, 1.0 and 1.5 mg/ml) and the dipping time from 1 to 300 min, did not show significant variation in absorbance spectra (absorbance at 680 nm = 0.0455 ± 0.0015). The ellipsometry measurement showed the estimated average bilayer thickness of poly($_L$-lysine)/CPTA and poly($_L$-lysine)/CR was 19 Å and 22 Å, respectively. Differences in the film growth between the organic dyes was probably due to CPTA (MW 921 with four sulfonate groups) tended to form H-aggregates to allow two sulfonate groups to be located in the upper and lower faces of CPTA layer, and satisfied the mechanism of the alternate adsorption. The results suggested that the adsorption of the dye layer reached saturation very rapidly and the dye molecules tended to form certain orientation during the adsorption process.

The PESA technique was also demonstrated to have a unique ability to incorporate several types of biomolecules such as enzymes [Lvov et al, 1995; Nabok et al, 2000], antibodies [Caruso et al, 1997] and DNA [Decher et al, 1994] into the polymer matrix. These biomolecules are ideal for PESA deposition because of their natural electric charge can be controlled by the pH of a buffer solution beyond the isoelectric point of the biomolecules. This technique provides a very natural environment for the biomolecules because the immobilization process was performed in a mild condition, and did not involve any modification of the biomolecules structures.

A multifunctional composite film can easily be formed with the PESA method, since it is possible to incorporate active biomolecules and chromophores molecules with transducing characteristics into the same polymer matrix. This composite PESA film can serve as a sensing membrane, combining functions of molecular recognition and transduction, which is suitable for enzyme or immune sensors. For instance, composite

films containing enzymes urease and cholinesterase, and respective indicators, cyclotetrachromotropylene (CTCT) and Thymol Blue was successfully deposited on glass substrate using the PESA method [Nabok et al, 2000]. Biosensing characteristics of the sensing membranes were studied using the UV-visible spectroscopy technique. The membranes were hydrophilic and permeable for small analyte molecules, which allowed biosensing activity, such as the registration of the enzyme reaction and inhibition, by the optical measurement.

2.4 Summary

This chapter contains a comprehensive review of enzyme sensors developed for water analysis. The principles of detection of pesticides and heavy metal ions using the inhibition of cholinesterase enzyme and urease, respectively, were explained in detail. The enzyme sensors based upon electrochemical approaches (particularly amperometric technique) were more sensitive than the optical method previously exploited. Consequently, the majority of enzyme sensors and sensor arrays were based on the electrochemical principles.

The design and implementation of planar optical waveguides for biosensing were also described in detail. The theory of multiple internal reflections was revised, and its application in several types of waveguide structures as ATR, TIRF and interferometer biosensors was reviewed. The ATR sensors were found to be more versatile, but its sensitivity especially towards the affinity reaction was substantially lower than that in other biosensors. One factor that allowed the TIRF or interferometer sensors to achieve high sensitivity was the use of specially designed planar optical waveguides, such as $SiO_2/SiON$ or SiO_2/Si_3N_4, having a thinner waveguiding layer than that in the macroscopic glass slide structures.

Finally, detailed descriptions on a universal deposition method namely polyelectrolyte self-assembly (PESA) technique was given. The theory and the application of the PESA method to form multi-function sensing membranes was reviewed. The PESA method proved to be suitable for the formation of composite membranes for optical enzyme sensors.

CHAPTER 3

CONSTRUCTION AND CHARACTERISATION OF

THE SINGLE CHANNEL ENZYME SENSOR

3.1   Optical Devices of the Planar Waveguide Enzyme Sensor

3.1.1   Planar waveguide transducer

The main idea of the proposed optical biosensor lies in multiple reflections of the light beam in the SiO_2/Si_3N_4 planar waveguide having a large difference in the refractive indices of the core and cladding. This waveguide, shown schematically in Figure 3.1, was provided by Prof. Yuri M. Shirshov from the Institute of Semiconductor Physics of the National Academy of Sciences of Ukraine. It was produced by standard silicon planar technology, where the Si_3N_4 waveguiding core layer of 0.19 μm thickness was deposited by LPCVD process on a thermally formed SiO_2 substrate layer with a thickness of 1.5 μm. The Si_3N_4 layer was covered with another 1.5 μm thick SiO_2 layer using the PECVD process. The refractive indices are typically 1.46 and 2.0 for SiO_2 and Si_3N_4 layers, respectively. The above parameters for core and cladding layers were chosen to provide a single mode light propagation [Shirshov et al, 1998], and this condition can be confirmed by using equation 2.11, where M = 1 at $\lambda = 635$ nm.

Ambient *ri4*

— L = 4 mm —

Membrane (nf, *df)* SiO_2

(1.5 pm)

Figure 3.1. Schematic diagram of light propagation through the planar waveguide.

A sensing window of 4 mm x 6 mm, formed in the central area of the top SiO_2 layer using a photolithography and wet etching (with hydrofluoric acid) technique, has exposed the surface of the Si_3N_4 layer to the environment. Due to the etching process, the Si_3N_4 surface became positively charged because of the presence of $Si-NH_2$ groups. The polarity of this surface was further enhanced by refreshing it with 5 % diluted hydrofluoric acid. This positive charge was required for the PESA technique to start the deposition of the sensing membrane with a compound, which had a negative surface charge. The Si_3N_4 surface was first deposited with the organic dye, namely cyclotetrachromotropylene. Details on this compound and the formation of the sensing membrane are explained in Section 3.2.

3.1.2   Experimental set-up for a single channel enzyme sensor

The effect of single enzyme reactions on light intensity, as well as the process of polyelectrolyte deposition, was studied in-*situ* using an optical experimental set-up, shown schematically in Figure 3.2. A diode laser (Coherent 31-0110) with a wavelength of 635 nm was used as a light source to produce an elliptical beam with the length and width of 5.6 mm and 1.5 mm, respectively. Then, a semi-cylindrical lens was used to focus the beam into a narrow horizontal line with a thickness of about 0.5 mm on the edge of the Si_3N_4 planar waveguide. A reaction cell having a volume of 0.2 cm^3 was tightly sealed with a square shape rubber frame, and was placed on top of the planar waveguide (see Figure 3.3). The rubber seal had a 6 x 8 mm square opening in the middle to avoid any contact with the surface of the waveguide window.
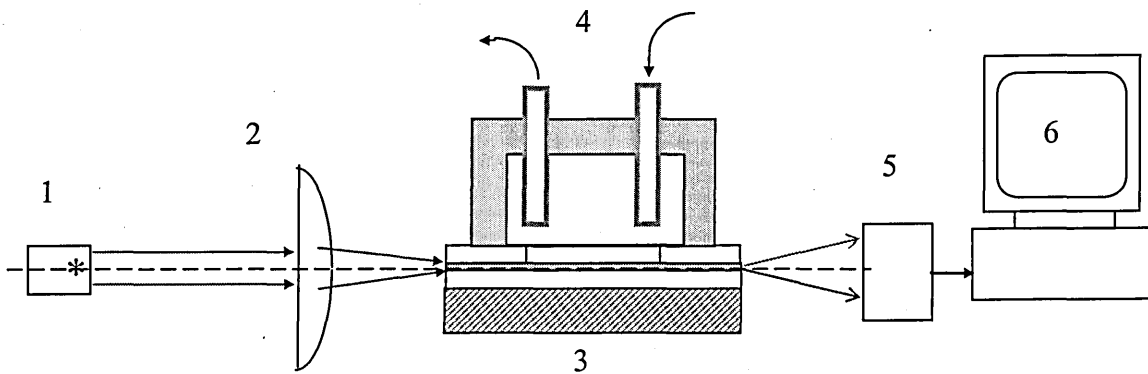
Figure 3.2. Schematic diagram of the planar waveguide experimental set-up. (1) HeNe laser source, (2) cylindrical lens, (3) the planar waveguide, (4) reaction cell with inlet and outlet, (5) optical power meter, (6) interfaced to the PC.
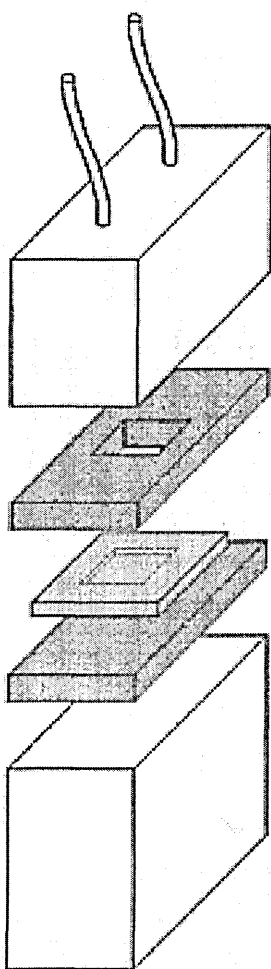
Figure 3.3. Expanded diagram of the reaction cell showing rubber seals (dark grey) and planar waveguide (light grey).

Coupling of the beam into the Si_3N_4 waveguiding layer was achieved by adjusting the position of the waveguide with a three-directional micropositioner. A photodetector (Anritsu Model MA9411A) of an optical powermeter, with an active area of 9.5 mm in diameter was placed immediately after the output end of the waveguide. The photodetector was able to capture light within the wavelength range of 0.38 μm to 1.15 μm and within the power range of 0.01 nW to 10 mW. The optical power meter (Anritsu Model ML9001A) was connected to a PC via a GPIB card.

The end-fire coupling approach caused large loses to the output light intensity due to the irregular surface of the waveguide edge. Light was reflected out more than being coupled into the waveguide at the desired incidence angle. The light intensity was dropped from 2 mW down to the range of 300 – 700 nW. The end-fire coupling was not the best method to couple the light into the waveguide as compared to the prism or grating method reviewed in Chapter 2. Nevertheless, a quite high density of light scattered within the waveguide sensing windows was observed, as shown in Figure 3.4. The intensity of light propagating in the Si_3N_4 planar waveguide was found to be adequate for the registration of some specific bio-chemical reactions, within the deposited nanocomposite membrane on the sensing window.

Figure 3.4. Picture shows amounts of light propagating under the sensing windows of the Si_3N_4 planar waveguide.

3.2 The Formations of Nanocomposite Membrane using PESA Technique

3.2.1 Materials

The polymer namely poly(allylamine hydrochloride) (PAH), was used as a polycation for PESA deposition. PAH is a pH-dependent charged compound, and it is fully ionized at a pH lower than 7.0 [Mendelsohn et al, 2000]. This compound, purchased from Aldrich, has a positive surface charge, derived from NH_3^+ groups in its structural formula, as shown in Figure 3.5. The advantage of using PAH was that its charge is located at the far end of the side chain, which was easily accessible for the compensation by other ionic molecules. The molecular weight of PAH was about 70000 g/mole. It has a pH of 4.37 when diluted to 10^{-5} M concentration in an ultrapure water. The ultrapure water was obtained by reversed osmosis using RiOs^{TM} Water Purification Systems followed by ion exchange and filtration steps using Super-Q^{TM} Plus Water Purification Systems. The concentration of PAH used for the deposition was 2 mg/ml (2.857×10^{-5} M). This concentration was considered to be appropriate to provide enough charge for PESA deposition, as demonstrated by Lvov et al [1995]. Furthermore, a high concentration of the polyelectrolyte caused desorption of the other macromolecules, such as organic dyes [Ariga et al, 1997] (as discussed in Chapter 2.3).

Cyclotetrachromotropylene (CTCT) was chosen as an organic indicator for the enzyme sensor because of its ability to change the absorption spectrum in a wide pH range between pH 3 to 13 [Poh and Lim, 1990]. As shown in Figure 3.6, the boat-like three-dimensional conformation with four $SO_3^-Na^+$ groups provided negative surface

$$-(CH_2-CH)_{\overline{n}}$$
$$|$$
$$CH_2$$
$$|$$
$$NH_3^+ \ Cl^-$$
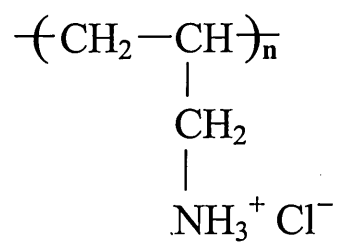
Figure 3.5. Chemical structure of poly(allylamine hydrochloride) (PAH).
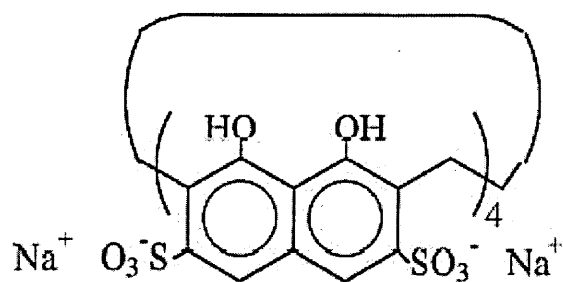
Figure 3.6. Chemical structure of Cyclotetrachromotropylene (CTCT).

charges suitable for the PESA deposition. CTCT was synthesised in house by the reaction of chromotropic acid disodium salt solution with an excess amount of formaldehyde (1:5) in a stoppered flask for a week [Poh et al, 1989]. After evaporation of the water from the dark red aqueous solution, CTCT in the form of a dark red plastic-like substance was obtained. This organic indicator decomposed at above 400°C, and it was soluble in water. The cyclic tetrameric structure afforded the ability to form complexes with some metal ions [Poh et al, 1990], aromatic hydrocarbons [Poh and Koay, 1990], amines [Poh and Lim, 1990], amino acids [Poh and Tan, 1994] and pesticides [Poh et al, 1993]. However, this complexation occurred only if the mixture was in 1:1 stoichiometry ratio.

It was reported that CTCT showed an absorption band at λ_{max} = 540 nm with a shoulder at 570 nm in the visible range [Poh et al 1989]. The molecule turned green in alkaline solution, and λ_{max} then shifted to 640 nm. This change was due to the deprotonation of CTCT compound, and its original red colour was restored in an acidic solution. The molecular weight of CTCT is 1497.048 g/mole and the pH was 4.41 when diluted to 10^{-4} M in ultrapure water. The concentration of CTCT used for the sensing membrane development was 1 mg/ml, which was equivalent to 6.6798×10^{-4} M. A similar concentration of CTCT was used by Nabok et al [2000] to prepare a multilayer PAH/CTCT membrane by alternate dipping of a glass slide in the CTCT and PAH solutions.

Three types of enzymes were tested as sensitive elements in the nanocomposite membrane. These materials were urease from jack beans, acetylcholine esterase (AChE) from electric eel and butyrylcholine esterase (BChE) from horse serum, which were purchased from Sigma-Aldrich. Enzyme molecules were known to have both negatively

charged carboxylic acid groups and positively charged amino groups in their structure. The electrostatic balance between these groups depended on the pH of the buffer solution in which the enzyme was kept. The enzyme molecule was electrically neutral at the isoelectric point, where the electrostatic balance was achieved. In this study, the enzymes urease and AChE had their isoelectric point about pH 5, while the isoelectric point of BChE was pH 7. Therefore, these solutes were dissolved in Trizmabase-HCl buffer solutions at pH 8.3 to make them negatively charged. This was necessary for the PESA deposition on the positively charged PAH layer.

The concentration for each enzyme was chosen to be 100 units, equivalent to 0.3-7 mg/ml. The particular choice depended on their activity as shown in Table 3.1. Generally, one unit of enzyme was sufficient to catalyse 1 μmole of the respective substratum per minute under standard conditions. According to the experimental results of Lvov et al [1995], the amount of enzyme deposited on the polyelectrolyte layer was about 5 to 10 % of the enzyme concentration in solution. Therefore, it is assumed that 5 to 10 units of the selected enzymes can be successfully deposited on the PAH layer, which is an adequate quantity to perform the enzyme reaction. Figure 3.7 shows the reactions catalysed by these enzymes. Obviously, pH changes will occur due to the production of acidic or alkaline compounds during the enzyme reaction. The concentrations of the substrata used were as follows: 100 mM urea for Urease reaction; 10 mM of butyrylcholine chloride for BChE reaction; and 10 mM of acetylcholine chloride for AChE reaction. All substrata were dissolved in Trizmabase-HCl buffer solutions at pH 7.

Table 3.1. Concentration of enzymes equivalent to 100 units activity.

Enzymes	Activity (units/mg)	Concentration (mg/ml)
Urease	54.3	1.84
AChE	301	0.33
BChE	13	7.69

$$urea \ + \ water \ \xrightarrow{\ Urease\ } \ carbon \ dioxide \ + \ ammonia$$

(a)

$$acetylcholine \ + \ water \ \xrightarrow{\ AChE\ } \ choline \ + \ acetic \ acid$$

(b)

$$butyrylcholine \ + \ water \ \xrightarrow{\ BChE\ } \ choline \ + \ butyryl \ acid$$

(c)
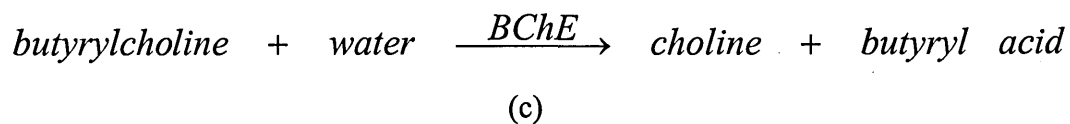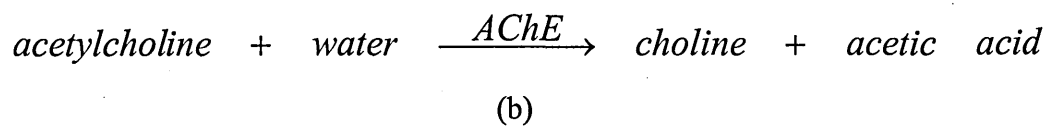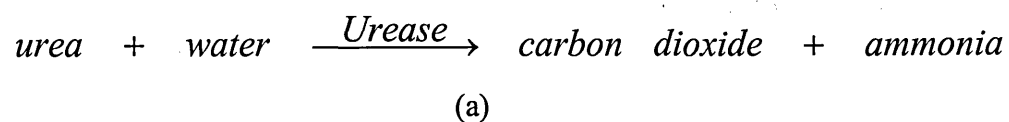
Figure 3.7. Reaction catalysed by the selected enzyme.

3.2.2 PESA set-up and deposition process

Fully computer controlled, experimental set-up for polyelectrolyte self-assembly deposition has been previously designed and built in-house [Nabok et al, 1999]. A block-diagram of the set-up is shown in Figure 3.8. It consisted of a rotated plastic disc and a dipping mechanism driven by a stepper-motor. The sample, i.e. a glass slide was clamped in a holder at the arm of the dipping mechanism. Two beakers containing polycation and polyanion solutions were placed onto the rotated plastic disc alternated with two beakers of ultrapure water.

A computer program was written in BASIC to control the PESA set-up to perform the following coating procedure. The sample was immersed into a beaker containing polyelectrolyte solution typically for 10 to 20 min at room temperature, by moving down the arm of the dipping mechanism. Next, the sample was withdrawn from the solution and the disc was rotated by 90° to position the sample above the beaker of water. Then the sample was rinsed four times by dipping in ultrapure water. The disc was rotated by 90° again to position the sample above the beaker of another polyelectrolyte or organic dye solution. The procedure stopped after the required numbers of cycles were completed.

The characterisation of the nanocomposite membrane developed in this study was performed using a UV-visible spectroscopy technique as well as the planar waveguide set-up. Microscopic glass slides were used for the measurement of the UV-visible absorption spectra of the PESA membrane. They were cut into small 9 x 50 mm^2 rectangular shapes to fit into a 10 x 10 x 45 mm^3 cuvette. Prior to membrane deposition, the surface of the glass slide was modified to enhance their negative charge
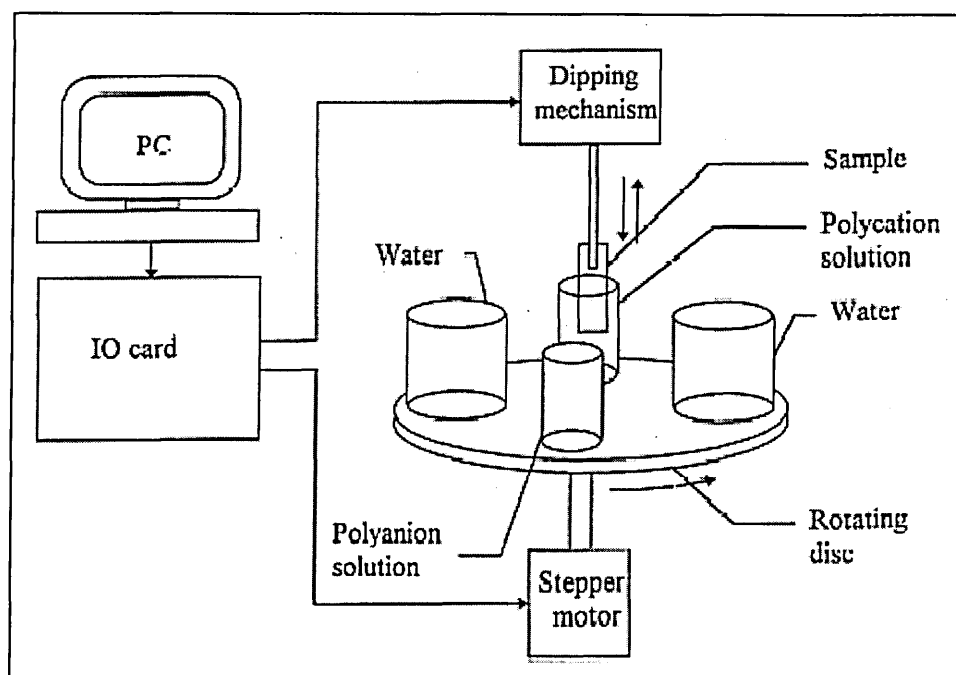
Figure 3.8. A block-diagram of the experimental set-up for polyelectrolyte self-assembly film deposition [after Nabok et al, 1999].

using an ultra sonic bath containing a mixture of 1 % of potassium hydroxide (KOH), 60 % of ethanol and 39 % of water, for 30 minutes at 60 °C [Lvov et al, 1997]. On the surface of soda-lime glass, there exist molecular groups linked to silicon, such as (-Si-O-Si-), (-Si-OH) and (-Si-O-Na-). The treatment tended to increase the concentration of OH⁻ ions on the glass surface by producing more silanol groups (-Si-OH) in the silica network.

The membrane deposition on the glass slide was entirely performed using the PESA set-up. The deposition routine of the PAH/CTCT membrane began with the formation of PAH and CTCT layers by prolonged soaking of the glass slide for 20 min each in the compound solution. Then, the process was followed by the sequential dipping in solutions of PAH and CTCT for 10 minutes. Intermediate rinsing in ultrapure water for about 1 minute was carried out after each dipping of the glass slide. In the case of the planar waveguide, the deposition routine was the same but started with the deposition of CTCT, since the surface of silicon nitride in the sensing window was made positively charged. Apart from using the PESA set-up, the membrane deposition on the planar waveguide was also performed in-situ using the planar waveguide set-up. The enzyme layers were then transferred onto the top surface of either glass/(PAH/CTCT)$_n$/PAH or Si$_3$N$_4$/(CTCT/PAH)$_m$ structures and finally covered with PAH layers. The results of both membrane structures are shown in Figure 3.9.

PAH

Enzyme

PAH

CTCT

PAH

Glass slide

(a)

PAH

Enzyme

PAH

$>$ x m

CTCT

Si_3N_4 planar waveguide

(b)
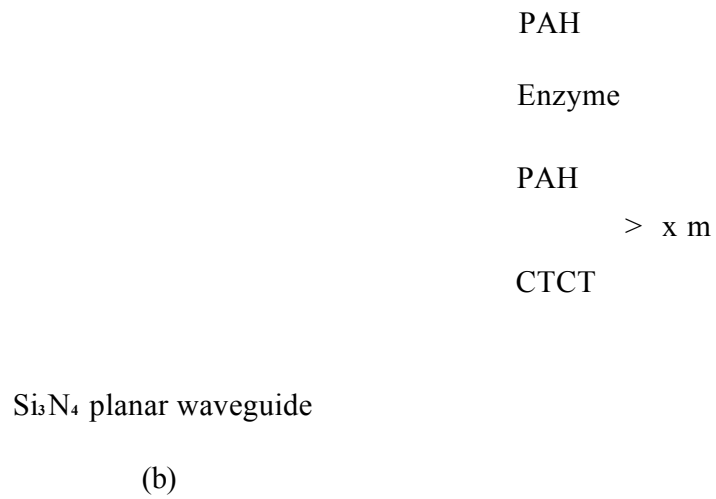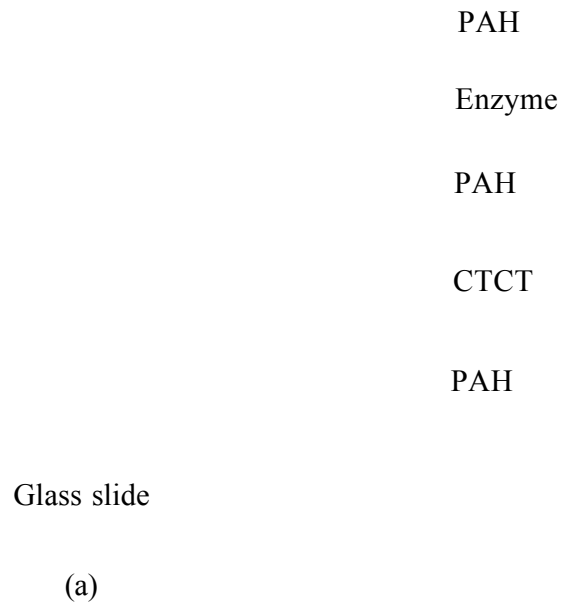
Figure 3.9. Nanocomposite membrane structure, (a) on the glass slide, and (b) on the Si_3N_4 surface of the planar waveguide.

3.3 Characterisation of the Nanocomposite Membrane

3.3.1 Monitoring of CTCT/PAH membrane deposition

Changes in the output signal intensity and UV-visible absorption spectra were observed when different numbers of CTCT layers were deposited on the planar waveguide and microscopic glass slides, respectively. The UV-visible absorption spectra of the CTCT/PAH membrane in Figure 3.10 shows a non linear dependence of the absorbance on the number of layers. A value of the normalised attenuation ratio $\frac{\Delta I}{I_o} = 4.3 \times 10^{-4}$ per layer was found for relatively thin PESA films containing 16 layers or less. The Beer's law absorption coefficient for the CTCT/PAH bilayer was determined to be $5.7 \times 10^5 \, m^{-1}$.

In-situ monitoring of CTCT/PAH membranes deposition on a planar waveguide was carried out using the optical experimental arrangement as described earlier. The adsorption kinetics of this process is shown in Figure 3.11. The output signal intensity decreased substantially after each layer of CTCT was deposited. The deposition of the PAH transparent layers had no influence on the light propagation. The attenuation of the initial light intensity by a factor of 10 was observed after four CTCT/PAH layers were deposited, and the normalised attenuation ratio $\frac{\Delta I}{I_o}$ was found to be 0.4 per layer. This large optical attenuation, which was 3 orders of magnitude greater than in the UV-visible spectroscopy, was primarily due to multiple reflections taking place at the interface between the core and the cladding of the waveguide.

0.25

0.2   0.01

                                     0.001   :

                                  0.0001

            24   16   24   32
                                          number of layers

0.05

      300   400   500   600   700   800
                      Wavelength (nm)
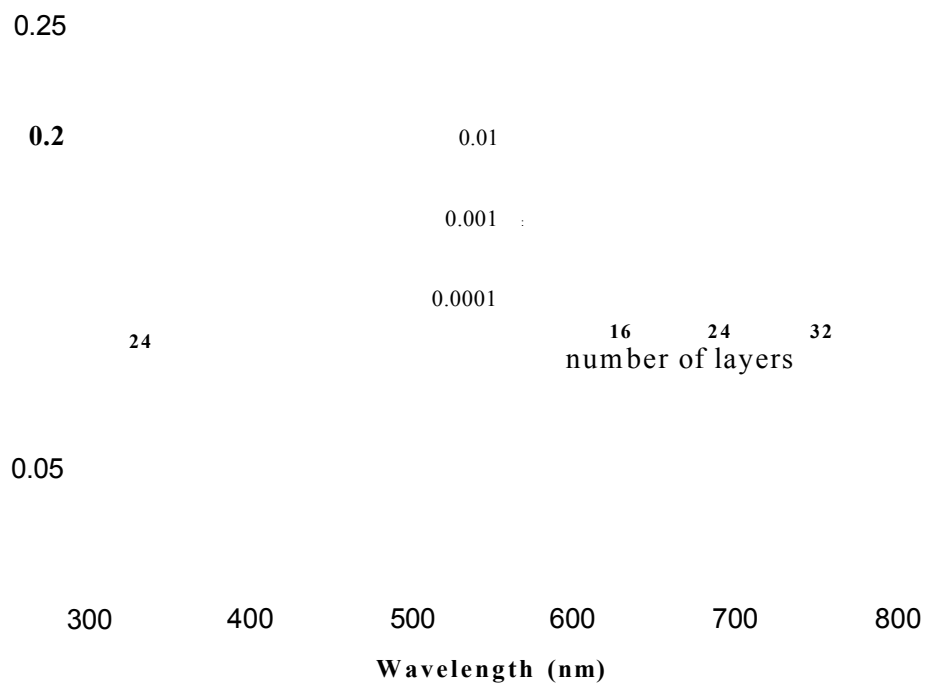
Figure 3.10. UV-vis absorption spectra of PAH/CTCT membrane. Number of layers is shown near respective curves. The inset shows the dependence of the absorbance at 635 nm on the number of layers.
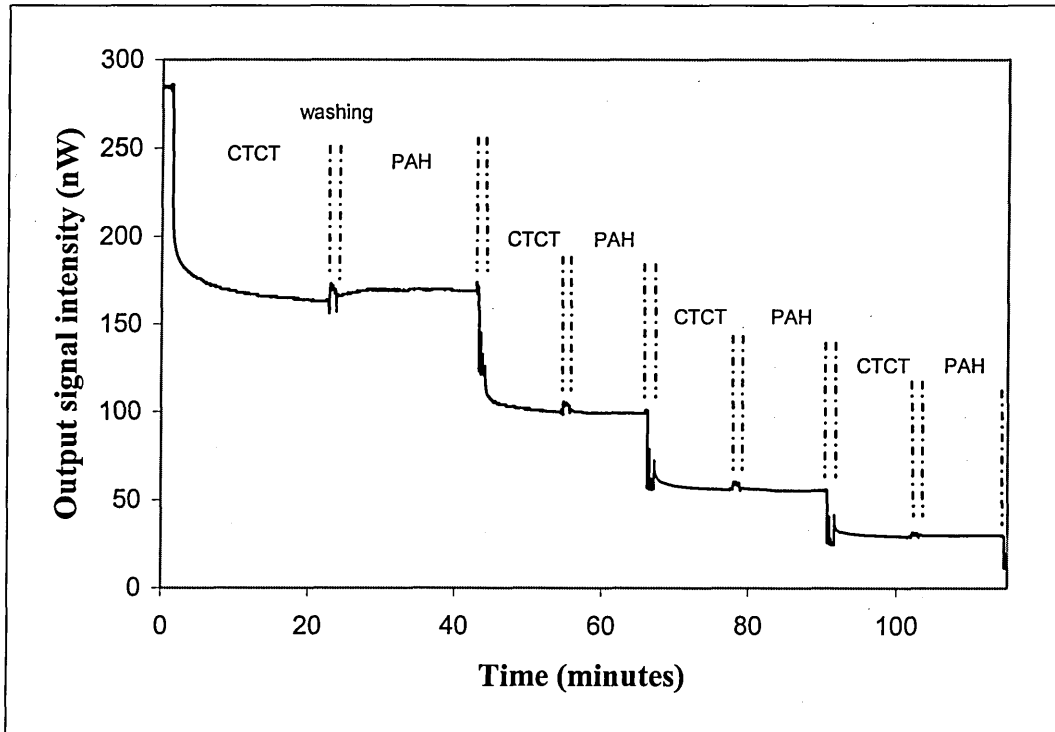
Figure 3.11. *In-situ* monitoring of the CTCT/PAH deposition onto the planar waveguide. Time intervals for the CTCT and the PAH adsorption steps and washing are shown

The number of reflections N at the interface was determined using equation (2.16). The self-consistent solution of equations (2.12) and (2.13) gave the values of θ_m $\approx 72.8^{\circ}$ for the single mode propagation. Based on this incidence angle, the interaction length was calculated to be 2 nm using equation (2.18). Therefore, the number of reflections at the interface of the sensing windows was equal to 670. This value is 15 times lower than that theoretically predicted by equation (2.10). Nevertheless, these calculations showed that the sensitivity of the Si_3N_4 waveguide was greater than that of the SiON waveguide [Walker et al, 1993; Plowman et al, 1998] by a factor of three. Thus, the potential of Si_3N_4 waveguides as the optical transducers to achieve much improved sensitivity in the ATR technique was demonstrated.

3.3.2   The effect of pH on the CTCT/PAH membrane

The functioning of the CTCT/PAH membrane as an indicator was investigated with both planar waveguide and UV-visible spectroscopy measurements in buffer solutions of different pH. A set of typical responses of the planar waveguide coating with the CTCT/PAH membrane, on exposure to different pH solution is shown in Figure 3.12. It is seen that the output signal intensity was increased by the pH of less than 5.5 of pure water. However, the signal intensity was diminished by high pH. These results agree with those obtained from the UV-visible absorption spectra of Figure 3.13. The absorbance of light by the membrane was increased in alkali solutions, while it was decreased in acidic solutions.
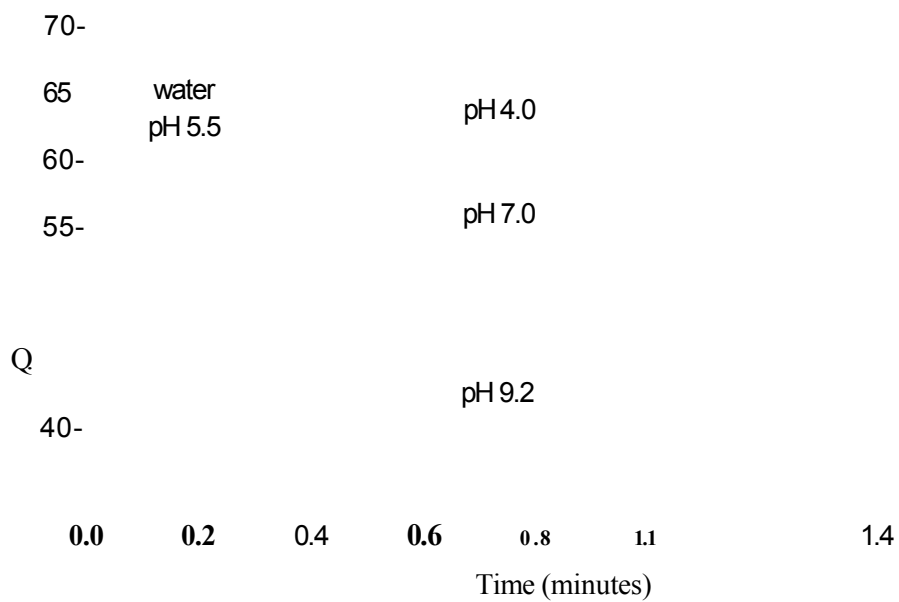
Figure 3.12. The effect of pH on the planar waveguide coated with CTCT/PAH membrane.

0.09 i
0.08 -
0.07 -
0.06 -
§ 0.05
-Q

XI
< 0.03
0.02 .
0.01 .

0.02
0.015 -
0.01 -

pH 9.2   M
pH 7.0
water (pH 5.5)
pH 4.0

600   610   620   630   640   650

350   450   550   650   750   850

Wavelength (nm)
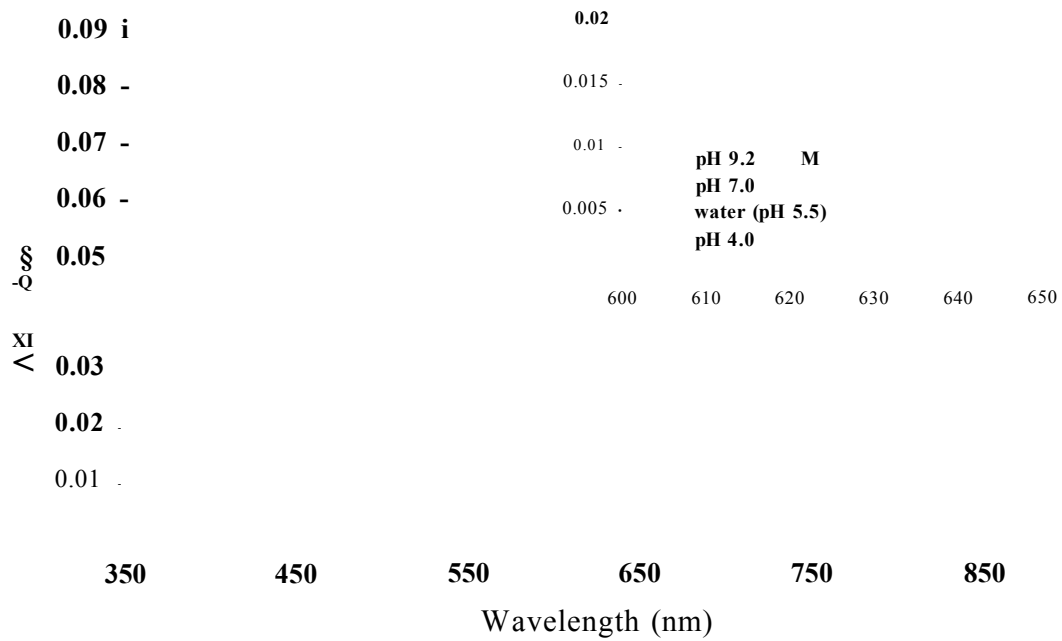
Figure 3.13. The effect of pH on UV-visible absorption spectra of CTCT/PAH membrane.

As pointed out earlier, the observed spectral changes were caused by deprotonation of CTCT molecules showing an improved response of this composite organic indicator for high pH. The fact that the planar waveguide method was more sensitive to pH changes than the UV-visible spectroscopy technique is apparent. This result also suggested that the planar waveguide arrangement was capable of registering the occurrence of pH changes during the enzymatic reaction.

3.4 The Performance of Planar Waveguide Enzyme Sensor

3.4.1 Registration of the enzyme reactions

The sensitivity of the Si_3N_4 planar waveguide transducer to enzyme reactions was investigated in order to illustrate the performance of the proposed planar waveguide set-up as an enzyme sensor. The experiment was conducted in two sequences. First, the effect of a substratum on the planar waveguide transducer coated with the CTCT/PAH membrane was investigated. A layer of enzyme was then deposited on top of the existing membrane and the effect on the respective substratum was recorded again. The results of both sequences were compared to the noise signal.

Following the above procedure, it was found in this study that the planar waveguides coated with the (CTCT/PAH)$_4$/(enzyme/PAH) membrane successfully registered the respective enzyme reaction. This registration also proved that the enzymes were successfully immobilised on top of the CTCT/PAH membrane. As shown in Figure 3.14, in the case of the AChE layer on top of the CTCT/PAH membrane, the output signal intensity of the planar waveguide enzyme sensor increased with the time of soaking in 10 mM acetylcholine chloride solution, in comparison to the one without the AChE layer. The reduction in local pH in the membrane, caused by the decomposition of acetylcholine chloride to choline and acetic acid, resulted in the protonation of the CTCT molecules and respective characteristic changes in the CTCT spectrum within the range of 580 to 700 nm.
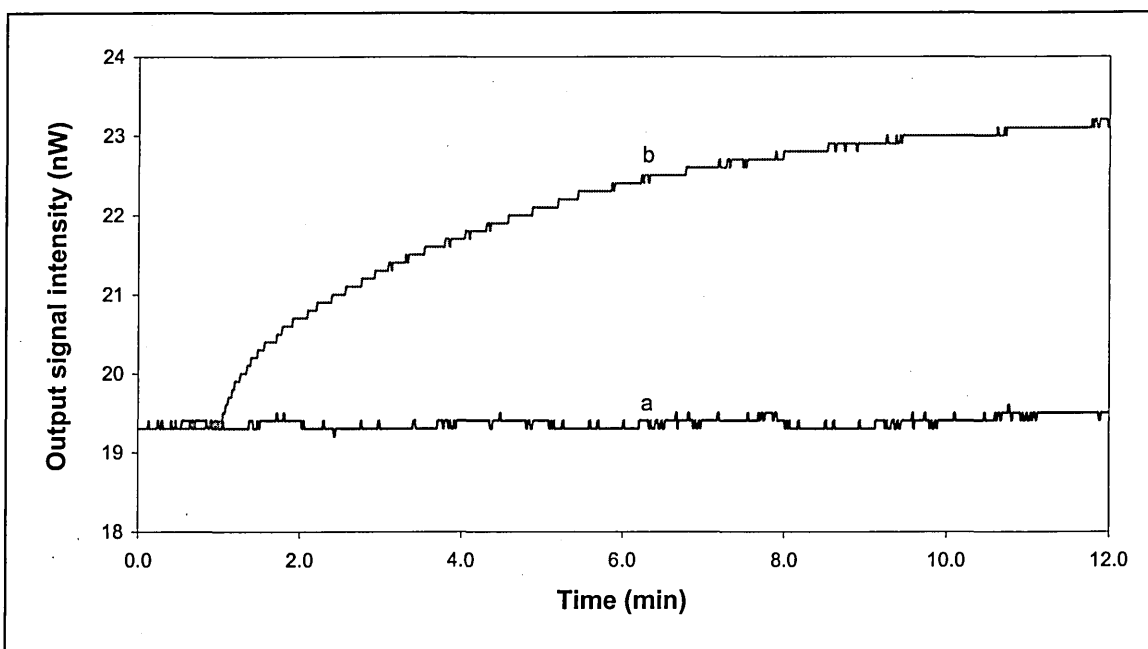
Figure 3.14. Kinetics of the AChE reaction:

(a) effect of 10 mM acetylcholine on the CTCT/PAH membrane,

(b) effect of 10 mM acetylcholine on the (CTCT/PAH)$_4$/(AChE/PAH) membrane.

A similar effect to the CTCT molecules was observed by soaking the planar waveguide coated with a (CTCT/PAH)$_4$/(BChE/PAH) film in a 10 mM butyrylcholine chloride solution. Figure 3.15 shows the output signal intensity increased with time indicating the production of choline and butyryl acid during the BChE enzyme reaction. It corresponded well to the spectral changes caused by the ionisation of hydroxyl groups in the CTCT molecules described previously.

Another type of enzyme reaction studied was the decomposition of urea catalysed by the enzyme urease. The production of ammonia caused an increase in local pH in the film and allowed the registration of this type of reaction with the CTCT indicator molecules. The exposure of the planar waveguide coated with the (CTCT/PAH)$_4$/(urease/PAH) membrane to 100 mM urea solution produced a decrease in the output signal intensity, as shown in Figure 3.16. The observed behaviour was believed to be due to the deprotonation of the hydroxyl groups in the CTCT molecules producing a respective increase in the absorbance of the CTCT indicator at 630 nm. This is in agreement with the results of the optical spectral study of this reaction in the (CTCT/PAH)/urease composite membrane reported earlier [Nabok et al, 1999].

The response of the planar waveguide set-up for all enzyme reactions is significant. As it was noticed from the effect of the respective substratum on the CTCT/PAH membrane, the noise signal was about 0.05 to 0.1 nW. Changes in the output signal intensity due to the enzymatic reaction was about 4 to 5 nW. Thus, the signal to noise ratio could be as large as 100. This value was considered adequate to provide a sufficient dynamic range for the registration of any suppressed response, when the planar waveguide coated with the (CTCT/PAH)$_4$/(enzyme/PAH) membrane was exposed to some toxic agents.
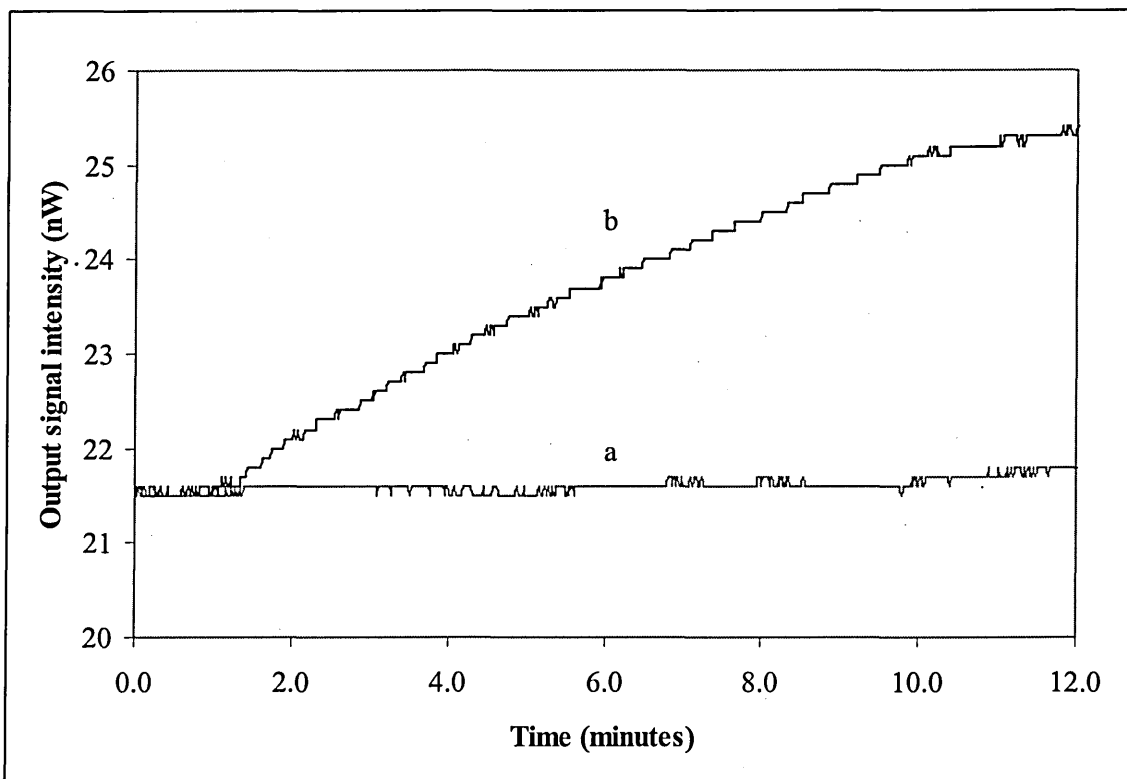
Figure 3.15. Kinetics of the BChE reaction:

(a) effect of 10 mM butyrylcholine on the CTCT/PAH membrane,

(b) effect of 10 mM butyrylcholine on the $(CTCT/PAH)_4/(BChE/PAH)$ membrane.
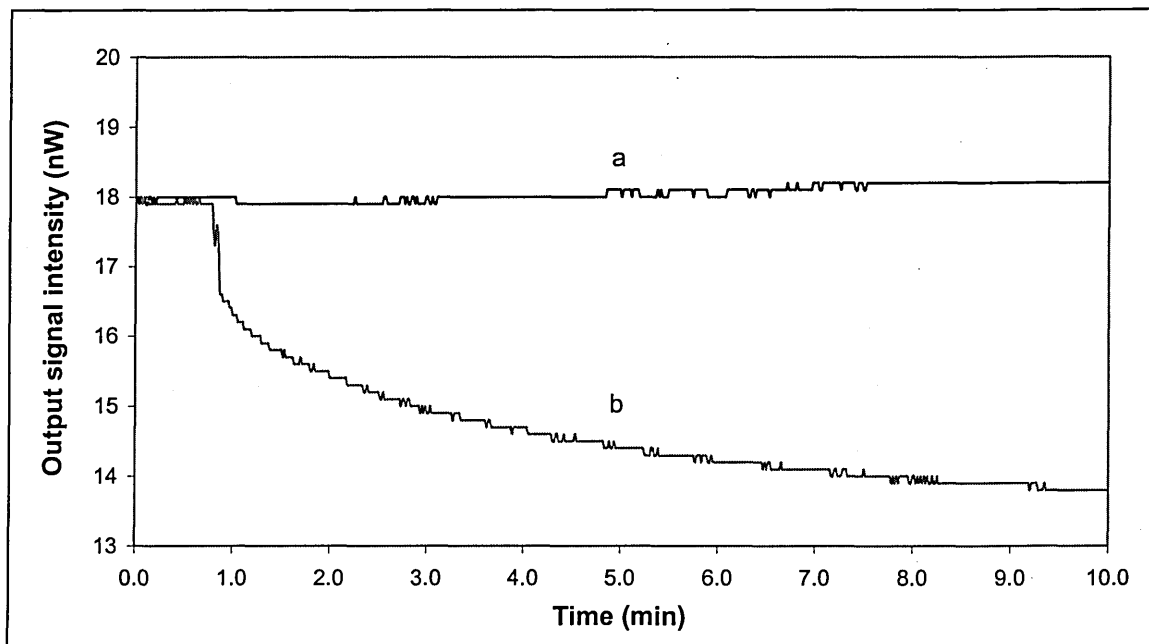
Figure 3.16. Kinetics of the urease reaction:

(a) effect of 100 mM urea on the CTCT/PAH films,

(b) effect of 100 mM urea on the (CTCT/PAH)$_4$/(urease/PAH) membrane.

3.4.2 Sensitivity of the enzyme sensor towards selected pollutants

This section presents the preliminary result of the enzyme sensor response regarding the effect of the selected pollutants on the enzyme activity. The effects of lead and cadmium ions on urease activity demonstrate the capability of the planar waveguide enzyme sensor in detecting the presence of toxic agents in the sample solution. The details of these measurements and the effect of other pollutants are discussed in Chapter 5.

Exposing the planar waveguide coated with $(CTCT/PAH)_4/(urease/PAH)$ membrane in the urea solution after the inactivation process in heavy metal ions solution, reduced the response of the urease enzyme reaction. Figures 3.17 and 3.18 show the effect of lead and cadmium ions on the kinetics of the enzyme reaction in the $(CTCT/PAH)_4/(urease/PAH)$ membrane, respectively. The concentration of 1 ppb of lead ions caused almost 60 % reduction in the response after 10 minutes of measurements. At the same time, the drop of residual output intensity of about 25 % was observed for cadmium ions.

The residual activity of the enzyme (defined in Chapter 5 page 129), correlated to the concentration of lead and cadmium ions, is shown in Figure 3.19. The observed behaviour was believed to be due to the inhibition of the urease enzyme by heavy metal ions.
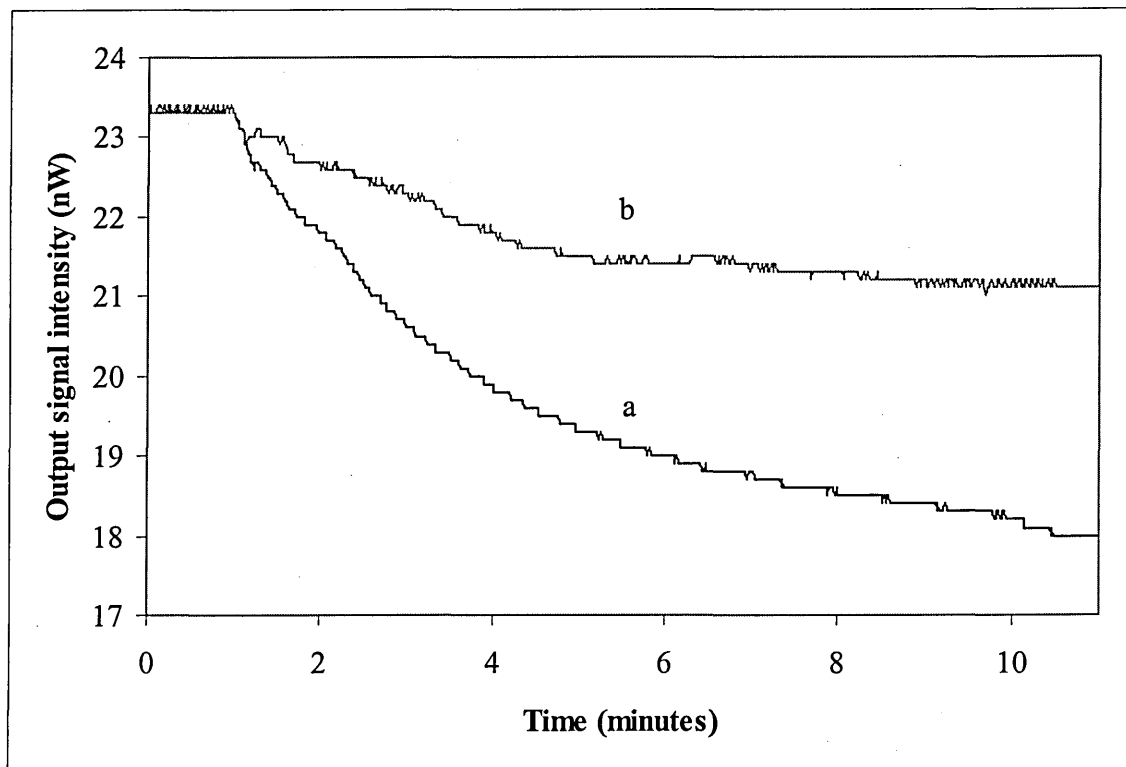
Figure 3.17. The effect of lead ions on the kinetics of enzyme reaction in the (CTCT/PAH)$_4$/(urease/PAH) membrane; (a) the response to 100 mM urea, (b) the response to 100 mM urea after inhibition of urease by 1 ppb of lead ions..
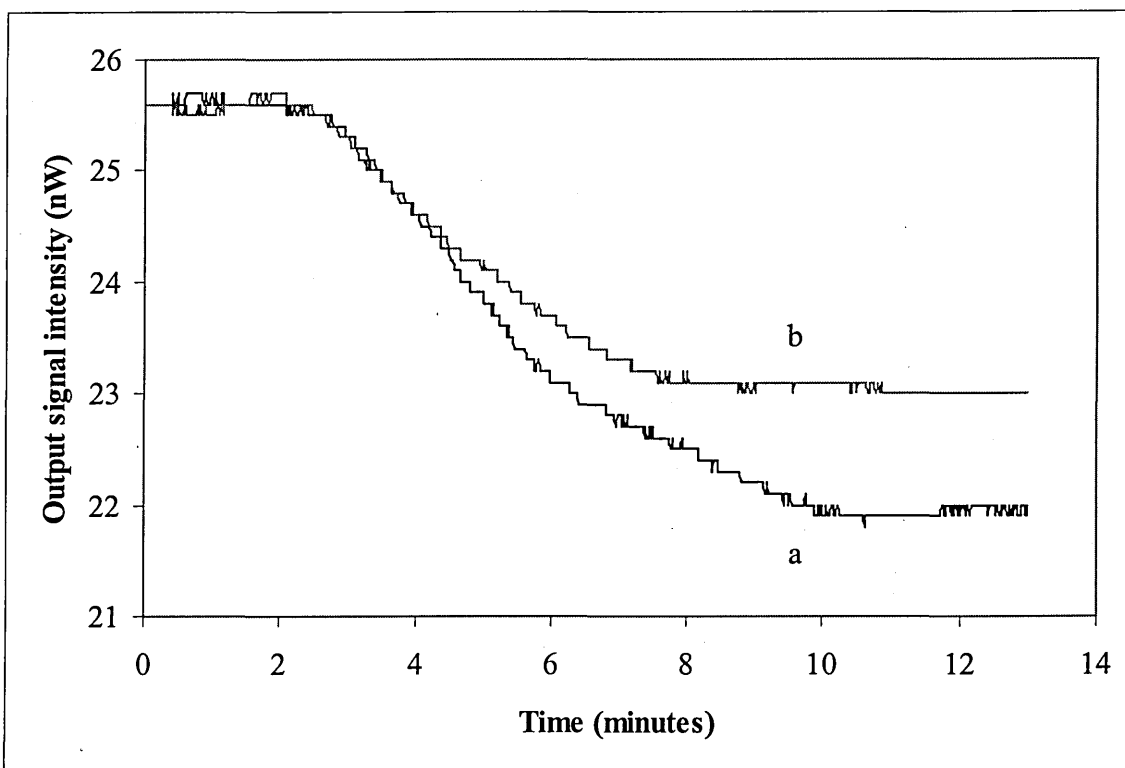
Figure 3.18. The effect of cadmium ions on the kinetics of enzyme reaction in the (CTCT/PAH)$_4$/(urease/PAH) membrane; (a) the response to 100 mM urea, (b) the response to 100 mM urea after inhibition of urease by 1 ppb of cadmium ions.
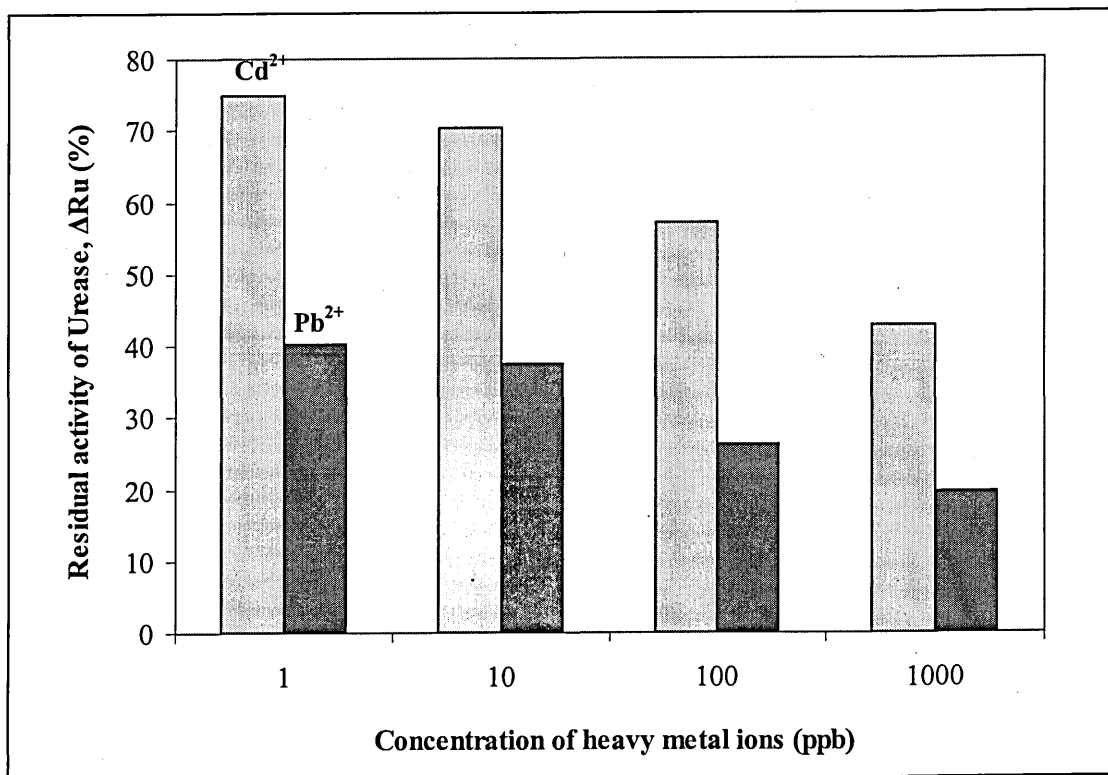
Figure 3.19. Residual activity of urease as a function of lead and cadmium ions concentration.

3.5 Summary

The SiO$_2$/Si$_3$N$_4$ planar waveguides produced by standard silicon planar technology and previously used as a polarization interferometer transducer for immunosensors were successfully exploited in this study as attenuated total reflection transducers. It was realised by a simple optical experimental set-up, which was used to measure the attenuation of light intensity after multiple interaction with the nanocomposite membrane deposited on the sensing window of the planar waveguide.

The sensitive PESA membrane containing the CTCT indicator was characterised using a UV-visible spectroscopy technique and the planar waveguide set-up. Large optical attenuation was found in the waveguide, with three orders of magnitude greater than in the UV-visible spectroscopy technique. The analysis of the experimental data showed that the large difference in refractive indices of core and cladding layers of the Si$_3$N$_4$ planar waveguides, gave rise to an increase in sensitivity by a factor of 3 over previously reported waveguiding structures.

This study also proved that, the intensity of light propagating in the Si$_3$N$_4$ planar waveguide is adequate for the registration of some specific bio-chemical reactions, within the deposited nanocomposite membrane on the sensing window. Individual enzyme reactions, as well as their inhibition by the toxic agents, were successfully registered by monitoring the change in intensity of light output from the planar waveguide. The remarkable result was that the traces of the tested pollutants in concentrations down to 1 ppb could be registered with the proposed enzyme sensor.

The present results provide a background for further development of sensor arrays, containing different chromophore/enzyme pairs, which are capable of registration and recognition of different industrial and agricultural pollutants in extremely small concentrations. The work on the development of the ATR optical enzyme sensor arrays for water pollution monitoring is explained in the following chapter.

CHAPTER 4

THE DEVELOPMENT OF MULTI-CHANNEL

ENZYME SENSOR

4.1   The Design of a Multi-Channel Enzyme Sensor

In order to achieve a simultaneous registration of different enzyme reactions, several changes were implemented in the single channel planar waveguide set-up. A multi-channel flow cell, and a special shutter rotated by a stepper motor was introduced into the sensor system. The configuration of the modified experimental set-up is shown schematically in Figure 4.1. This setup allowed the deposition of nanocomposite membranes with different types of enzyme on the surface of four waveguide windows. Consequently, the light beam was guided to propagate through each channel. The above process was achieved due to the unique design of the flow cell and the rotating shutter.

The flow cell consisted of two components, shown in Figure 4.2. The upper component was made of a hard plastic with eight holes of diameter 4 mm for solution inlets and outlets. The lower part was made of a hard rubber with a symmetric pattern of narrow channels and 1 mm holes. Thus, by combining the two parts, the sample solutions were able to pass through the narrow channels, and then enter each of the four reaction chambers at the bottom of the cell via the 1 mm holes. This multi-channel flow cell was placed on top of the Si_3N_4 planar waveguide transducer and the Anritsu light detector was put immediately after the other end of the cell.

2

Top view

Figure 4.1. Schematic diagram of the experimental set-up for the enzyme sensor array. (1) HeNe laser source, (2) two semi-cylindrical lenses, (3) shutter with asymmetric slits rotated by a stepper motor, (4) SisN₄ planar waveguide with multi-channel flow cell, (5) Anritsu light detector.

(a)

(b)

four individual
reaction chambers

(c)
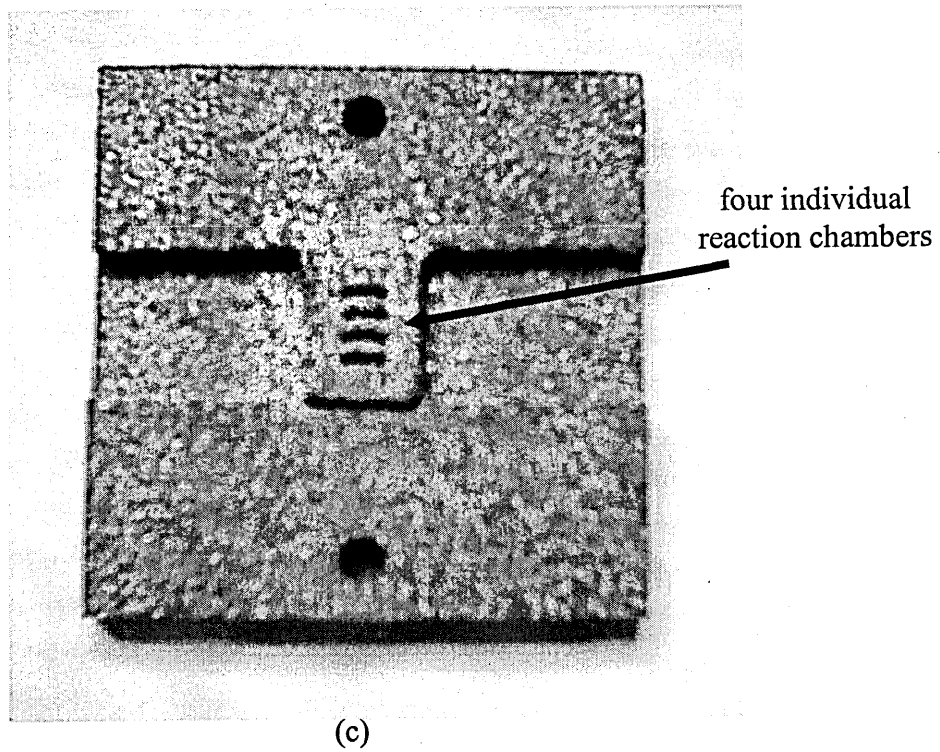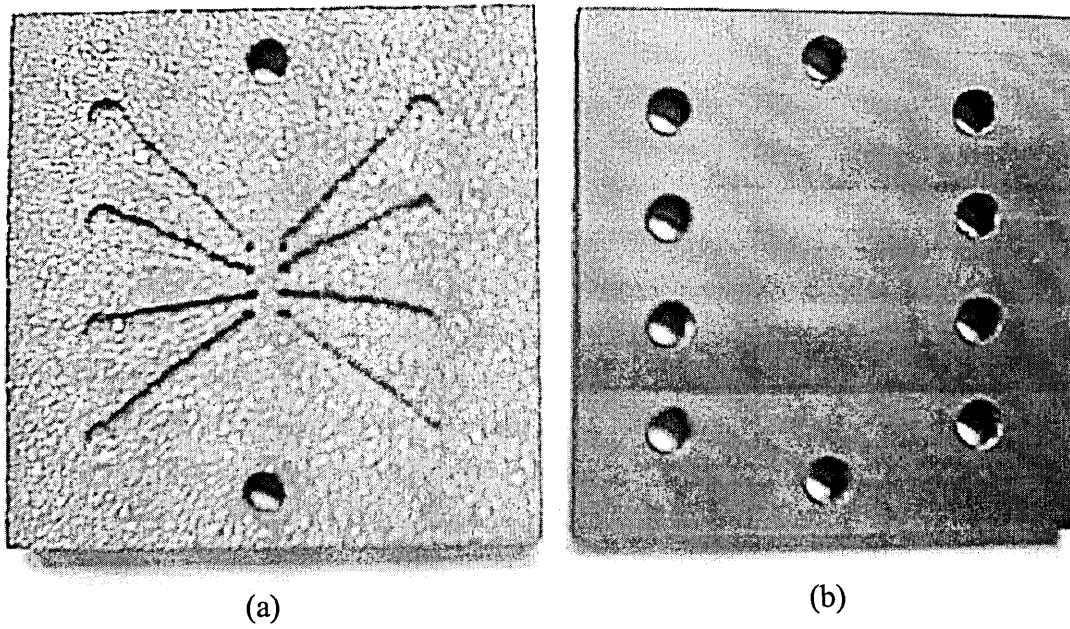
Figure 4.2. The component of the multi-channel flow cell. (a) Lower part made of a hard rubber, (b) upper part made of a hard plastic, (c) bottom view of the lower part.

The purpose of this cell construction was to ease the process of solution injection into the small reaction chamber. Unfortunately, the design allowed the photodetector to be 2 cm away from the edge of the waveguide and this reduced the signal down to the noise level. Therefore, the cell was partially removed to allow the photodetector to be placed closer to the edge of the waveguide. Figure 4.3 shows a photograph of the multi-channel flow cell after alteration.

The size of the opening in each chamber was 1 x 4 mm, and the gap between each chamber was 1 mm. Therefore, the distance across each of these chambers was about 7 mm. However, the widths of the waveguide window and the laser beam were only about 6 mm and 5.6 mm, respectively. Thus, in order to accommodate all the reaction chambers, the following procedure was performed: 1) the waveguide window was made 1 mm wider on each side by etching the SiO_2 layer in 5 % hydrofluoric acid for 5 minutes; 2) an additional semi-cylindrical lens was placed vertically in front of the light source to increase the width of the beam to 12 mm on the edge of the waveguide.

A special shutter was used to guide the light beam to propagate through a certain channel. This shutter had four identical 2 mm wide slits around its perimeter. The distance from each slit to the central line of the shutter was made slightly different as illustrated in Figure 4.4. As a result, when the shutter rotated by 90° every second, the position of the slit at point X was slightly shifted, and a portion of light beam allowed through to propagate under different channels.

Figure 4.5 shows a photograph of the main components of the proposed set-up of the enzyme sensor array. Further explanation about the operation of this sensor array set-up was given in the following section.

Figure 4.3. The view of multi-channel flow cell after the alteration process.
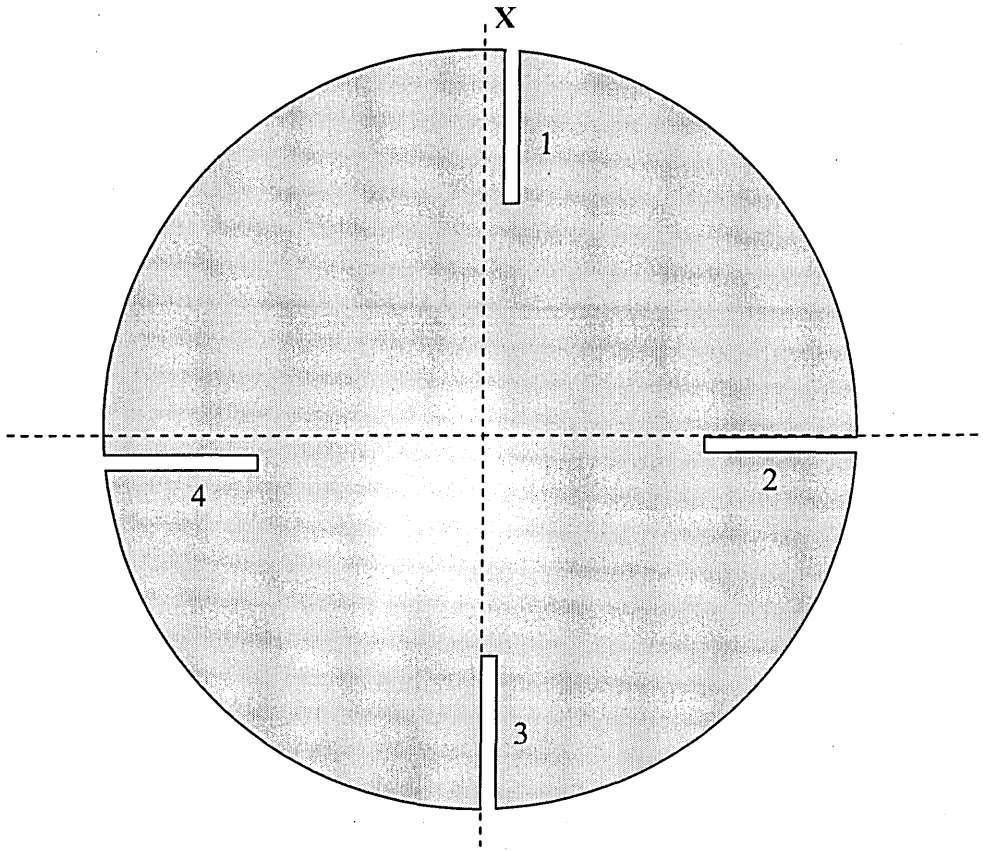
Figure 4.4. Schematic diagram of the shutter shows the exact location of the slits.

Figure 4.5. The experimental set-up of the enzyme sensor array. (A) HeNe diode laser , (B) vertical semi-cylindrical lens, (C) horizontal semi-cylindrical lens, (D) shutter with asymmetric slits rotated by a stepper motor, (E) Si_3N_4 planar waveguide with multi-channel flow cell, (F) Anritsu light detector.

4.2 Software for Multi-Channel Experimental Set-up

The operation of the proposed sensor array set-up was controlled with dedicated software written with the LabVIEW programming language. The main function of the software was to synchronize the rotation of the shutter by the stepper motor and the data acquisition with the optical power meter. This task was important in order to make sure that the output signal was measured from each channel illuminated by the laser beam through the slit in the shutter. The software performed the task of communication between the main instruments (stepper motor and optical power meter) in a sequence illustrated in Figure 4.6. The communication process was repeated four times to provide the measurements of responses from four channels.

As shown in Figure 4.7, the intensity of the output beam was measured before the software has sent the transmission signal to the stepper motor. The acquired data was stored and displayed as the response of appropriate channels. In order to rotate the shutter by 90°, 50 pulses of 1 kHz TTL signal were generated to drive the stepper motor. This procedure was carried out by sending 0 and 5 V transmission signals with a 1 ms interval to the stepper motor control board. Both signals were sent in a series of 50 iterations through the computer parallel port. Since the stepper motor used had a single step of 1.8°, the series of 50 produced TTL pulses caused the stepper motor (and thus the shutter) to rotate by 90° in 0.1 seconds.

Multi-channel
flow cell

Photodetector

Power meter

Light source

1

GPIB
communication

Stepper motor
and shutter

2

PC

Parallel port
communication
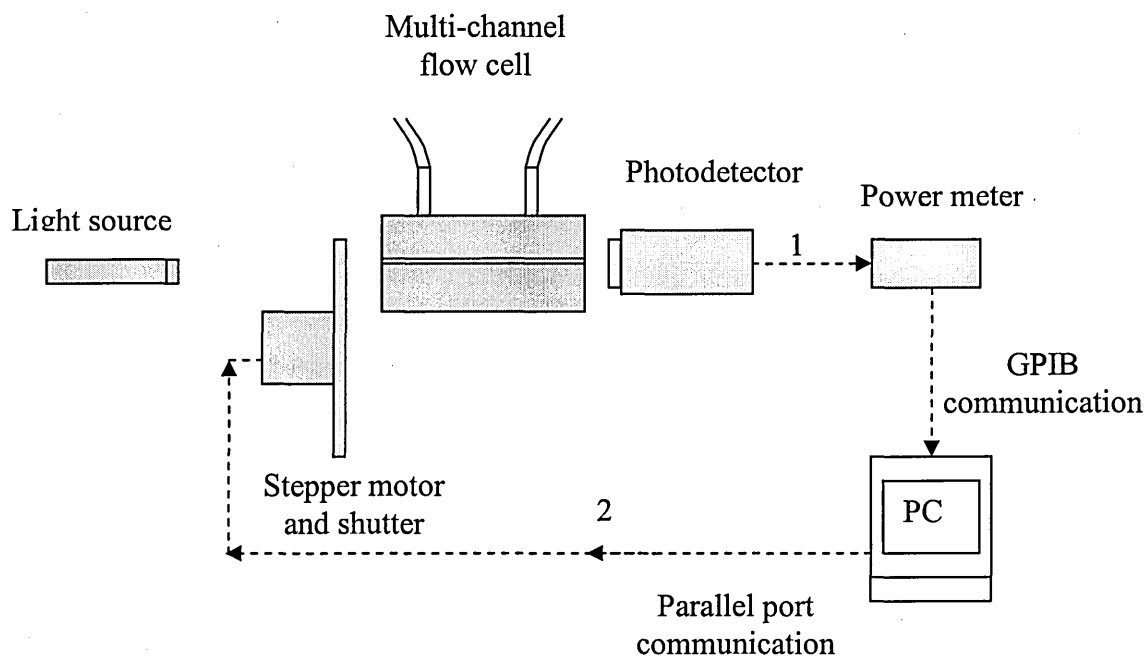
Figure 4.6. Illustration of the communication sequence between the software and the main instruments.
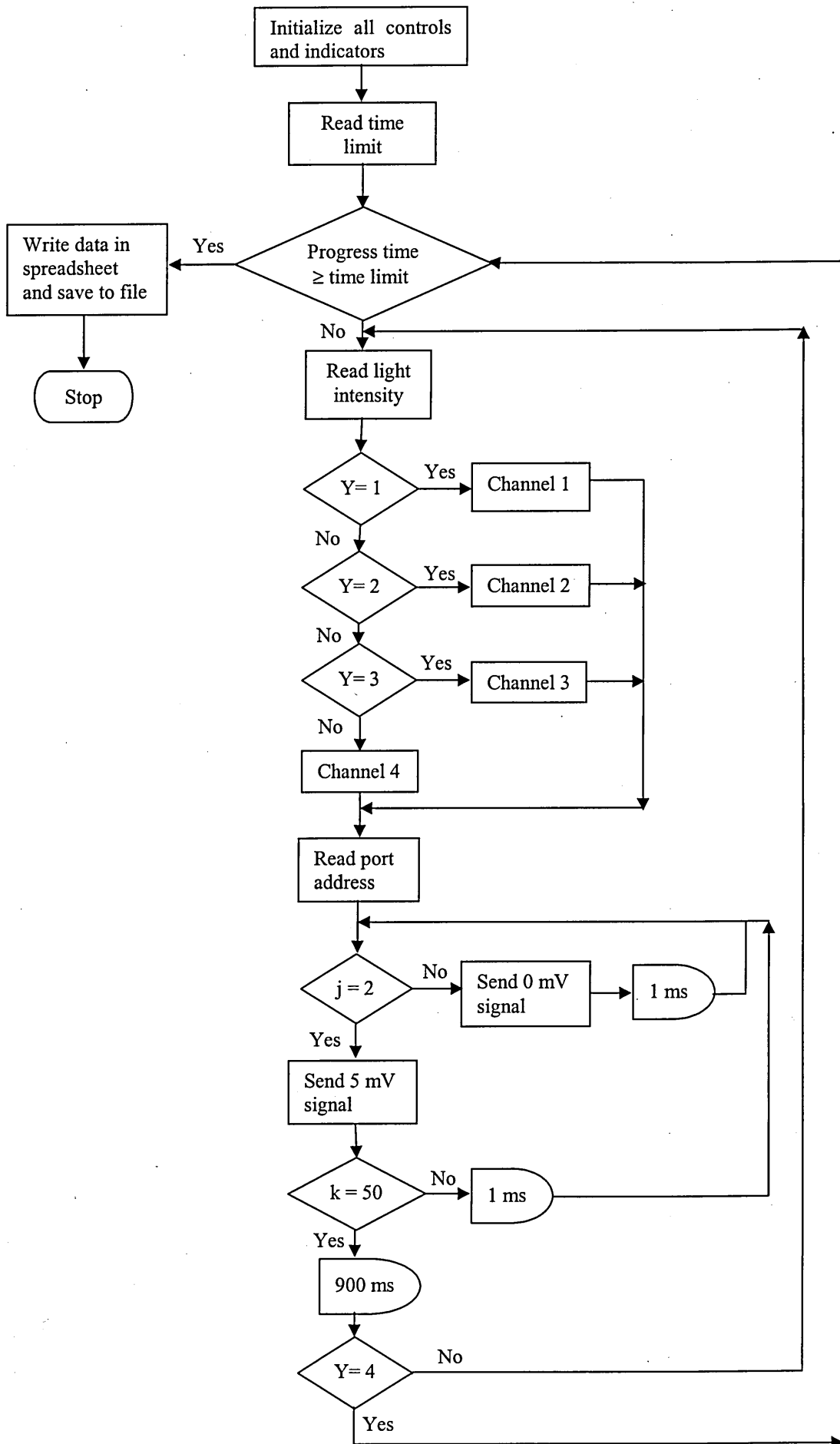
Figure 4.7. The flow process of the operating programme.

110

The operating programme had a time delay of 0.9 seconds after the 90° rotation of the shutter. This intermediate pause allowed the software to record a stable output response from a channel. Experimental results of the sensor array were displayed by four graphs at the LabVIEW graphic window as shown in Figure 4.8. The graphs were plotted concurrently with every measurement of the output signal intensity. This feature of the developed programme enabled the kinetic response of the sensor array to be observed during the experimental work. The details of this LabVIEW programme are given in the appendix.
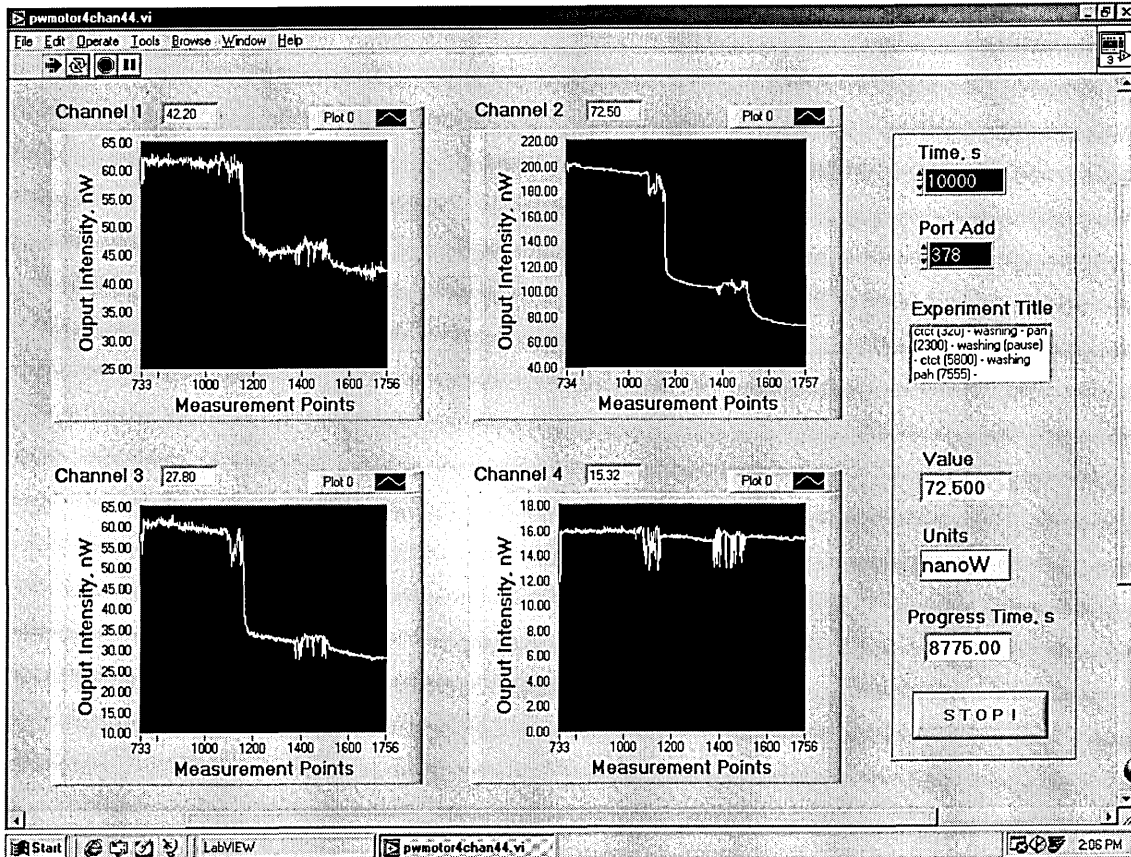
Figure 4.8. The front panel of the software shows four graphs of the channels responses.

4.3   Signal Calibration and Channel Addressability

A series of tests were performed with a view to evaluating the light intensity distribution across the waveguide. Measurements of light intensity both initial (before coupling into waveguide) and output (coming out from the waveguide) were carried out.

It was found that the light intensity was distributed non-uniformly along the laser beam stripe, giving different light intensities in different channels. The highest intensity was obtained at the centre of the light beam (maximum value of about 1 mW). The intensity then decreased about 10 times at the edges of the light beam. As shown in Figure 4.9, the light intensity in the first and fourth slit was substantially lower than that in the second and third slit. Consequently, when the light was coupled into the planar waveguide, it was unable to provide adequate responses for channel 1 and 4 (see Figure 4.10). The output signal intensity from both channels was too low to monitor the deposition of one or two layers of the CTCT.

In order to overcome this problem, the measurements were performed in three channels. The output signal intensity from these three channels was increased by repositioning the slits towards the centre of the light beam. As shown in Figure 4.11, the light intensity from the first and third slit was only two times lower than that from the second slit. This condition provided adequate response signals for the three channels as shown in Figure 4.12. Although the response signal of the multi-channel sensor was from 3 to 7 times lower than that of the single channel sensor, it was enough for *in-situ* PESA deposition and registration of any enzyme reaction.
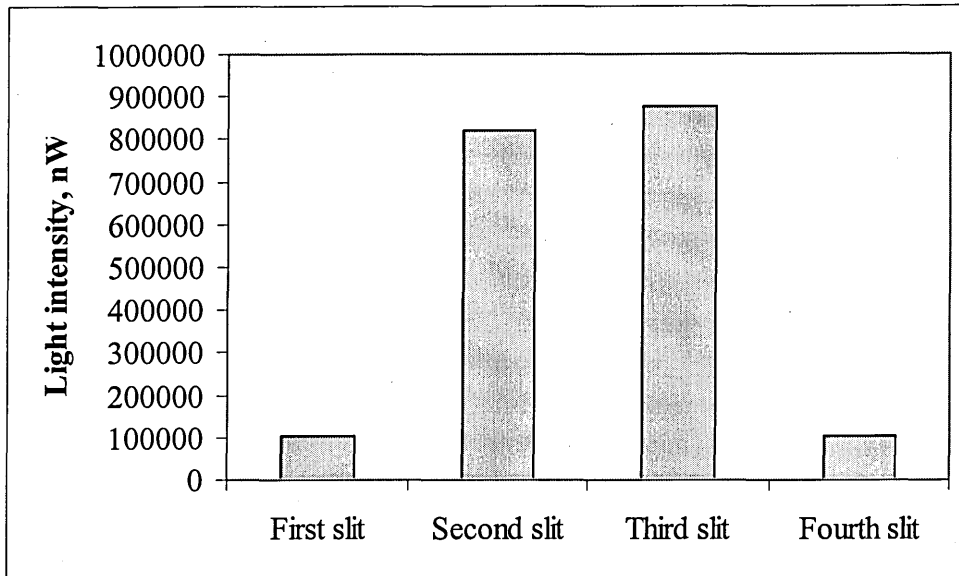
Figure 4.9. The intensity of lights after passing through the four slits.
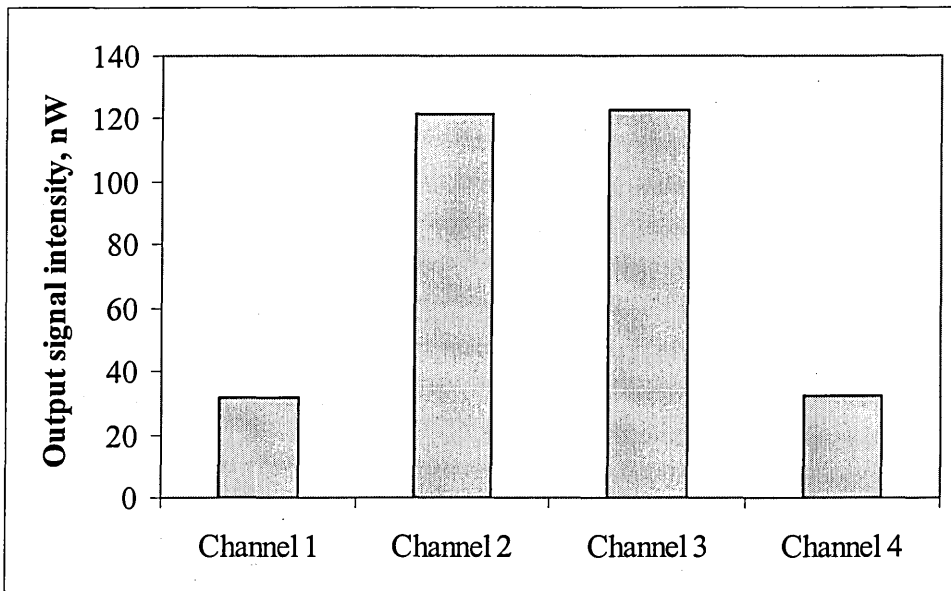
Figure 4.10. Channel responses after the guided light propagated in the waveguide.
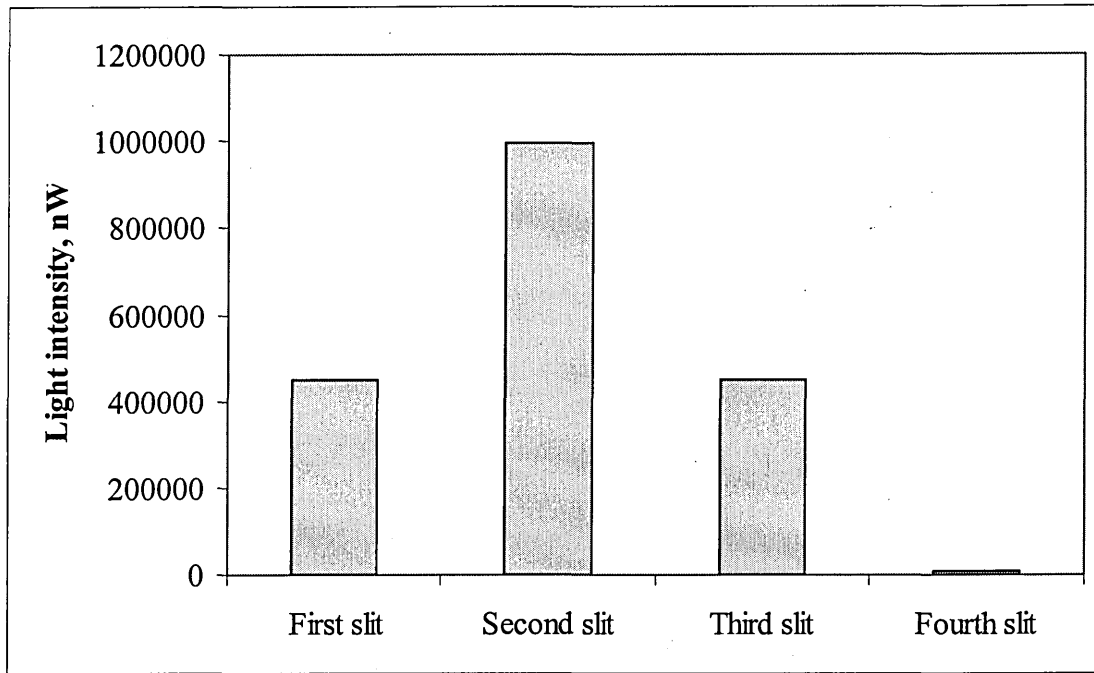
Figure 4.11. The improvement of light intensity after reposition of the slits towards the centre of the light beam.
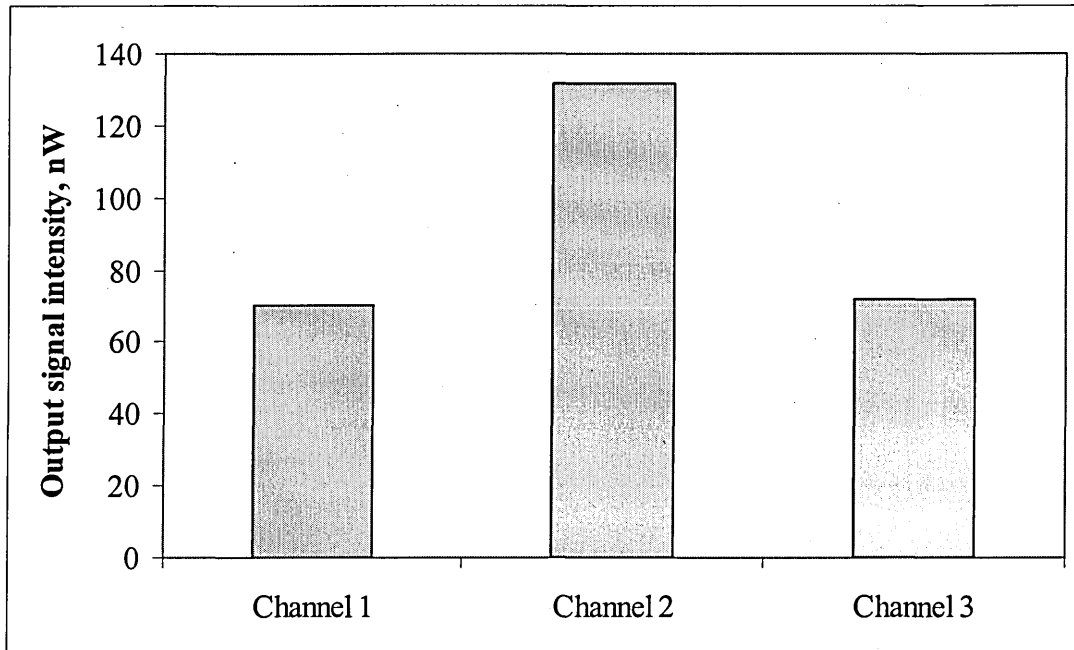
Figure 4.12. The improved responses of the three channels.

Prior to PESA deposition, the flow cell of the sensor array was tested for any leakage between its channels. A no leakage condition is important to allow split formation of nanocomposite membranes on the sensing window of the planar waveguide. The test was performed by injecting water into the channels in a sequence, beginning with channel 1, and then followed by channel 2 and 3 at 60 seconds interval. When each channel was filled with water, the output signal intensity increased due to the change of the refractive index from 1.0 (air) to 1.3 (water) in the sensing window of the Si_3N_4 planar waveguide. The results of this test, shown in Figure 4.13, proved that there was no leakage in the multi-channel flow cell, as the step change in the sensor response only occurred on the particular wet channel.

In-situ deposition of the CTCT/PAH membranes on the Si_3N_4 planar waveguide was carried out simultaneously by a series of manual injections of the CTCT and PAH solutions into the three channels of the flow cell. The adsorption kinetics of this process was found to be similar to the deposition of the CTCT/PAH membranes in a single channel planar waveguide as described previously. As shown in Figure 4.14, despite the small area of the sensing window and a low intensity of light, a significant decrease of the output signal was observed after each deposition of the CTCT layer. The normalised attenuation ratio $\dfrac{\Delta I}{I_o}$ was found to be 0.4 per layer of the CTCT in each channel. This result suggested that the sensitivity of each channel in the enzyme sensor array was comparable to the sensitivity of the single channel enzyme sensor. However, the formation of the CTCT/PAH membranes were limited to two bilayers only in order to obtain sufficient sensor responses from channels 1 and 3.
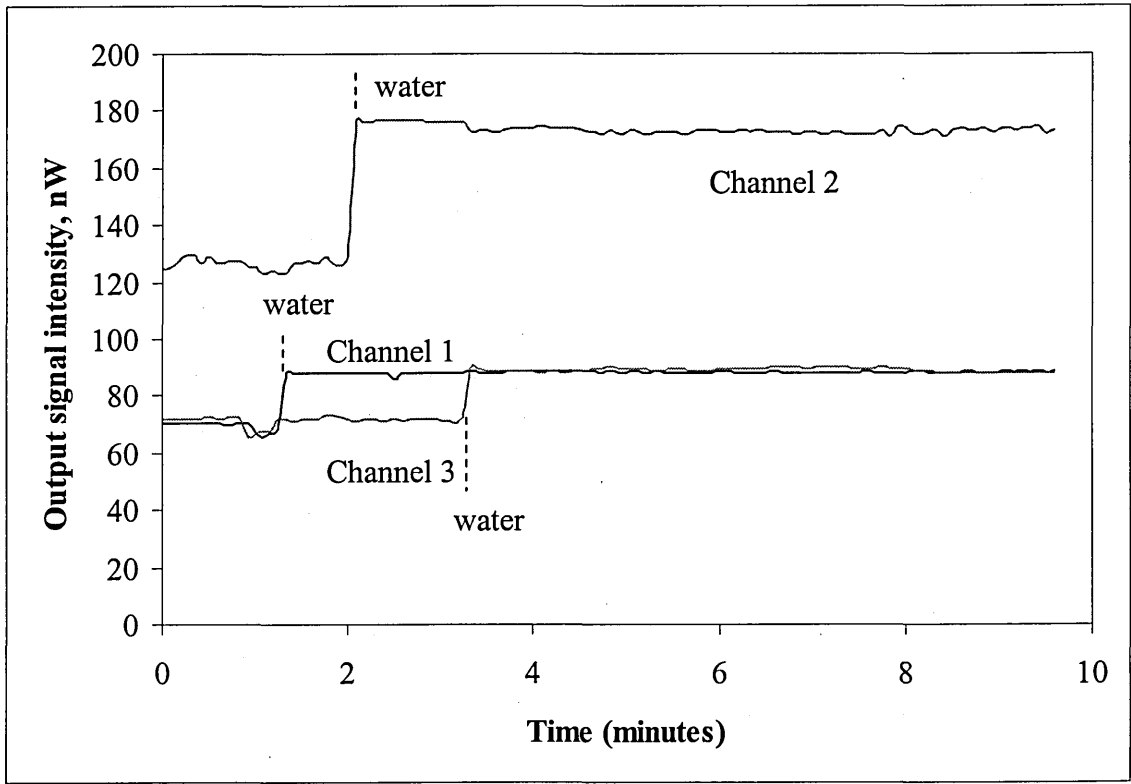
Figure 4.13. Results of the leaking testing on each channel. Time intervals where water was introduced into each channel are indicated.

300 T

250

200

Channel 2

150   CTCT   PAH

100
        L
            Channel 3   CTCT   PAH

50

^Channel 1

                        100   120

Time (minutes)
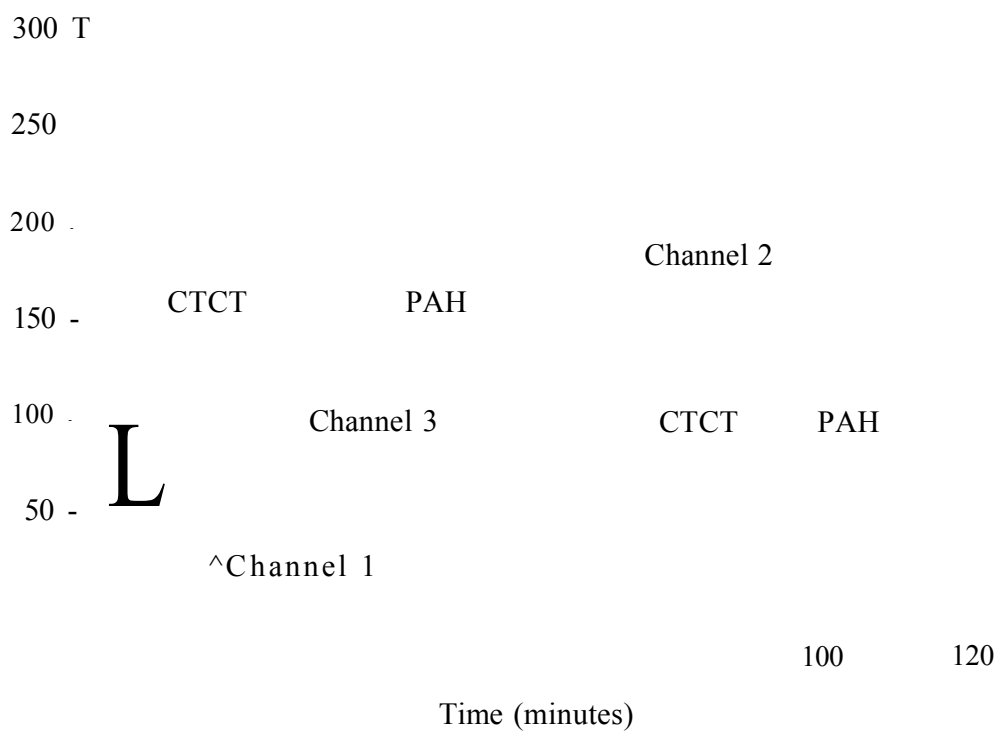
Figure 4.14. *In-situ* deposition of the CTCT/PAH membranes onto the planar waveguide for each channel.

4.4 Simultaneous Registration of Several Enzyme Reactions

The feasibility study of the developed sensor array to produce significant responses on the activity of different enzymes was implemented simultaneously on the three effective channels. The reactions of the enzymes AChE and BChE were analysed in channel 1 and 3, respectively. Concurrently, channel 2 was used to examine the activity of the urease. The experiment was performed by manually injecting the respective substrata into appropriate channels in two sets: before and after the deposition of the particular enzyme on the CTCT/PAH membrane. The respective substrata and the composition of the sensitive membrane deposited in the channels are shown in Table 4.1.

Figure 4.15 shows the response of each channel on exposure to the specific substratum. It is obvious that the enzyme sensor array successfully registered the activities of the immobilized enzymes. The change in the output signal intensity was correlated to the reaction of the particular enzyme in the channels. For instance, the decrease in the intensity of the output signal with time indicates the decomposition of urea occurring in channel 2. On the other hand, the output signal intensity from channels 1 and 3 increased with time demonstrating the production of acetyl and butyryl acid during the AChE and BChE reaction.

It became very evident from the results obtained that the response of each channel in the sensor array was similar to the response of the single channel planar waveguide. Generally, the changes in the output signal intensity due to the enzyme reactions were found to be about 4 to 5 nW after 10 minutes exposure to the respective substratum. The sensor response was 100 times higher than the background signal

observed from the substrata affect on the CTCT/PAH membrane. This indicates that the enzyme sensor array had sufficient dynamic range for the registration of the suppressed response caused by pollutants.

Table 4.1. Membrane configuration and substratum applied to each channel of the enzyme sensor array.

Channel	Membrane configuration	Substratum
1	(CTCT/PAH)$_2$/(AChE/PAH)	10 mM acetylcholine chloride
2	(CTCT/PAH)$_2$/(urease/PAH)	100 mM urea
3	(CTCT/PAH)$_2$/(BChE/PAH)	10 mM butyrylcholine chloride
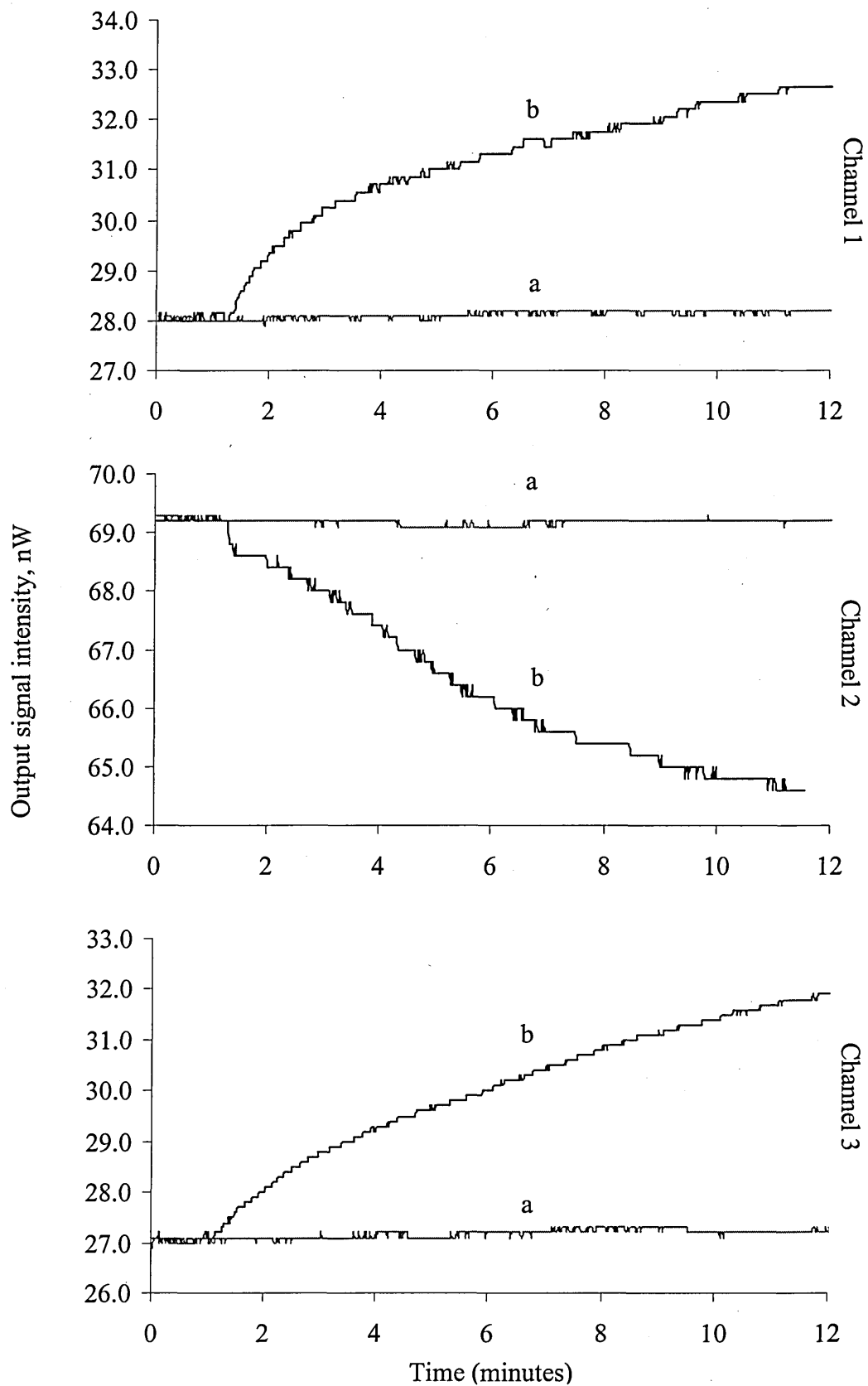
Figure 4.15. Responses of the enzyme sensor array when exposed to the respective substratum (a) without the enzyme layer, and (b) with the enzyme layer on top of the CTCT/PAH membrane.

4.5   Summary

The multi-channel enzyme sensor was designed and developed. It was based on a single light source (laser) in the shape of a light stripe focused and coupled into the three-channel waveguide. Addressing of the channels was achieved with the mechanical shutter. Dedicated LabVIEW software was written to control the channel addressing and data acquisition. A series of tests proved the feasibility of the multi-channel enzyme sensor to register three enzyme reactions simultaneously. The responses agreed with those obtained by the single channel enzyme sensor. The results further suggested that the multi-channel enzyme sensor was capable of registering and recognizing different types of pollutants according to their effect on the enzymes activities.

CHAPTER 5

RECOGNITION OF POLLUTANTS BY THE

PLANAR WAVEGUIDE ENZYME SENSORS

5.1 Type of Pollutants and Samples Preparation

The following metal salts and pesticides were used to study the response of the planar waveguide enzyme sensor to different concentrations of pollutants: cadmium chloride ($CdCl_2$), nickel chloride ($NiCl_2$), lead nitrate ($Pb(NO_3)_2$), imidacloprid, paraoxon and 2,2-dichlorovinyl dimethyl phosphate (DVDP). All compounds are highly soluble in water. The metal salts are dissolved as cation (Cd^{2+}, Ni^{2+}, Pb^{2+}) and anion ($(NO_3)^{2-}$, Cl^{2-}) components. It was assumed that both chloride and nitrate anions exhibit practically no effect on the sensing membrane, particularly on the activity of immobilized enzymes. Imidacloprid is a chloro-nicotinyl pesticide and it was produced as a substitution of highly toxic phosphororganic pesticides, such as DVDP and paraoxon [Cox, 2001]. Different classes of pesticides were used in order to investigate the sensitivity of the enzyme sensors to pollutants of different toxicity. The pollutants were diluted a number of times in ultrapure water to reach concentrations in the range from 100 part per million (ppm) down to 1 part per billion (ppb). The dilution process began with the preparation of sample solutions of 100 ppm and 10 ppm concentration by dissolving 1 mg of respective compound in 10 ml and 100 ml of ultrapure water. The dilution process was performed at room temperature in a well-stirred condition to obtain a homogeneous mixture of the sample solutions.

5.2 Measurement Procedure for Pollutants Registration

Two approaches were exploited to measure the pollutants level in sample solutions. The first method was based on the registration of the sensor response in the mixture of the substratum and the sample solutions. At the beginning, the measurements of the respective enzyme reactions were performed in pure substratum solutions. Then, residual activities of enzymes in equal volume mixtures (0.5 *ml*/0.5 *ml*) of substrata and diluted pollutant solutions were recorded. The measurements were conducted continuously by increasing the concentration of the pollutant in the sample solution within the range from 1 ppb to 100 ppm. After each exposure to the mixture, the reaction cell was rinsed several times with ultrapure water. The ratio of the enzyme activity in the sample mixture and pure substratum solution was correlated to the different level of the pollutant in the solution tested.

This approach was used to study the effect of imidacloprid pesticide on urease activity. As shown in Figure 5.1, the enzyme sensor successfully registered the urease residual activities when continuously exposed to mixture solutions containing different concentration of imidacloprid. The sensor response was gradually decreased in each exposure with increasing imidacloprid concentration within the range from 10 ppb to 100 ppm (Figure 5.1, curve b to curve f). The preliminary explanation of this observation was believed to be due to the inhibition effect of imidacloprid on urease. However, this inhibition effect was found to be nonpermanent as full recovery of urease activity was achieved after rinsing with ultrapure water (Figure 5.1, curve a and g).
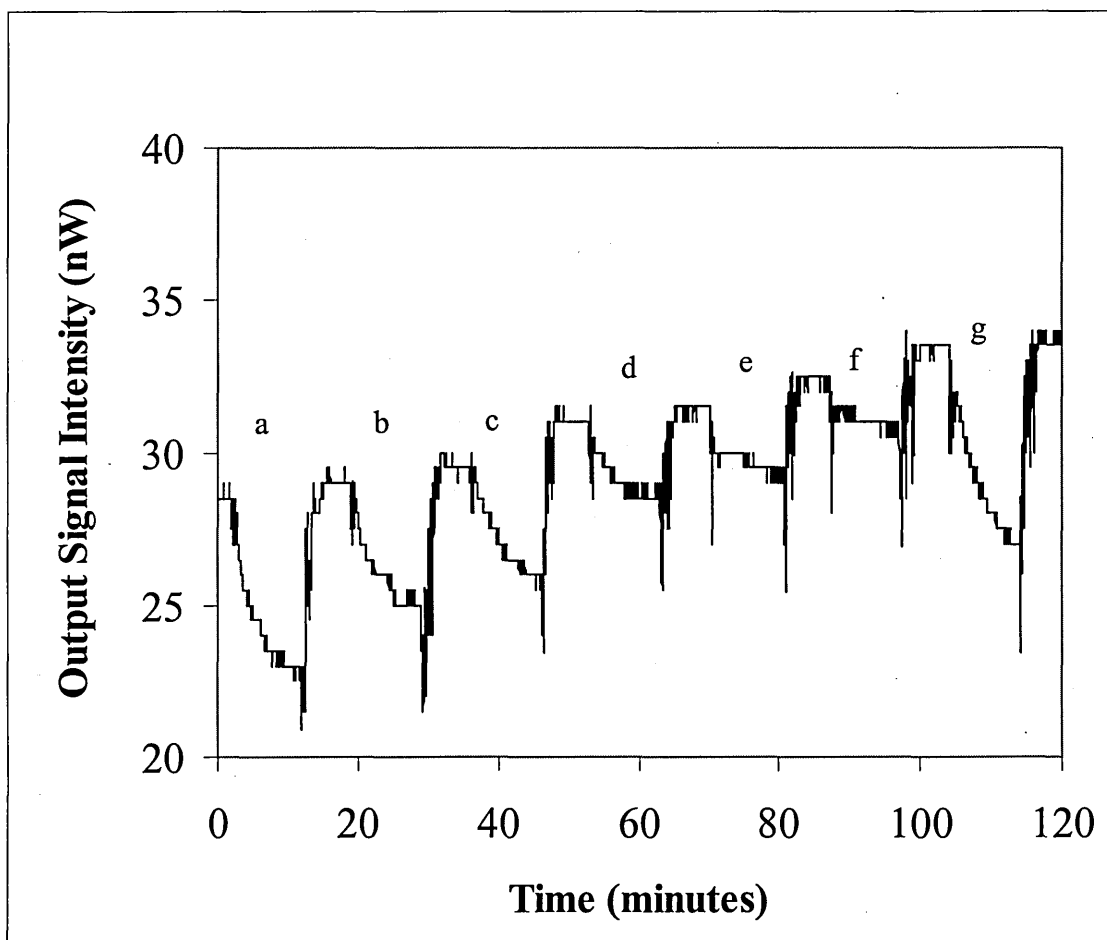
Figure 5.1. Response of the planar waveguide enzyme sensor coated with (CTCT/PAH)$_4$/(urease/PAH) membrane after exposure to the pure 100 mM urea solution (a and g) and mixed solution of 100 mM urea and different concentrations of imidacloprid at 0.01 ppm (b), 0.1 ppm (c), 1 ppm (d), 10 ppm (e), 100 ppm (f).

A few drawbacks of the first experimental approach were found from this study. Despite the fact that the reversible inhibition effect of imidacloprid was reversible, other factors also had an affect on the sensor response during the measurements. The pH of the mixture was not defined, and therefore the result of the experiment was unknown. Due to the small volume (1 ml) of the solution mixture, it is difficult to measure changes in pH after mixing the urea and imidacloprid solutions. However, changes in the output signal intensity were found when the waveguide coated with the nanocomposite membrane without urease, were exposed to the mixed urea and imidacloprid solution. As shown in Figure 5.2, the sensor response was slightly increased at high concentrations of imidacloprid, most likely because the solution became more acidic. This may have possibly had a significant impact on the sensor output signal during measurements of urease residual activity.

The 100 % recovery of the urease activity may also mean that the imidacloprid pesticide did not inhibit the enzyme. The sensor response in the mixed solutions was found to decrease possibly due to the limited access for urea molecules to the urease layer covered with adsorbed imidacloprid molecules. This assumption was based on a smaller size of the urea molecule having a molecular weight of 60 g/mole as compared to the imidacloprid molecule having a molecular weight of 256 g/mole. It was also possible that imidacloprid formed a barrier layer on top of the sensing membrane. The first method was not suitable for the irreversible inhibition of enzymes since measurements were carried out continuously. In this case, the sensor response could be masked by the effect of the preceding concentration of pollutants, and the registration of the pollutant level by simple comparison of the final enzyme activity with its initial activity was not possible.
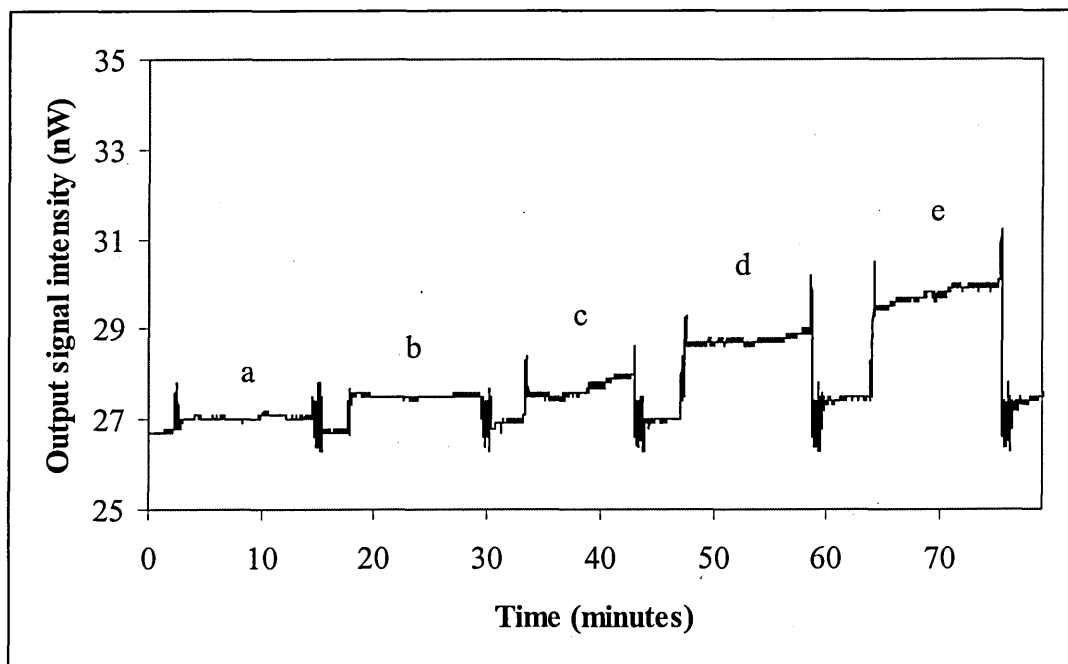
Figure 5.2. Response of the planar waveguide enzyme sensor coated with (CTCT/PAH)$_4$ membrane after exposure to the mixed solution of 100 mM urea and different concentrations of imidacloprid at 0.01 ppm (a), 0.1 ppm (b), 1 ppm (c), 10 ppm (d), 100 ppm (e).

In the second method, the inhibition process and the measurement of the enzyme activity were separated, as shown in Figure 5.3. The substrata were dissolved in mildly concentrated (1 mM) Trismabase-HCL buffer pH 7.3 to standardise the pH at the start of the enzyme reactions. The buffer solution was also injected into the reaction cell before each measurement to stabilize the sensor response in neutral conditions. The routine began with the registration of the sensor response to an enzyme reaction in the substratum solution. Then, a sample solution containing only the pollutant was injected into the reaction cell and held there for 15 minutes. After this inactivation process, the response to the enzyme reaction was recorded again under similar conditions as before. The reaction cell was rinsed with the ultrapure water after each step of the measurement. The evaluation of the pollutant concentration in the sample solution was performed by comparing the sensor response of the enzyme reaction before and after the inhibition.

Since each measurement started at a different background level of sensor signal, the absolute response (ΔI) was defined as a difference between the initial (I_b) and final (I_f) values of the output signal:

$$\Delta I = \mid I_b - I_f \mid \qquad (5.1)$$

Thus, the relative response of the sensor (also called residual activity of the enzyme) can be calculated as,

$$\Delta R = \frac{\Delta I_r}{\Delta I_o} \times 100\% \qquad (5.2)$$

where ΔI_o and ΔI_r are the response values of the initial enzyme reaction and that after the inhibition process, respectively.

Ov\u) A4isu^|in psifois 411d m o

The study of the pollutant level in water was carried out at room temperature. Optimal measuring time of enzyme reactions in all cases was within 10 minutes, while optimal time of enzyme incubation in the sample solution was chosen to be 15 minutes. These optimal times were based on an earlier report [Starodub et al, 1998], which found smaller exposure times have resulted in a decrease of sensitivity of the analysis, and on the other hand, no noticeable rise in the sensitivity achieved by increasing the exposure time.

Figure 5.4 shows the result of the inhibition effect of 100 ppb Pb^{2+} ions on urease obtained by both measurement methods. Obviously, the first method showed a higher reduction in the urease activity than the second one. This is probably because factors other than the inhibition effect of the pollutants contributed to the sensor response in the first method. The second method was more time consuming than the first one, however, the results obtained were more reliable since the reduction in the enzyme activity was absolute and caused by pollutants. Therefore, the second method was chosen for further investigations described in the following sections.
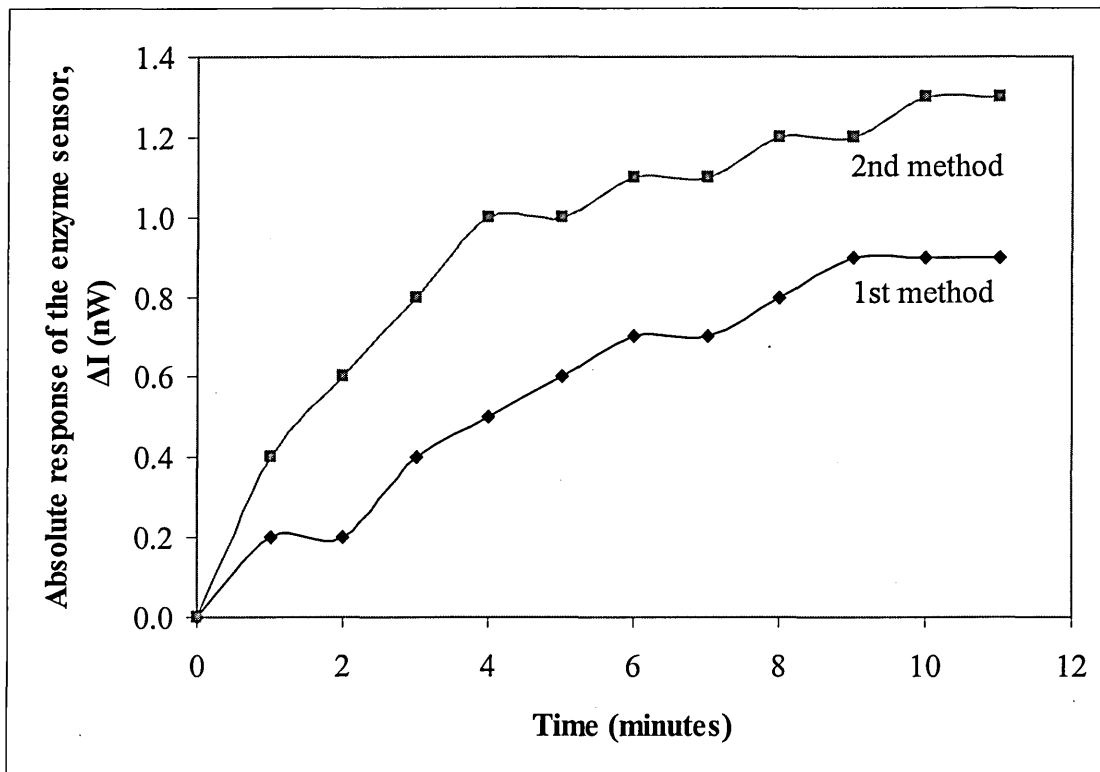
Figure 5.4. Absolute sensor response measured by the first and second method after exposure to 100 ppb Pb^{2+} ions.

5.3 The Reliability of the Sensor Response

The reproducibility of experimental results was studied by repeating at least three times the measurements of enzymes reactions and their inhibition. For example, the registration of urease reaction in a pure urea solution was performed three times after the deposition of nanocomposite membrane on the planar waveguide. As shown in Figure 5.5, the output signals were in good agreement and their relative standard deviation of 2.2 % was acceptable. Thus, sensor response to the initial enzyme reaction (ΔI_o) can be used as a reference for the calculation of the pollutants concentration.

The measurements of the urease reaction were also repeated using three SiO_2/Si_3N_4 planar waveguides. Unfortunately, it was difficult to receive the same signal from different planar waveguide devices. As shown in Figure 5.6 (curve a, b and c), the planar waveguides coated with the same concentration of urease produced a variation in the output signal of about 8 %, when exposed to 100 mM urea solution. Similar deviation was observed for the measurements of the urease activity after 15 minutes incubation in 100 ppb lead ions (Figure 5.6, curve d, e and f).

Nevertheless, the relative response of the sensor signals calculated by Equation 5.2 was found to be consistent for all planar waveguides. Table 5.1 and Figure 5.7 show the average values and standard deviations of the sensor relative response for a series of measurements of urease inhibition by the lead ions. A tolerance of less than 5 % was obtained even when the measurements were carried out using different planar waveguides. This result proves a feasibility of the registration approach based on the relative changes in the sensor output signal.

133

25

24

22

21

20

19

18

0   2   4   6   8   10
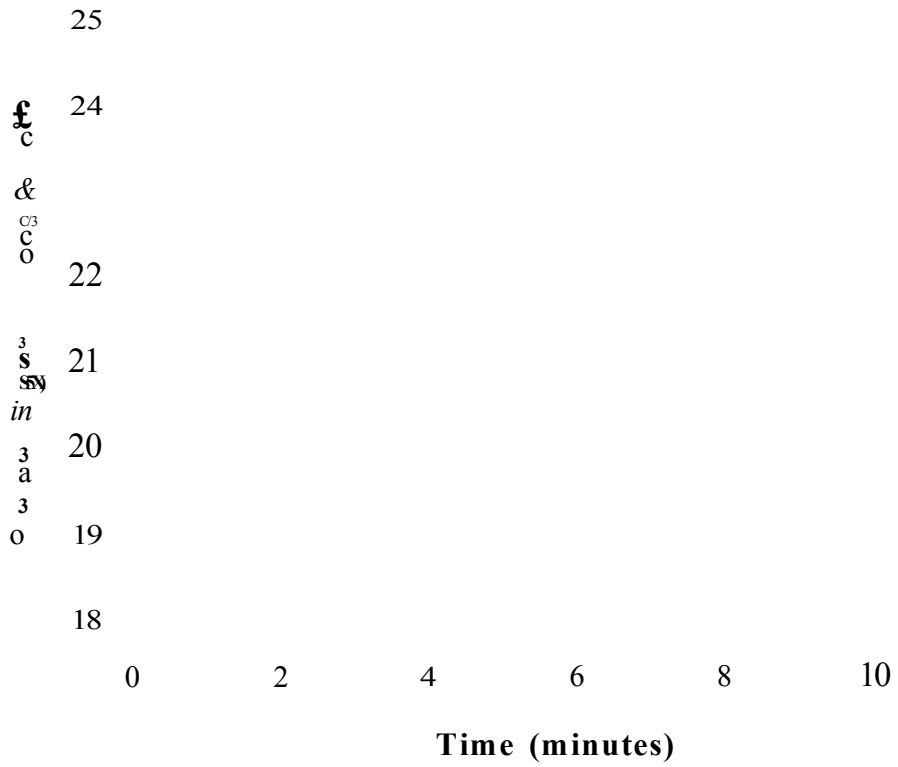
Time (minutes)

Figure 5.5. Response of single channel enzyme sensor to a series of urease reaction on the same SiCVSis^ planar waveguide.

4   6   8

Time (minutes)

Figure 5.6. Absolute sensor responses to initial urease reaction (curve a, b and c) and that after inhibition by 100 ppb lead ions (curve d, e, and f), measured using three SiO_2/Si_3N_4 planar waveguides: PW1 (b and e), PW2 (a and b) and PW3 (c and d).

Table 5.1. Calculation of the standard deviation of the sensor relative response for urease inhibition by 100 ppb of lead ions.

	Planar waveguide		
	PW1	PW2	PW3
ΔI_o (nW)	4.6	5.1	3.9
ΔI_r (nW)	1.3	1.4	1.0
Residual activity of urease, ΔR_u (%)	28.3	27.4	25.6
Average residual activity of urease, $\overline{\Delta R}_u$ (%)	27.1		
Standard deviation, SD (%)	1.12		
Relative standard deviation, RSD (%)	4.1		
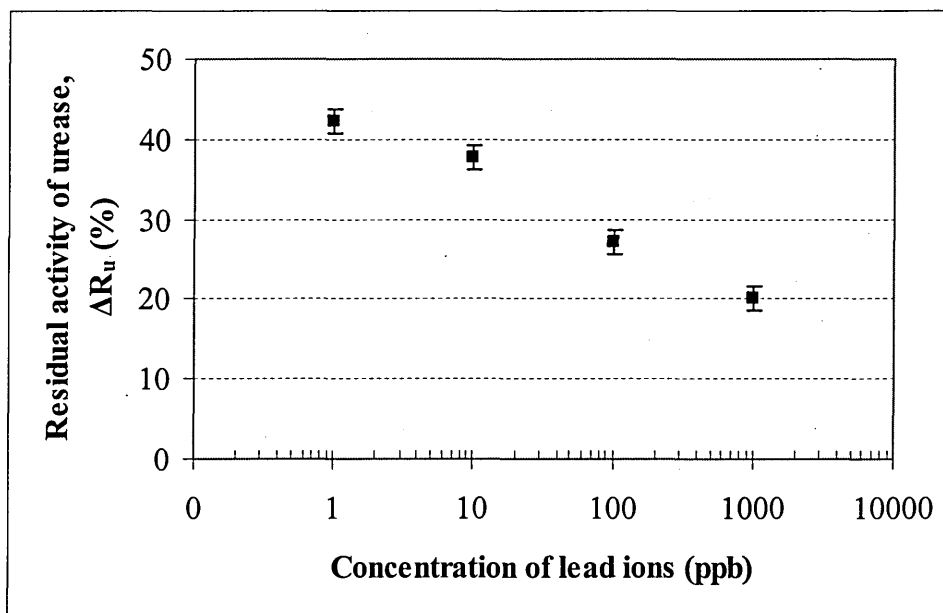
Figure 5.7. The relative response of the enzyme sensor at different concentration of lead ions. The responses were reproducible within the tolerance of less than 5 %.

136

5.4 Simultaneous Registration of Heavy Metal Ions using the Enzyme Sensor Array

A series of experiments were carried out in order to analyse the effect of lead, cadmium and nickel ions on the activity of the immobilised enzymes in the three-channel enzyme sensor array. The inhibition of the cholinesterase enzymes (AChE and BChE) by metal ions were detected in channel 1 and 3, respectively. The effect of metal ions on the urease reaction was simultaneously investigated in channel 2. All the enzymes were exposed to different concentrations of the heavy metal ions in a range from 1 ppb to 1000 ppb.

Figure 5.8 presents the relative responses of channel 2 to different concentrations of heavy metal ions. The results show that the metal ions strongly and irreversibly suppress the activity of urease to different extents. The residual activity of urease was found to decrease from 75 % down to 19.6 %, as the concentration of metal ions increased from 1 ppb to 1000 ppb. As one can see, lead ions are a stronger urease inhibitor than the other two metal ions. The toxicity of heavy metal ions towards urease was found to decrease in the following decreasing order: $Pb^{2+} > Ni^{2+} > Cd^{2+}$. These findings, however, differ from previous observations of the inhibition of urease by heavy metal ions in ppm range [Zhylyak et al, 1995; Preininger and Wolfbeis 1996; Kukla et al, 1999]. The concentrations studied in the present investigation were, however, smaller by three orders of magnitude.

70 -

60

50 -

40 -   ;2+

30 -

                                                   2+

10 -

                        100   1000   29

Concentration of heavy metal ions (ppb)
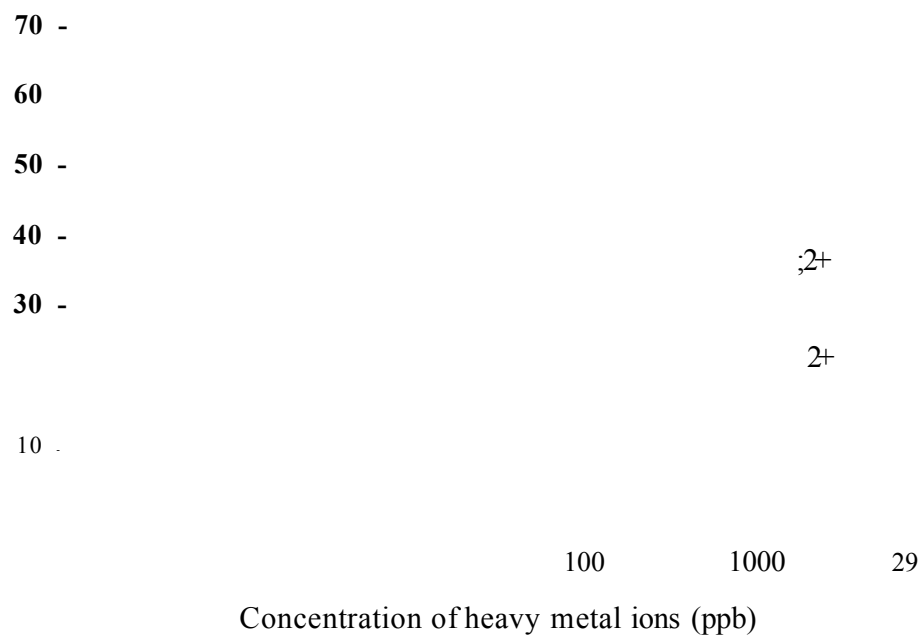
Figure 5.8. Residual activity of urease as a function of the concentrations of the following heavy metal ions: lead (Pb2+), nickel (Ni2+) and cadmium (Cd2+).

The dependences of residual activities of AChE and BChE on the concentration of heavy metal ions are shown in Figure 5.9 and Figure 5.10. The heavy metal ions were found to be less toxic to both cholinesterase enzymes than to urease. The relative responses of the sensor signals were found to decrease from 90 % to 50.1 % for the AChE reaction and from 87.9 % to 58.3 % for the BChE reaction, after being exposed to different concentrations of metal ions. This result is in agreement with the one obtained by Starodub et al (1999). Nickel and cadmium had similar inhibition levels on the activity of the cholinesterase enzymes. The inhibition effect was slightly higher on AChE than BChE. The toxicity of heavy metal ions towards cholinesterase enzymes was found to decrease in the following orders: $Cd^{2+} > Ni^{2+} > Pb^{2+}$ for AChE and $Pb^{2+} > Cd^{2+} > Ni^{2+}$ for BChE.

The inhibition pattern of metal ions became obvious when the three-dimensional plot of residual activity of the enzymes is illustrated (see Figure 5.11). The areas of sensor responses to different heavy metal ions are well separated, so the three compounds can be easily distinguished according to their toxic level at different concentrations.
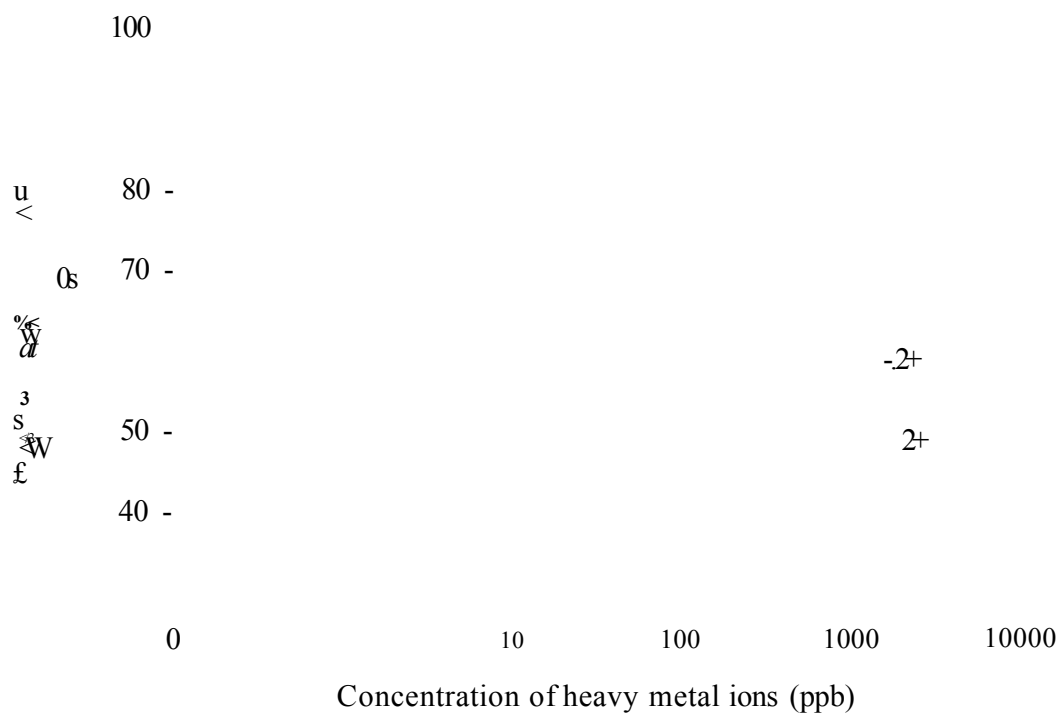
Figure 5.9. Residual activity of AChE as a function of the concentrations of the following heavy metal ions: lead (Pb2+), nickel (Ni2+) and cadmium (Cd2+).

85 -

80 -

75   •2+

70 -

65 -

60

55 -   2+

  100   1000   10000

Concentration of heavy metal ions (ppb)
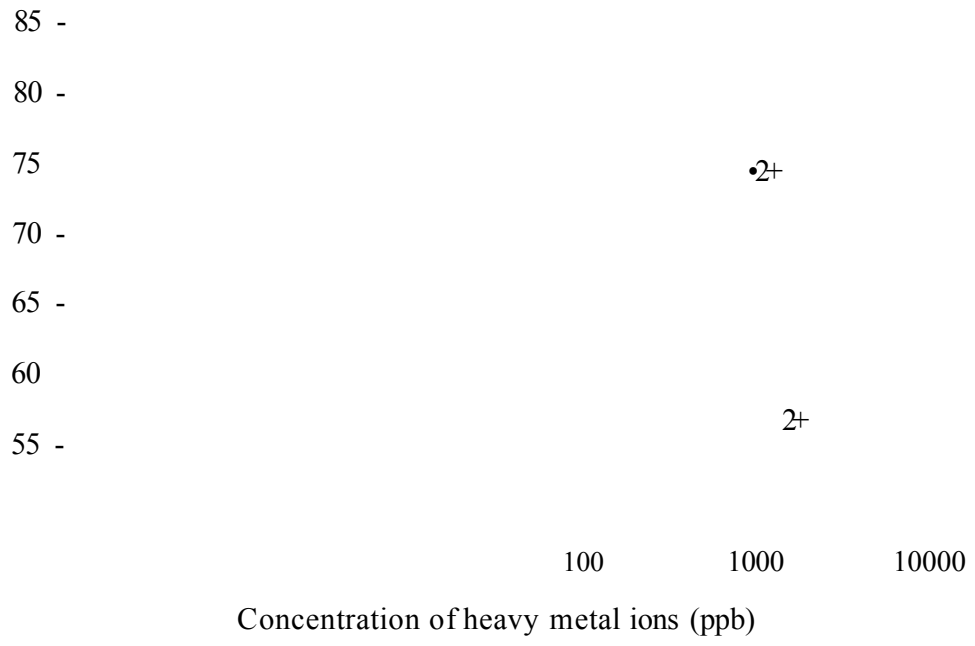
Figure 5.10. Residual activity of BChE as a function of the concentrations of the following heavy metal ions: lead (Pb2+), cadmium (Cd2+) and nickel (Ni2+).

Nickbl

Cadmium

TOO ppb

lOOOppb

1000 ppb
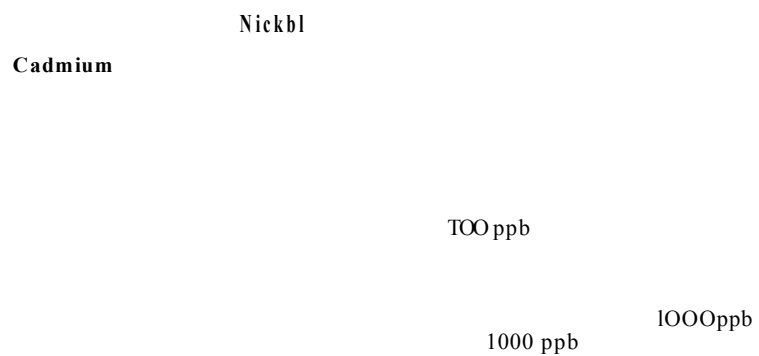
Figure 5.11. Residual activities of urease (ARy), AChE (ARa) and BChE (ARB) corresponding to different concentrations of heavy metal ions.

5.5 Simultaneous Registration of Pesticides using the Enzyme Sensor Array

This section presents the responses of the multi-channel enzyme sensor to the presence of traces of pesticides imidacloprid, DDVP and paraoxon. Data was obtained by simultaneous exposure of the three sensing channels of an enzyme sensor array to different concentration of pesticides in the range from 1 ppb to 1000 ppb. The sensitivity of the sensor array to the pesticide traces was then analysed according to the residual activities of enzymes in each channel.

Figure 5.12 shows the residual activities of enzymes after exposure to different concentrations of imidacloprid. The response of channel 2 produced a 100 % relative signal indicating that no inhibition of urease by imidacloprid was observed. The full recovery of the urease activity was found after rinsing the multi-channel flow cell with water. This result corresponds to the imidacloprid effect on urease obtained with a single channel sensor, as discussed in Section 5.2. At the same time, the reduction of the sensor response to imidacloprid was observed for the other two enzymes. The relative response of the sensors were found to decrease from 78.4 % to 49.6 % for AChE, and from 68.4 % to 37.0 % for BChE, as the concentration of imidacloprid increased from 1 ppb to 1000 ppb.

120

100 -

urease

80 -

AChE

40 -

BChE

20 -

100   1000   10000

Concentration of imidacloprid (ppb)
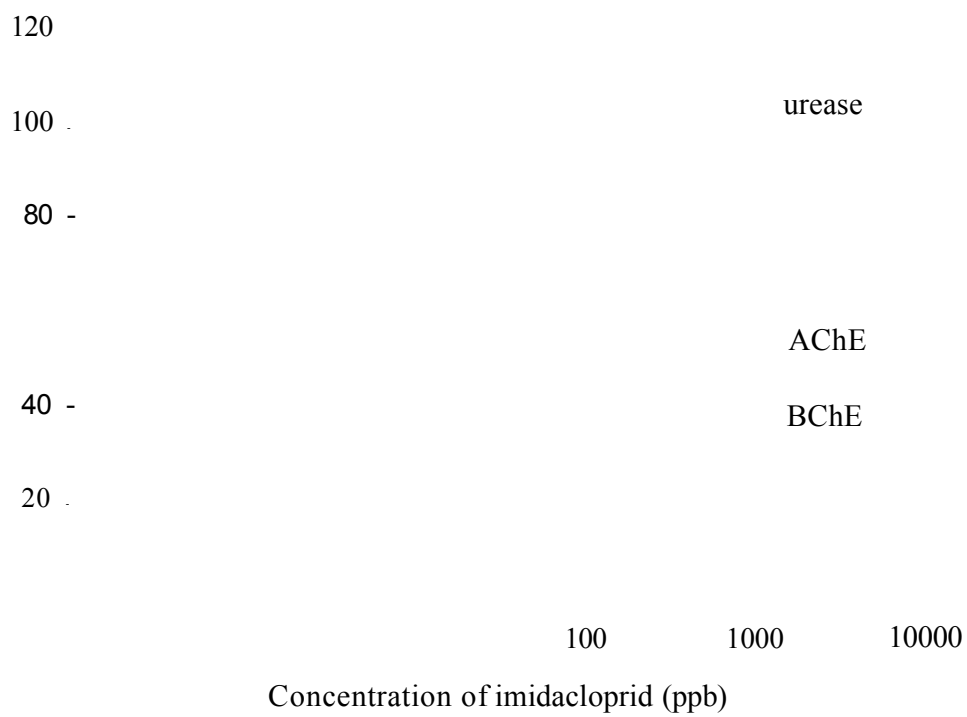
Figure 5.12. Residual activity of enzymes after inhibited by imidacloprid.

The residual activities of enzymes after their inhibition by DVDP pesticide is presented in Figure 5.13. Apparently, the urease activity was strongly suppressed by DVDP. In contrast to the effect of imidacloprid, the urease activity dropped from 42.9 % to 25.0 % due to the presence of 1 ppb to 1000 ppb of DVDP, respectively. In addition, the sensor responses were found to be much smaller than the response produced by nickel or cadmium ions on urease. DVDP was also found to be highly toxic for enzymes AChE and BChE. The residual activities of AChE and BChE decrease from 76.9 % to 45.4 % and from 52.4 % to 33.3 %, respectively, as the concentration of DVDP increase from 1 ppb to 1000 ppb.

Figure 5.14 presents the results of the inhibition effects of paraoxon. As could be seen, the highest inhibition effect of paraoxon was on the enzyme BChE, where the sensor responses were found to decrease from 62.5 % down to 40.6 %. In comparison to DVDP and imidacloprid, paraoxon showed a moderate inhibition effect on the enzyme urease. The residual activity of enzyme urease was found to decrease from 89.4 % down to 70.1 %, as paraoxon concentration increased from 1 ppb to 1000 ppb. On the other hand, the inhibition effect of paraoxon on AChE was similar to the effect of DVDP and imidacloprid. The residual activity of AChE decreased consistently from 72.5 % to 48.5 %, with the increases in the paraoxon concentration from 1 ppb to 1000 ppb.

It was observed that all pesticides studied have higher inhibition effects on BChE than AChE, and these results are in agreement with previously reported results [Arkhypova et al, 2001; Dzyadevych et al, 2005]. Regarding the effect of pesticides on urease, DVDP shows an unexpected result of a strong suppression of the urease activity as compared to other enzymes. This result contradicts the effect of paraoxon and imidacloprid on urease, as well as the result of the previous study [Starodub et al, 1999].

so

70

60

£ £ 50 "I   AChE

I 2 4 0

30   BChE

20 -=   urease

10

                    10   100   1000   10000

              Concentration of DVDP (ppb)
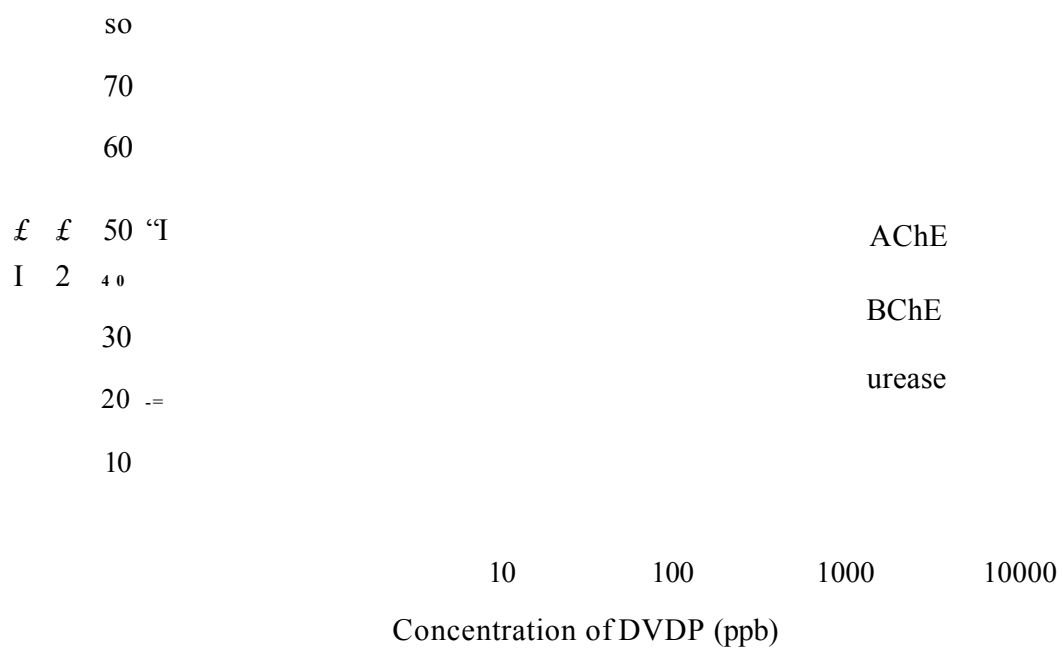
Figure 5.13. Residual activity of enzymes after inhibited by DVDP.

100

90 -

80 -

urease

60 -

50 -   AChE

40 -   BChE

100   1000   10000

Concentration of paraoxon (ppb)
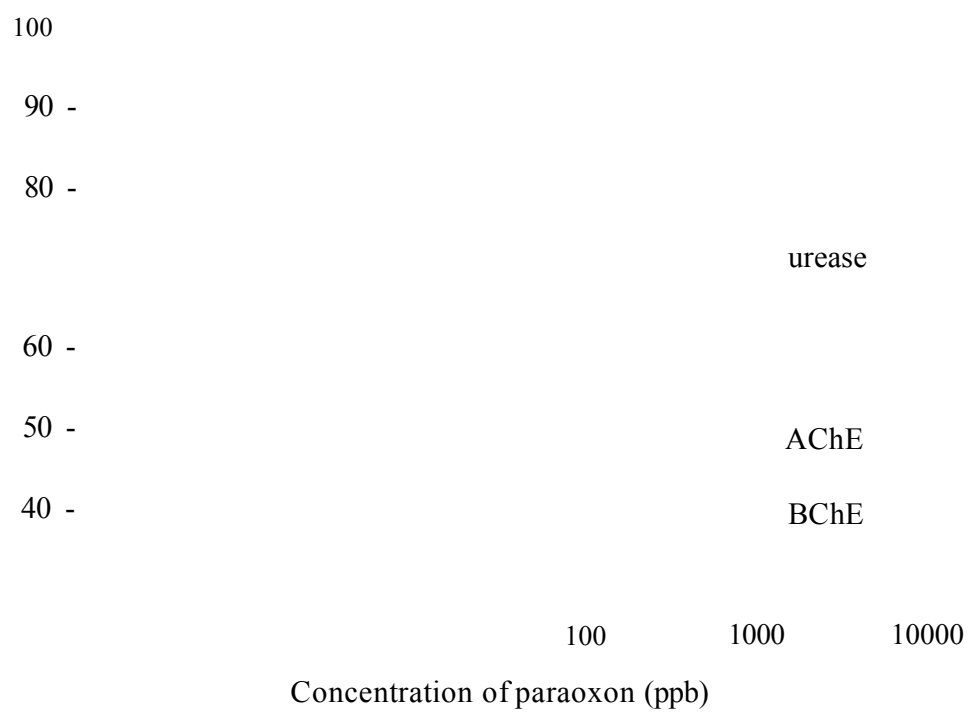
Figure 5.14. Residual activity of enzymes after inhibited by paraoxon.

The anamolous behaviour of DVDP may be attributed to the presence of traces of heavy metal ions in DVDP's sample solution. The obtained result showed that the multi-channel enzyme sensor is capable of detecting the effect of a mixture of pollutants on the enzymes activity, and this will be discussed in the following section.

5.6 Response of the Enzyme Sensor Array to the Binary Mixtures of Pollutants

The potential use of the enzyme sensor array for multi-analyte detection was investigated further in solutions containing binary mixtures of pollutants. Two types of sample solutions were prepared. The first sample was formed by mixing two pesticides solutions, paraoxon and imidacloprid, in different concentrations from 1 ppb to 1000 ppb (Mix1). The second sample consisted of the mixture of diluted solutions of paraoxon and cadmium ions (Mix2). Paraoxon was chosen as the basic pollutant in the mixtures, because of its moderate effect on the activity of the enzymes.

Experimental results show that the inhibition effect of Mix1 on AChE and BChE was higher than the effect of paraoxon or imidacloprid alone (Figure 5.15a and 5.15c). The residual activities of AChE and BChE were found to decrease from 53.2 % to 30.7 % and from 43.3 % to 25.7 %, respectively, as the concentration of paraoxon and imidacloprid in Mix1 increase from 1 ppb to 1000 ppb. On the other hand, the sensor responses on the inhibition of urease by Mix1 were found to be similar to the effect of paraoxon alone (Figure 5.15b). This result confirmed that imidacloprid did not inhibit urease and therefore the toxicity of Mix1 to urease was dominated by paraoxon.

100

Imidacloprid

40

Paraoxon

20

Mixl

100   1000   10000

Concentration of pollutants (ppb)

(a)

120

Imidacloprid

100

Paraoxon

Mixl

■D

100   1000   10000

Concentration of pollutants (ppb)

(b)

Imidacloprid

Paraoxon

Mixl

100   1000   10000
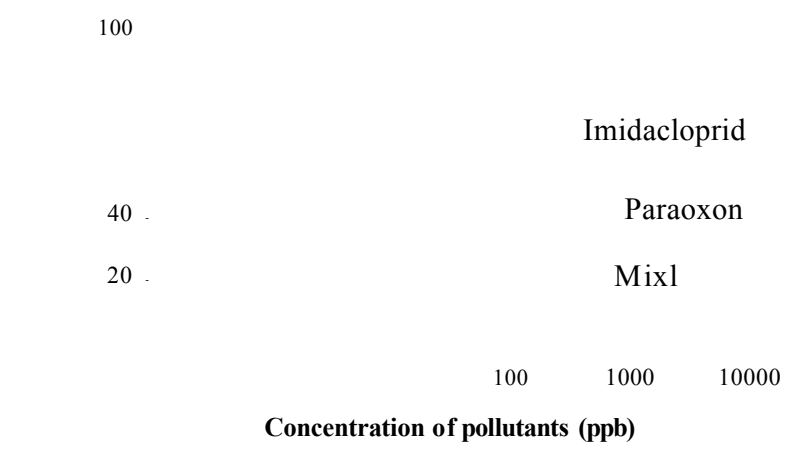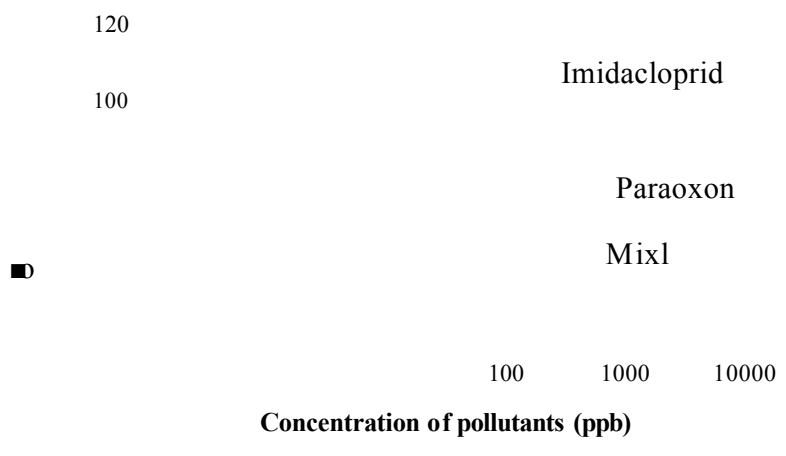
Concentration of pollutants (ppb)
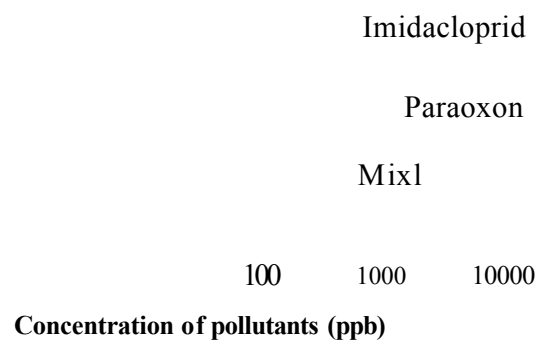
(C)

Figure 5.15. Residual activity of enzymes after exposed to Mixl.

The effects of Mix2 on the sensor response are summarised in Figure 5.16a to 5.16c. Different results for the sensor response were obtained when the enzymes were exposed to Mix2. As shown in Figure 5.16b, the mixture of paraoxon and cadmium ions strongly suppressed the urease activity. The inhibition of urease by Mix2 was slightly higher than that by cadmium ions. The residual activity of urease was found to decrease from 70.2 % to 37.1 %, as the concentration of paraoxon and cadmium ions in Mix2 increased from 1 ppb to 1000 ppb. The sensor responses on the inhibition of AChE and BChE by Mix2 were found to be similar to the effect of paraoxon alone (Figure 5.16a and 5.16c). Apparently, the presence of cadmium ions did not affect the activity of the cholinesterase enzymes. This result suggests that the residual activity of these enzymes was strongly affected by their most toxic pollutant present in the mixture solution. Therefore, in the binary mixture containing paraoxon and cadmium ions, sensor responses on the urease reaction were highly influenced by the cadmium ions, whereas the activities of the cholinesterase enzymes were strongly inhibited by paraoxon pesticide.

A similar pattern of inhibition by the mixture of pollutants was also demonstrated by Arkhypova et al [2001]. The inhibition of urease and the cholinesterase enzymes were found to be strongly affected by heavy metal ions and pesticides respectively, after being exposed to the mixtures containing pesticides (trichlorfon and carbofuran) and heavy metal ions (mercury and silver ions). Arkhypova et al [2001] also found that the combined inhibition effects of mixtures containing trichlorfon and carbofuran on BChE and AChE was higher than the effects of a single pesticide. This result corresponds to the combined inhibition effects of paraoxon and imidacloprid in Mix1 on the activity of BChE and AChE, as presented previously (see Figure 5.19).

100

80 -

Cadmium

60 -

Paraoxon

40 -

Mix2

100   1000   10000

Concentration of pollutants (ppb)

(a)

100

Paraoxon

Cadmium

Mix2

1   10   100   1000   10000

Concentration of pollutants (ppb)

(b)

100

Cadmium

Paraoxon

Mix2

100   1000   10000
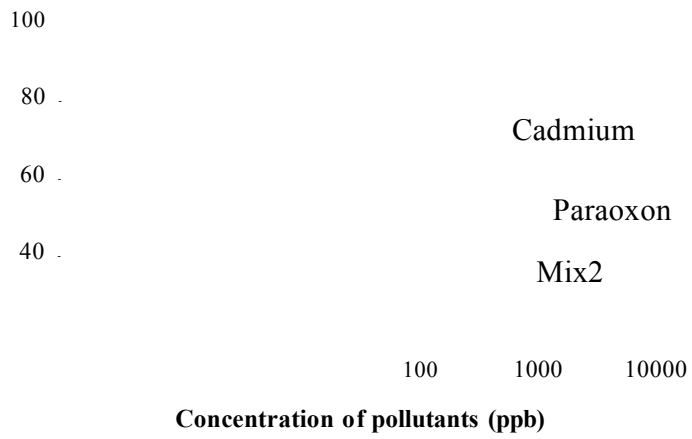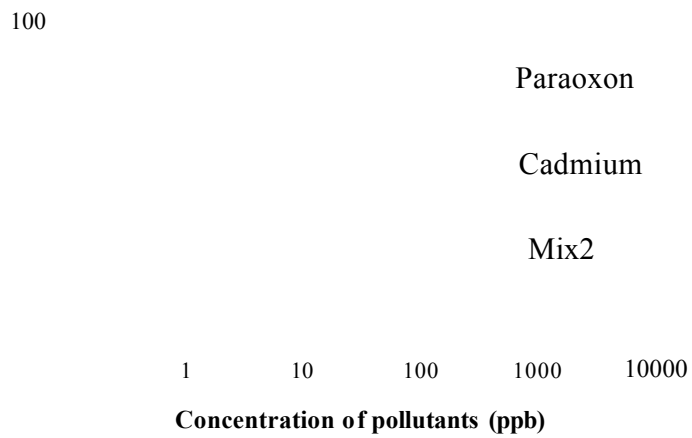
Concentration of pollutants (ppb)
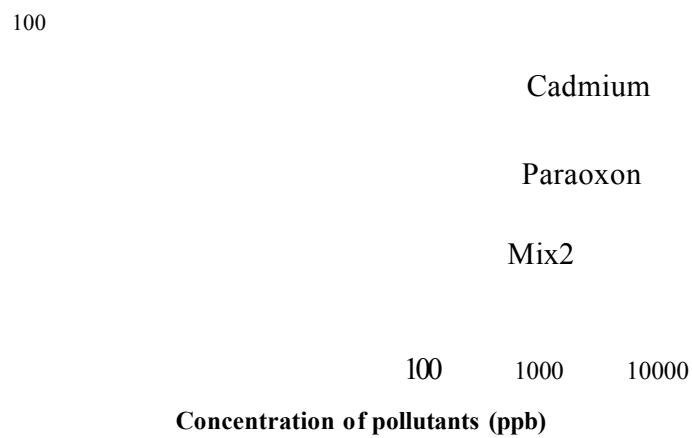
(C)

Figure 5.16. Residual activity of enzymes after exposed to Mix2.

A three-dimensional plot of the residual activity for the three enzymes (AChE, BChE, urease) shown in Figure 5.17, clearly illustrates the sensor array response to each pollutant and binary mixtures. The position of Mix1 (mixture of paraoxon and imidacloprid) was found close to the pesticide area, while the position of Mix2 (mixture of paraoxon and cadmium ions) was shifted towards heavy metal ions area. These plots demonstrated the dependence of both specificity and accuracy (in the determination of toxic agents) on the increase of the number of analyzing enzyme sensors. It also places the emphasis on the need to design a pattern recognition algorithm to enable identification of specific pollutants and their multi-component mixtures.

Nickel

Lead
⊢~*A*~
100. ppb

&- **Paraoxon**

ARA

DVDP
Paraoxon
Imidacloprid
Lead
Cadmium
Nickel
Mixl
Mix2
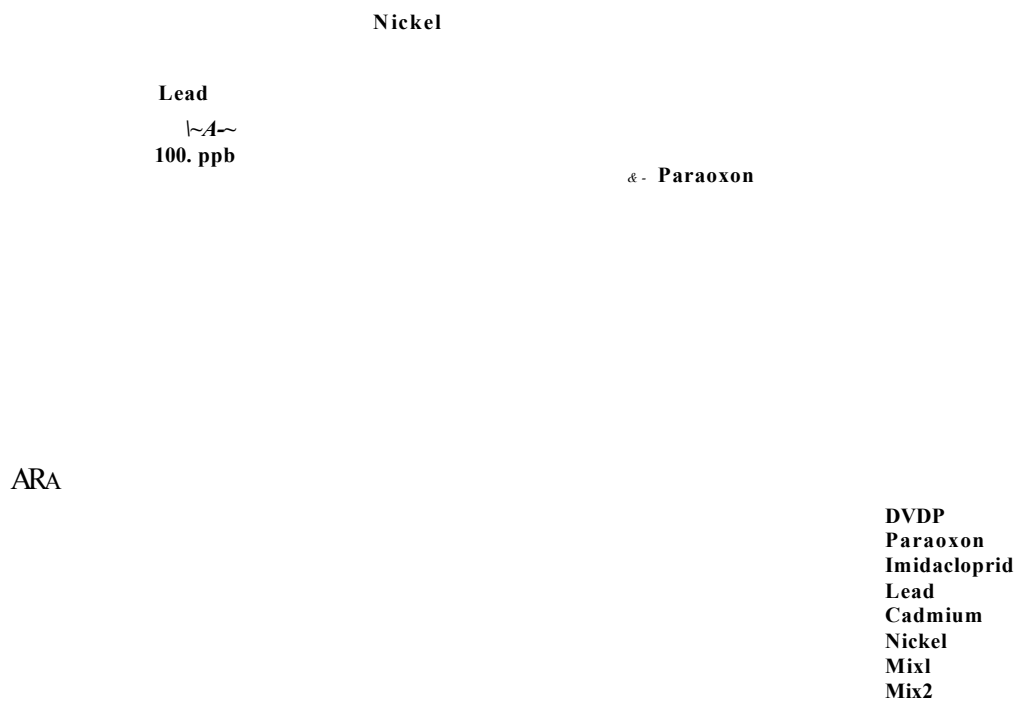
Figure 5.17. Residual activities of urease (ARu), AChE (ARA) and BChE (ARB) corresponding to the different concentrations of pollutants.

5.7 Analysis of Pollutants using Artificial Neural Network Algorithm

The experimental data presented previously shows a distinct pattern of sensor responses to certain pollutants in water. According to literature, such data patterns were treated by various pattern recognition algorithms including principal component analysis [Vlasov et al, 2000], partial least squares [Mortensen et al, 2000], multiple correspondence analysis [Arkhypova et al, 2001], multiple linear regression [Natale et al, 1997], and artificial neural networks [Bachmann and Schmid, 1999]. Among these methods, Shaffer et al [1999] demonstrated that the neural network based algorithms have the highest accuracy in classifying sets of data obtained from chemical sensor arrays.

Artificial neural network (ANN) also performed very well in solving overlapping signal distributions or difficult non-linear quantifications [Gutés et al, 2005]. A variety of applications that deployed ANN as a tool for multi-component analysis, have been reported particularly in chemical sensing and biosensing purposes. The examples of such applications are: the determination of pesticides using enzyme sensors and immunosensors [Bachmann et al, 2000; Reder et al, 2003], the classification of neurotoxins [Gholmieh et al, 2003], the analysis of ethanol-glucose mixtures [Lobanov et al, 2001] and the quantification of metals and inorganic pollutants in groundwaters [Rudnitskaya et al, 2001]. These complex analytical systems are sometimes defined as an 'electronic tongue' due to their capability to recognise both the quantitative and qualitative composition of solutions by mimicking the concept of human sensing [Vlasov et al, 2000].

Commonly, ANN consists of simple processing elements or 'neurons' grouped together to form three types of layers known as input, hidden and output layers (Figure 5.18). The neurons are linked with each other in a particular configuration, so that the output from neurons of one layer becomes the input to the neurons in the next layer. In each neuron, the input signal (x_i) is multiplied by a weight factor (w_i). The weighted input signals are added together and transferred to an activation function (F) that generates an output signal (y_{neu}) of a neuron. The activation function can have any form, from a pure linear dependence to an elaborate exponential function, like the hyperbolic tangent (tan-sigmoid) function:

$$F_{\text{tan-sigmoid}}(S) = [\exp(S) - \exp(-S)]/[\exp(S) + \exp(-S)] \tag{5.1}$$

in which

$$S = \sum_{i=1}^{p} w_i x_i \tag{5.2}$$

where S is the sum of p weighted input signals. ANN typically requires a large set of data and long training times. Generally, the networks are trained, so that a particular input leads to a specific target output. During training, the weights of the network are iteratively adjusted to minimize the average squared error between the network outputs (a) and the target outputs (t), normally known as mean square error (MSE):

$$\text{MSE} = \frac{1}{n}\sum_{i=1}^{n}(e_i)^2 = \frac{1}{n}\sum_{i=1}^{n}(t_i - a_i)^2 \tag{5.3}$$

where n is the total number of the network inputs.
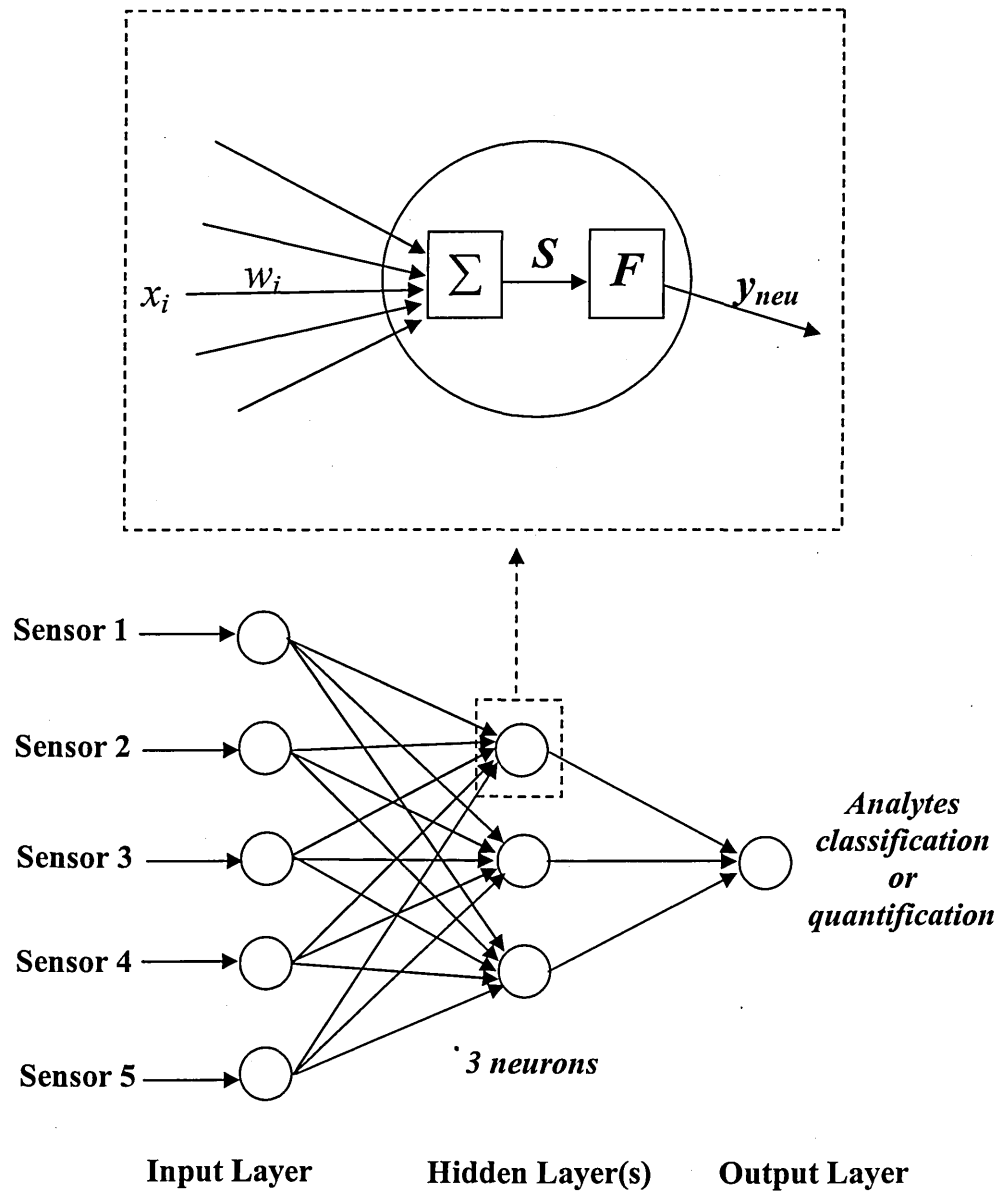
Figure 5.18. Typical computational neural network architecture.

The weights of the network are optimised by several different training algorithms, such as Levenberg-Marquardt [Shaffer et al, 1999; Natale et al, 1997], resilient backpropagation [Bachmann et al, 2000; Lobanov et al, 2001], scaled conjugate gradient [Reder et al, 2003] and Bayesian regularization [Gutés et al, 2005] algorithms.

Based on its adaptability in the sensing application, ANN was implemented as a pattern recognition tool for data analysis of the developed multi-channel enzyme sensor. MATLAB software (version 6.1, Mathworks, Natick, MA) was employed for the ANN modelling, using the supplied functions and algorithms in MATLAB Neural Network Toolbox (version 4.0, Mathworks, Natick, MA). Prior to ANN processing, the experimental results from the repeated measurements were divided into two data sets, which were used for training and testing of the network models. Table 5.2 shows the data set applied for the network training in order to identify the pollutants. The ANN training procedure exploited the Levenberg-Marquardt algorithm to optimize the weights of a hidden layer. This algorithm appeared to be the fastest method for the network training using the limited experimental data of this study. The training was performed for 10000 epochs (repetitions) with the error (*mse*) goal set to 1×10^{-10}. The neural network models, which produced the minimum error for each training run, were selected for processing the cumulative data of the sensor array.

For qualitative and quantitative analysis, nine separate network models were produced and trained as described above. One of the neural networks was used to classify the pollutants. This contained seven neurons in the hidden layer, as illustrated in Figure 5.19. The number of neurons in the input layer was set to three, equal to the number of channels in the sensor array. Three neurons in the output layer were used to describe a three-digit binary code, representing the type of pollutants (see Table 5.2).

Table 5.2. Data set for training the neural network to classify the pollutants.

Concentration of pollutants (ppb) [a]						Input value			Set output (target) value		
Pb^{2+}	Cd^{2+}	Ni^{2+}	DP	Para	Imid	R_A, %	R_U, %	R_B, %	(Binary code)		
1	0	0	0	0	0	90.5	40.2	78.3	0	0	1
0	1	0	0	0	0	81.2	75	87.4	1	0	0
0	0	1	0	0	0	81.7	60.2	87.9	1	0	1
0	0	0	1	0	0	76.9	42.9	52.4	0	0	0
0	0	0	0	1	0	72.5	89.4	62.5	0	1	0
0	0	0	0	0	1	78.4	100	68.4	0	1	1
0	0	0	0	1	1	53.2	87.4	43.3	1	1	0
0	1	0	0	1	0	68.1	70.2	61	1	1	1
10	0	0	0	0	0	81.1	37.6	71.4	0	0	1
0	10	0	0	0	0	77.7	70.3	83.1	1	0	0
0	0	10	0	0	0	77.1	52.6	83.3	1	0	1
0	0	0	10	0	0	66.7	35.7	47.2	0	0	0
0	0	0	0	10	0	63.6	85.9	57.1	0	1	0
0	0	0	0	0	10	72	100	61.4	0	1	1
0	0	0	0	10	10	45.1	81.8	37.8	1	1	0
0	10	0	0	10	0	60.3	62.6	53.7	1	1	1
100	0	0	0	0	0	72.3	26.2	66.7	0	0	1
0	100	0	0	0	0	71.4	57.1	72.4	1	0	0
0	0	100	0	0	0	71.7	39.2	77.8	1	0	1
0	0	0	100	0	0	59.8	32.1	40.9	0	0	0
0	0	0	0	100	0	56.7	78.3	47.3	0	1	0
0	0	0	0	0	100	66	100	49.6	0	1	1
0	0	0	0	100	100	38.6	77.3	31.5	1	1	0
0	100	0	0	100	0	55.8	53.2	47.3	1	1	1
1000	0	0	0	0	0	50.1	19.6	58.3	0	0	1
0	1000	0	0	0	0	62.5	42.9	66.7	1	0	0
0	0	1000	0	0	0	61.5	31.1	66.7	1	0	1
0	0	0	1000	0	0	45.4	25	33.3	0	0	0
0	0	0	0	1000	0	48.5	70.1	40.6	0	1	0
0	0	0	0	0	1000	49.6	100	37.1	0	1	1
0	0	0	0	1000	1000	30.7	67.3	25.7	1	1	0
0	1000	0	0	1000	0	42.8	37.1	37.9	1	1	1

[a] DP for DVDP, Para for paraoxon and Imid for imidacloprid.

Input Layer **Hidden Layer** **Output Layer**

Residual activities of enzymes $\{ R_A, R_U, R_B$

Represent the type of pollutant

0
1
0
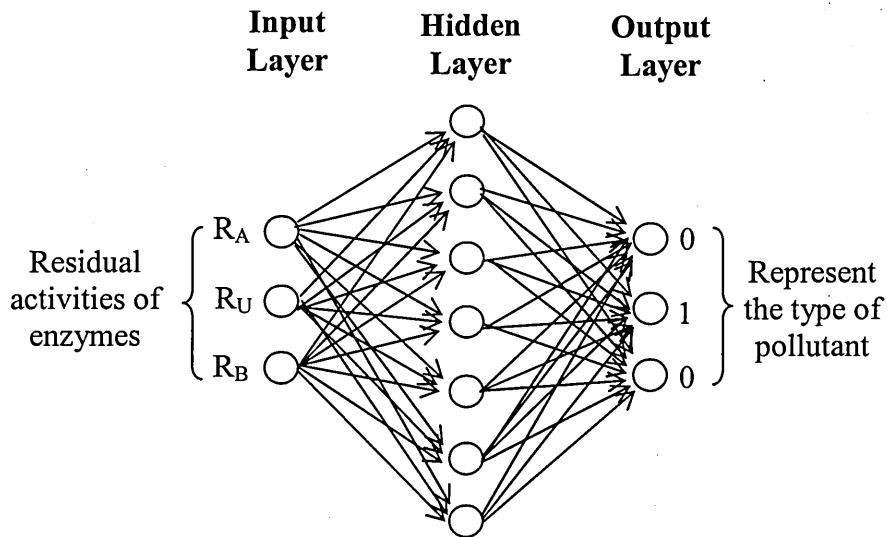
Neural network architecture for classifying the pollutants

Residual actiities of enzymes $\{ R_A, R_U, R_B$

Concentration of DVDP, lead and imidacloprid
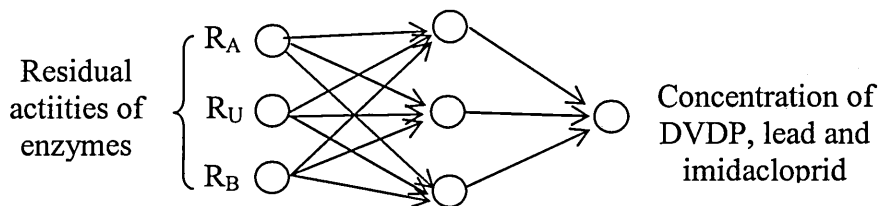
Neural network architecture for quantifying DVDP, Lead and Imidacloprid

Residual activities of enzymes $\{ R_A, R_U, R_B$

Concentration of cadmium, nickel, paraoxon, Mix1 and Mix2
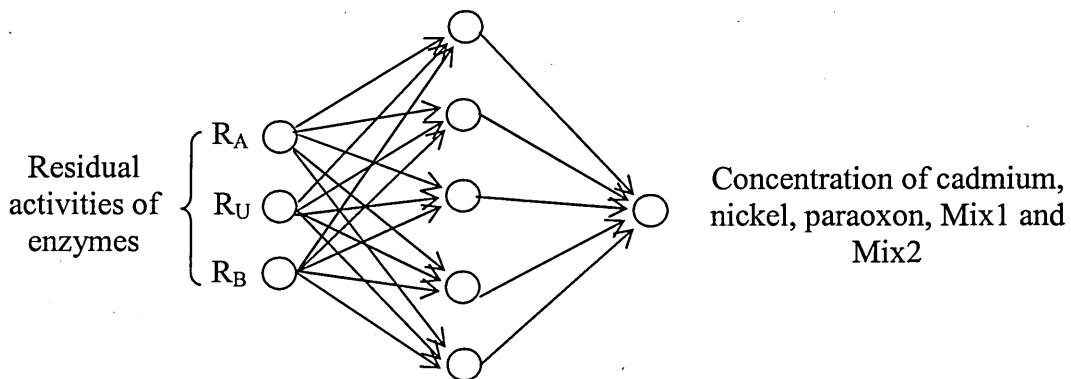
Neural network architecture for quantifying cadmium, nickel, paraoxon, Mix1 and Mix2

Figure 5.19. The architecture of the neural network algorithm after optimisation.

The other eight network models were designed to quantify each pollutant (cadmium, lead, nickel, imidacloprid, DVDP and paraoxon) and two binary mixtures (Mix1 and Mix2). The topology of these network models consisted of three and one neuron in the input and output layer, respectively. The number of neurons in the hidden layer was either three or five depending on the type of target pollutants (see Figure 5.19). A hyperbolic tangent was used as the activation function for the hidden neurons, and a log-sigmoid function was used for the output neurons in all nine neural network models.

The results of pollutants classification achieved with the neural network algorithms are shown in Table 5.3. The precision of the network model was evaluated using 22 randomly selected experimental data points. This test shows that 91 % of the test data was correctly classified. False classifications occurred during the determination of 1 ppb of paraoxon and 1000 ppb of Mix1 (mixture of paraoxon and imidacloprid). Classified pollutants were then quantified using the optimized individual network algorithm. The results were reasonable since the network models were trained using a limited amount of data. As shown in Figure 5.20, a high correlation between the target and evaluated concentration of pollutants was observed with an acceptable average error of 6.24 %. The successful classification and quantification of randomly selected data sets proves that the neural network models were able to generalize the information given and could be used to analyse unknown compounds or their mixtures, assuming that they belong to the group of six analytes used to build the models.

Table 5.3. Classification of selected pollutants by the neural network model.

Input value			Results				
R_A, %	R_U, %	R_B, %	Binary code			Pollutant	Accuracy
70.8	58.2	73.3	1	0	0	Cadmium	True
73.4	88.7	61.4	1	1	0	Mix1	False (Paraoxon)[a]
71.1	27.4	67.4	0	0	1	Lead	True
77.9	53.1	83.3	1	0	1	Nickel	True
60.2	31.4	42	0	0	0	DVDP	True
49.4	70.8	41	0	1	0	Paraoxon	True
37.4	76.8	32.7	1	1	0	Mix1	True
48.2	100	37.8	0	1	1	Imidacloprid	True
67.4	70.9	61.8	1	1	1	Mix2	True
65.3	36.2	48.1	0	0	0	DVDP	True
81	60.9	88.7	1	0	1	Nickel	True
56.3	54.7	48.5	1	1	1	Mix2	True
79.2	36.1	72.1	0	0	1	Lead	True
75.2	100	69	0	1	1	Imidacloprid	True
81.8	76.5	87	1	0	0	Cadmium	True
31.2	68.1	25.1	0	1	0	Paraoxon	False (Mix1)[a]
64.3	85.1	58.2	0	1	0	Paraoxon	True
44.7	24.1	33.9	0	0	0	DVDP	True
73	40.7	78.5	1	0	1	Nickel	True
78.9	71.1	82.5	1	0	0	Cadmium	True
77.3	57.7	46.7	0	1	0	Paraoxon	True
82.7	46.8	38.1	1	1	0	Mix1	True

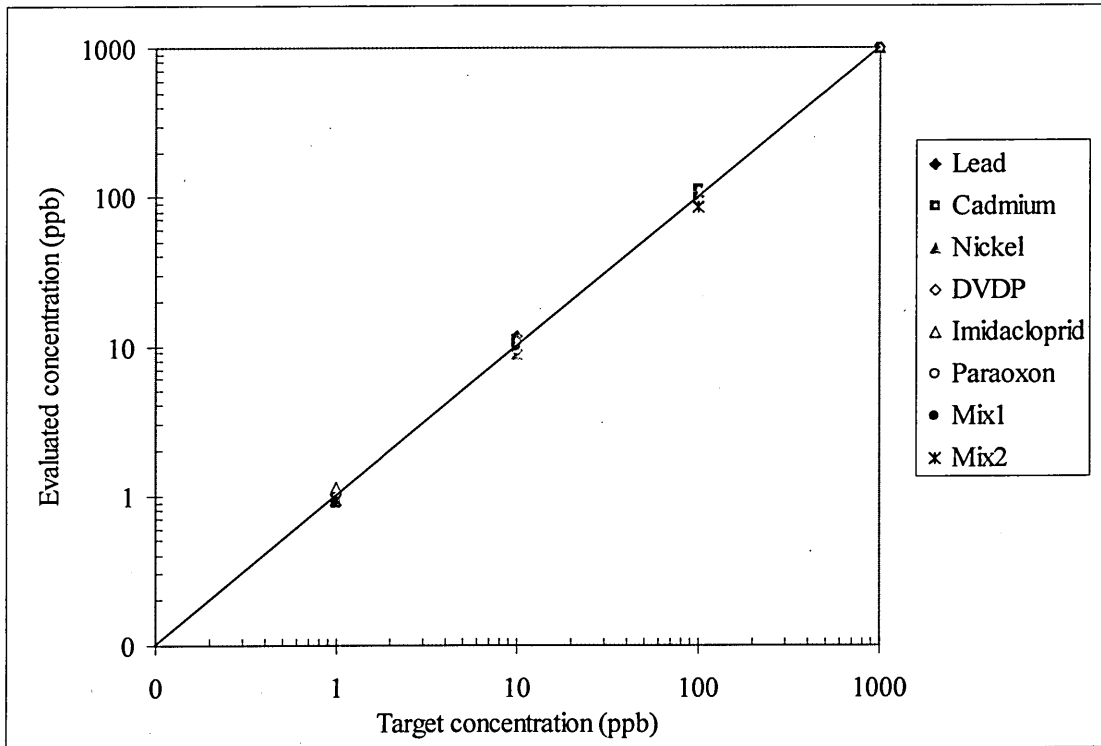[a] Parenthetical compound is the expected pollutant

162

Figure 5.20. Precision of the neural network algorithm in quantifying the pollutants.

163

5.8 Summary

The performance of the developed planar waveguide enzyme sensor as a multi-analyte detector was successfully tested with six types of pollutants. A series of experiments were conducted according to the measurement routine that separates the inhibition process and the evaluation of the enzymes activity. The reliability of the sensor responses was achieved using the relative changes in the sensor output signal, calculated from the ratio of the enzymes activity before and after the inhibition process. The relative responses to the effect of each pollutant on three types of enzymes (urease, AChE and BChE) were registered simultaneously using three sensing channels of the enzyme sensor array.

The analysis on the experimental results demonstrated that the multi-channel enzyme sensor was able to produce adequate responses to the presence of pollutants, in the concentration range from 1 ppb to 1000 ppb. Furthermore, the results showed that it was possible to discriminate each pollutant and two binary mixtures due to their different levels of inhibition on the activity of the enzymes. This has emphasised the implementation of the artificial neural network algorithm as a tool for the analysis of the distinct pattern of sensor responses. Despite a rather small amount of experimental data, the trained neural networks were able to classify and quantify the pollutants with acceptable errors of less than 10 %. More accurate and reliable results could be obtained by increasing the number of experimental data for each toxic agent and their mixtures.

CHAPTER 6

CONCLUSIONS AND RECOMMENDATIONS

6.1 Thesis Conclusions

The development of an optical enzyme sensor for in-situ monitoring of heavy metal ions and pesticides in water was the subject of study in this thesis. The research concentrated on the exploitation of light propagation in a SiO_2/Si_3N_4 planar waveguide as the optical transducing technique. According to literature, such planar waveguides were used as total internal reflection fluorescence and interferometer transducers for affinity biosensors. This present research work has expanded the implementation of these planar waveguides by utilizing them as attenuated total reflection (ATR) transducers for enzyme sensors. The formation of sensor sensitive membranes was realized with the universal polyelectrolyte self-assembly (PESA) deposition technique.

Multi-functional nanocomposite PESA membranes containing pairs of indicator/enzyme, such as CTCT/urease, CTCT/acetylcholine esterase and CTCT/butyrylcholine esterase were successfully deposited on the silicon nitride surface of the planar waveguide. The membranes produced were very stable, so that chromophore molecules cannot be washed out. On the other hand, the polymer matrix of the membrane was porous and hydrophilic enough to provide good permeation of small analyte molecules in aqueous solution. Study on enzyme reactions proved that the PESA method provides a natural environment for the enzymes encapsulated within the polymer matrix.

The experimental set-up of the enzyme sensor was based on end-fire coupling of an elliptical light beam to the edge of the planar waveguide. The intensity of light propagating in the planar waveguide was found to be adequate for in-situ monitoring of the deposition of PESA membranes. The initial light intensity was attenuated by a factor of 10 after the deposition of four CTCT/poly(allylamine hydrochloride) layers, and the normalised attenuation ratio $\frac{\Delta I}{I_o}$ was found to be 0.4 per layer. This large optical attenuation was 3 orders of magnitude greater than that in UV-visible spectroscopy.

This study has also found that a single channel enzyme sensor was able to register some specific bio-chemical reactions within the deposited PESA membrane on the planar waveguide sensing window. Individual enzyme reactions, as well as their inhibition by the toxic agents, were successfully registered by monitoring the changes in the intensity of light coming out from the planar waveguide. The presence of 1 ppb of cadmium and lead ions in sample solutions was successfully demonstrated. This result proved that the combination of a highly sensitive ATR technique and the superior PESA immobilisation method has substantially enhanced the performance of optical enzyme sensors.

The success of a single channel enzyme sensor has motivated the design and development of a laboratory scale enzyme sensor array. The experimental set-up was based on a single light stripe focused and coupled into the planar waveguide attached to a multi-channel reaction cell. The light was guided to excite the sensing windows of each channel in series by using a specially designed shutter. The feasibility of the multi-channel enzyme sensor towards the registration of three enzyme reactions simultaneously was proved by several tests. The response of each channel was found to be 100 times higher than the background signal. It showed that the enzyme sensor array

166

had sufficient dynamic range for the registration of the suppressed responses caused by pollutants.

The experimental results demonstrated that the multi-channel enzyme sensor was able to register six different pollutants belonging to two groups, namely heavy metal ions (cadmium, lead and nickel) and pesticides (imidacloprid, paraoxon and DVDP), in a concentration range from 1 ppb to 1000 ppb. The pollutants exhibited different levels of inhibition on the activity of the enzymes. A general discrimination between the pollutants was possible by plotting a three-dimensional graph of the residual activity of three enzymes (acetylcholine esterase, butyrylcholine esterase, and urease). The distinct pattern of sensor responses was analysed further by the implementation of artificial neural network algorithm. Despite the rather small amount of experimental data, the trained neural networks were able to classify and quantify the pollutants with an acceptable average accuracy of 6.24 %.

6.2 Recommendations for Future Work

Although considerable time and efforts were spent during this study for the development of the optical enzymes sensors, it was only a small part of a huge of work towards the development of a prototype biosensor device. In order to overcome certain limitations and to ensure the ability of the optical enzyme sensor for monitoring water pollutants in a real environment, further work needs to be done.

1. To use a large variety of pollutants concentrations as compared to the present study which only involving 1, 10, 100 and 1000 ppb, in order to have a better view on the distribution range of the sensor sensitivity.

2. To expose the optical enzyme sensor to more complex pollutant mixtures in order to further evaluate the ability of the sensor system to identify and quantify different type of pollutants.

3. To compare the acquired data with the results of any conventional analytical techniques, such as mass-spectrometry or liquid chromatography in order to verify the sensor performance.

4. To investigate the reversibility of the enzyme sensors after the inhibition by heavy metal ions and pesticides, using ethylene diamine tetra acetic acid (EDTA) and pyridine-2-aldoxime methiodide (PAM) as recovery agents for urease and cholinesterase enzymes, respectively.

5. To integrate the pattern recognition algorithm with the sensor array set-up in order to have simultaneous in-situ monitoring and analysis of pollutants in aqueous solutions.

6. To explore the possibility to miniaturize the multi-channel enzyme sensor set-up, for example, by using an LED array as the light source or a CCD array as the photodetector.

REFERENCES

Ali, M. B., Abdelghani, A., Ouada, H. B., Jaffrezic-Renault, N., and Lamartine, R., 2002, *Optical and electrochemical studies of thiacalix[4]arene film supported on Si/SiO₂ for ion-sensitive sensor*, Materials Science and Engineering: C, Volume 21, pp. 29-34.

Andreescu, S., Barthelmebs, L., and Marty, J. L., 2002, *Immobilization of acetylcholinesterase on screen-printed electrodes: comparative study between three immobilization methods and applications to the detection of organophosphorus insecticides*, Analytica Chimica Acta, Volume 464, pp. 171–180.

Andres, R. T., and Narayanaswamy, R., 1997, *Fibre-optic pesticide biosensor based on covalently immobilized acetylcholinesterase and thymol blue,* Talanta, Volume 44, pp. 1335-1352.

Angelino, S., and Gennaro, M. C., 1997, *An ion interaction RP-HPLC method for the determination of the eleven EPA priority pollutant phenols*, Analytica Chimica Acta, Volume 346, pp. 61-71.

Ariga, K., Lvov, Y., and Kunitake, T., 1997, *Assembling alternate dye-polyion molecular films by electrostatic layer-by-layer adsorption*, J. Am. Chem. Soc., Volume 119, pp. 2224-2231.

Arkhypova, V. N., Dzyadevych, S. V., Soldatkin, A. P., El'skaya, A. V., Jaffrezic-Renault, N., Jaffrezic, H., and Martelet, C., 2001, *Multibiosensor based on enzyme inhibition analysis for determination of different toxic substances*, Talanta, Volume 55, pp. 919-927.

Bachmann, T. T., and Schmid, R. D., 1999, *A disposable multielectrode biosensor for rapid simultaneous detection of the insecticides paraoxon and carbofuran at high resolution*, Analytica Chimica Acta, Volume 401, pp. 95-103.

Bachmann, T. T., Leca, B., Vilatte, F., Marty, J. L., Fournier, D. and Schmid, R. D., 2000, *Improved multianalyte detection of organophosphates and carbamates with disposable multielectrode biosensors using recombinant mutants of Drosophila acetylcholinesterase and artificial neural networks*, Biosensors and Bioelectronics, Volume 15, pp. 193-201.

Baronian, K. H. R., 2004, *The use of yeast and moulds as sensing elements in biosensors*, Biosensors and Bioelectronics, Volume 19, pp. 953-962.

Barzen, C., Brecht, A., and Gauglitz, G., 2002, *Optical multiple-analyte immunosensor for water pollution control*, Biosensors and Bioelectronics, Volume 17, pp. 289-295.

Bernabei, M., Chiavarini, S., and Cremisini, C., 1993, *Anticholinesterase activity measurement by a choline biosensor: application in water analysis*, Biosensors & Bioelectronics, Volume 8, pp. 265-271.

Bisenberger, M., Brächle, C., and Hampp, N., 1995, *A triple-step potential waveform at enzyme multisensors with thick-film gold electrodes for detection of glucose and sucrose*, Sensors and Actuators B: Chemical, Volume 28, pp. 181-189.

Bonnet, C., Andreescu, S., and Marty, J. L., 2003, *Adsorption: an easy and efficient immobilisation of acetylcholinesterase on screen-printed electrodes*, Analytica Chimica Acta, Volume 481, pp. 209-211.

Bovanova, L., and Brandsteterova, E., 2000, *Direct analysis of food samples by high-performance liquid chromatography*, Journal of Chromatography A, Volume 880, pp. 149-168.

Brosinger, F., Freimuth, H., Lacher, M., Ehrfeld, W., Gedig, E., Katerkamp, A., Spener, F., and Cammann, K., 1997, *A label-free affinity sensor with compensation of unspecific protein interaction by a highly sensitive integrated optical Mach-Zehnder interferometer on silicon*, Sensors and Actuators B: Chemical, Volume 44, pp. 350-355.

Campanella, L., Favero, G., Sammartino, M. P., and Tomassetti, M., 1998, *Further development of catalase, tyrosinase and glucose oxidase based organic phase enzyme electrode response as a function of organic solvent properties*, Talanta, Volume 46, pp. 595-606.

Caruso, F., Niikura, K., Furlong, D. N., Okahata, Y., 1999, *Assembly of alternating polyelectrolyte and protein multilayer films for immunosensing*, Langmuir, Volume 13, pp. 3427-3433.

Choi, J. W., Min, J., Jung, J. W., Rhee, H.W., and Lee, W. H., 1998, *Fiber-optic biosensor for the detection of organophosphorus compounds using AChE-immobilized viologen LB films*, Thin Solid Films, Volumes 327-329, 31, pp. 676-680.

Choi, J. W., Kim, Y. K., Lee, I. H., Min, J., and Lee, W. H., 2001, *Optical organophosphorus biosensor consisting of acetylcholinesterase/viologen hetero Langmuir-Blodgett film*, Biosensors & Bioelectronics, Volume 16, pp. 937-943.

Cobben, P. L. H. M., Egberink, R. J. M., Bomer, J. G., Bergveld, P., Verboom, W., Reinhoudt, D. N., 1992, *Transduction of selective recognition of heavy metal ions by chemically modified field effect transistors (CHEMFETs)*, J. Am. Chem. Soc., Volume 114, pp. 10573-10582.

Cooper, M., Campbell, A. L., and Crane, R. L., 1995, *Formation of polypeptide-dye multilayers by an electrostatic assembly technique*, Langmuir, Volume 11, pp. 2713-2718.

Cox, C., 2001, *Imidacloprid*, Journal of Pesticide Reform, Volume 21, pp. 15-21.

Choquette, S. J., Locascio-Brown, L., Durst, R. A., 1992, *Planar waveguide immunosensor with fluorescent liposome amplification*, Analytical Chemistry, Volume 64, pp. 55-60.

Cremisini, C., Sario, S. D., Mela, J., Pilloton, R., and Palleschi, G., 1995, *Evaluation of the use of free and immobilised acetylcholinesterase for paraoxon detection with an*

amperometric choline oxidase based biosensor, Analytica Chimica Acta, Volume 311, pp. 273-280.

Davis, J., Vaughan, D. H., and Cardosi, M. F., 1995, *Elements of biosensor construction, Enzyme and Microbial Technology*, Volume 17, pp. 1030-1035.

Decher, G., Hong, J.-D., and Schmitt, J., 1992, *Buildup of ultrathin multilayer films by a self-assembly process: III. Consecutively alternating adsorption of anionic and cationic polyelectrolytes on charged surfaces*, Thin Solid Films, Volume 210/211, pp. 831-835.

Decher, G., Lehr B., Lowack, K., Lvov, Y., and Schmitt, J., 1994, *New nanocomposite films for biosensors: layer-by-layer adsorbed films of polyelectrolytes, proteins or DNA,* Biosensors and Bioelectronics, Volume 9, pp 677-684.

Decher, G., 1997, *Fuzzy nanoassemblies: Toward layered polymeric multicomposites*, Science, Volume 277, pp.1232-1237.

DeGrandpre, M. D., Burgess, L. W., 1988, *Long path fiber-optic sensor for evanescent field absorbance measurements*, Analytical Chemistry,Volume 60, pp. 2582-2586.

DeGrandpre, M. D., Burgess, L. W., White, P. L., Goldman, D. S., 1990, *Thin film planar waveguide sensor for liquid phase absorbance measurements*, Analytical Chemistry,Volume 62, pp. 2012-2017.

Doong, R. A., and Tsai, H. C., 2001, *Immobilization and characterization of sol-gel-encapsulated acetylcholinesterase fiber-optic biosensor*, Analytica Chimica Acta, Volume 434, pp. 239-246.

Duveneck, G. L., Abel, A. P., Bopp, M. A., Kresbach, G. M. and Ehrat, M., 2002, *Planar waveguides for ultra-high sensitivity of the analysis of nucleic acids,* Analytica Chimica Acta, Volume 469, pp. 49-61.

Dzyadevych, S. V., Soldatkin, A. P., Arkhypova, V. N., V. El'skaya, A., Chovelon, J. M., Georgiou, C. A., Martelet, C., and Jaffrezic-Renault, N., 2005, *Early-warning electrochemical biosensor system for environmental monitoring based on enzyme inhibition, Sensors and Actuators B*: Chemical, Volume 105, pp. 81-87.

Farré, M., and Barceló, D., 2003, *Toxicity testing of wastewater and sewage sludge by biosensors, bioassays and chemical analysis*, TrAC Trends in Analytical Chemistry, Volume 22, pp. 299-310.

Fattinger, Ch., Koller, H., Schlatter, D., and Wehrli, P., 1993, *The difference interferometer: a highly sensitive optical probe for quantification of molecular surface concentration*, Biosensors and Bioelectronics, Volume 8, pp. 99-107.

Galassi, S., Mingazzini, M., and Battegazzore, M., 1993, *The use of biological methods for pesticide monitoring*, The Science of the Total Environment, Volume 132, pp. 399-414.

Gholmieh, G., Courellis, S., Fakheri, S., Cheung, E., Marmarelis, V., Baudry, M., and Berger, T., 2003, *Detection and classification of neurotoxins using a novel short-term plasticity quantification method*, Biosensors and Bioelectronics, Volume 18, pp. 1467-1478.

Gonzalez-Martinez, M. A., Puchades, R., and Maquieira, A., 2001, *Comparison of Multianalyte Immunosensor Formats for On-Line Determination of Organic Compounds*, Anal. Chemistry, Volume 73, pp. 4326-4332.

Gutés, A., Céspedes, F., Alegret, S. and Valle, M. D., 2005, *Determination of phenolic compounds by a polyphenol oxidase amperometric biosensor and artificial neural network analysis*, Biosensors and Bioelectronics, Volume 20, pp. 1668-1673.

Hamlaoui, M. L., Reybier, K., Marrakchi, M., Jaffrezic-Renault, N., Martelet, C., Kherrat, R., and Walcarius, A., 2002, *Development of a urea biosensor based on a polymeric membrane including zeolite*, Analytica Chimica Acta, Volume 466, pp. 39-45.

Hämmerle, M., and Hall, E. A. H., 1996, *Electrochemical enzyme sensor for formaldehyde operating in the gas phase*, Biosensors and Bioelectronics, Volume 11, pp.239-246.

Heideman, R. G., Kooyman, R. P. H., and Greve, J., 1991, *Development of an optical waveguide interferometric immunosensor,* Sensors and Actuators B: Chemical, Volume 4, pp. 297-299.

Heideman, R. G., Kooyman, R. P. H., and Greeve, J., 1993, *Performance of a highly sensitive optical waveguide Mach-Zehnder immunosensor*, Sensors and Actuators B, Volume 10, pp. 209-217.

Heideman, R. G., Kooyman, R. P. H., and Greve, J., 1994, *Immunoreactivity of adsorbed anti human chorionic gonadotropin studied with an optical waveguide interferometric sensor*, Biosensors and Bioelectronics, Volume 9, pp. 33-43.

Iler, R. K., 1966, *Multilayers of colloidal particles*, J. Colloid Interface Science, Volume 21, pp. 569-594.

Ivanov, A. N., Evtugyn, G. A., Gyurcsányi, R. E., Tóth, K., and Budnikov, H. C., 2000, *Comparative investigation of electrochemical cholinesterase biosensors for pesticide determination*, Analytica Chimica Acta, Volume 404, pp 55-65.

Jeanty, G., and Marty, J. L., 1998, *Detection of paraoxon by continuous flow system based enzyme sensor*, Biosensors & Bioelectronics, Volume 13, pp. 213-218.

Kasap, S. O., 2001, *Optoelectronic and photonics : principles and practices*, Prentice Hall, Upper Saddle River, NJ, pp. 50-98.

Karube, I., and Nomura, Y., 2000, *Enzyme sensors for environmental analysis*, Journal of Molecular Catalysis B: Enzymatic, Volume 10, pp. 177-181.

Klotz, A., Brecht, A., Barzen, C., Gauglitz, G., Harris, R. D., Quigley, G. R., Wilkinson, J.S., and Abuknesha, R.A., 1998, *Immunofluorescence sensor for water analysis*, Sensors & Actuators B, Volume 51, pp. 181-187.

174

Kok, F. N., Bozoglu, F., and Hasirci, V., 2002, *Construction of an acetylcholinesterase-choline oxidase biosensor for aldicarb determination, Biosensors and Bioelectronics*, Volume 17, pp. 531-539.

Kok, F. N., and Hasirci, V., 2004, *Determination of binary pesticide mixtures by an acetylcholinesterase–choline oxidase biosensor*, Biosensors and Bioelectronics, Volume 19, pp. 661-665.

Konda, L. N., and Pásztor, Z., 2001, *Environmental distribution of Acetochlor, Atrazine, Chlorpyrifos and Propisochlor under field conditions*, J. Agric. Food Chem., Volume 49, pp 3859-3863.

Kovács, B., Nagy G., Dombi, R., and Tóth, K., 2003, *Optical biosensor for urea with improved response time*, Biosensors and Bioelectronics, Volume 18, pp. 111-118.

Kukla, A. L., Kanjuk, N. I., Starodub, N. F, and Shirshov, Yu. M., 1999, *Multi-enzymatic electrochemical sensor: field measurements and their optimisation*, Analytica Chimica Acta, Volume 385, pp. 461-466.

Kunz, R.E., 1997, *Miniature integrated optical modules for chemical and biochemical sensing*, Sensors and Actuators B: Chemical, Volume 38, pp. 13-28.

Lechuga, L. M., Lenferink, A. T. M., Kooyman, R. P. H., and Greve, J., 1995, *Feasibility of evanescent wave interferometer immunosensors for pesticide detection: chemical aspects*, Sensors and Actuators B: Chemical, Volume 25, pp. 762-765.

Lee, H-S., Kim, Y. A., Cho, Y. A., and Lee, Y. T., 2002, *Oxidation of organophosphorus pesticides for the sensitive detection by a cholinesterase-based biosensor*, Chemosphere, Volume 46, pp. 571-576.

Li, W. J., Xian, M., Wang, Z.C., Sun, C. Q., Zhao, M. Y., 2001, *Alternate Deposition of Horseradish-Peroxidase and Bipolar Pyridine Salt on the Solid-Surface to Prepare Electrocatalytically Active Enzyme Thin-Film*, Thin Solid Films, Volume 386, pp. 121-126.

Liawruangrath, S., Oungpipat, W., Watanesk, S., Liawruangrath, B., Dongduend, C., and Purachat, P., 2001, *Asparagus-based amperometric sensor for fluoride determination*, Analytica Chimica Acta, Volume 448, pp. 37-46.

Lobanov, A. V., Borisov, I. A., Gordon, S. H., Greene, R. V., Leathers, T. D. and Reshetilov, A. N., 2001, *Analysis of ethanol-glucose mixtures by two microbial sensors: application of chemometrics and artificial neural networks for data processing*, Biosensors and Bioelectronics, Volume 16, pp. 1001-1007.

Lukosz, W., 1995, *Integrated optical chemical and direct biochemical sensors*, Sensors and Actuators B: Chemical, Volume 29, pp. 37-50.

Lukosz, W., Stamm, Ch., Moser, H. R., Ryf, R., and Dübendorfer, J., 1997, *Difference interferometer with new phase-measurement method as integrated-optical refractometer, humidity sensor and biosensor*, Sensors and Actuators B: Chemical, Volume 39, pp. 316-323.

Lvov, Y., Decher, G., and Moehwald, H., 1993, *Assembly, structural characterization, and thermal behavior of layer-by-layer deposited ultrathin films of poly(vinyl sulfate) and poly(allylamine)*, Langmuir, Volume 9, pp. 481-486.

Lvov, Y. M., and Decher, G., 1994, *Assembly of multilayer ordered films by alternating adsorption of oppositely charged macromolecules*, Crystallography Reports, Volume 39, pp. 628-647.

Lvov, Yu., Ariga, K., and Kunitake, T., 1995, *Assembly of multicomponent protein films by means of electrostatic layer-by-layer adsorption*, J. Am. Chem. Soc., Volume 117, pp. 6117-6123.

Mahendra, N., Gangaiya, P., Sotheeswaran, S., and Narayanaswamy, R, 2003, *Investigation of a fibre optic copper sensor based on immobilised [alpha]-benzoinoxime (cupron)*, Sensors and Actuators B: Chemical, Volume 90, pp. 118-123.

Malcik, N., Tunoglu, N., Caglar, P., and Wnek, G. E., 1998, *Fiber-optic cation determination using crown ether dyes immobilized on polymer membranes*, Sensors and Actuators B: Chemical, Volume 53, pp. 204-210.

Mallat, E., Barzen, C., Abuknesha, R., Gauglitz, G., and Barcelo, D., 2001, *Part per trillion level determination of isoproturon in certified and estuarine water samples with direct optical immunosensor*, Analytica Chimica Acta, Volume 426, pp. 209-216.

Mamedov, A. A., Belov, A., Giersig, M., Mamedova, N. N., and Kotov, N. A., 2001, *Nanorainbows: Graded Semiconductor Films from Quantum Dots*, J. Am. Chem. Soc., Volume 123, pp. 7738 –7739.

Marty, J. L., Garcia, D., and Rouillon, R., 1995, *Biosensors: potential in pesticide detection*, Trends in Analytical Chemistry, Volume 14, pp. 329-333.

Marty, J. L., Mionetto, N., Noguer, T., Ortega, F., and Roux, C., 1993, *Enzyme sensors for the detection of pesticides*, Biosensors and Bioelectronics, Volume 8, pp. 273-280.

Mazzei, F., Botr, F., Lorenti, G., Simonetti, G., Porcelli, F., Scibona, G., and Botr, C., 1995, *Plant tissue electrode for the determination of atrazine*, Analytica Chimica Acta, Volume 316, pp. 79-82.

Mlika, R., Ouada, H. B., Kalfat, R., Gamoudi, G., Mhenni, F., and Jaffrezic-Renault, N., 1997, *Thin sensitive organic membranes on selective iron-ion sensors*, Synthetic Metals, Volume 90, pp. 239-243.

Morillo, J., Usero, J., and Gracia, I., 2003, *Heavy metal distribution in marine sediments from the southwest coast of Spain*, Chemosphere, Volume 55, pp. 431–442.

Mortensen, J., Legin, A., Ipatov, A., Rudnitskaya, A., Vlasov, Y., and Hjuler, K., 2000, *A flow injection system based on chalcogenide glass sensors for the determination of heavy metals*, Analytica Chimica Acta, Volume 403, pp 273-277.

Mulchandani, A., Mulchandani, P., Kaneva, I., and Chen, W., 1998, *Biosensor for direct determination of organophosphate nerve agents using recombinant Escherichia coli with surface-expressed organophosphorus hydrolase. 1. Potentiometric microbial electrode*, Analytical Chemistry, Volume 70, pp. 4140-4145.

Nabok, A. V., Davis, F., Hassan, A. K., Ray, A. K., Majeed, R., and Z. Ghassemlooy, 1999, *Polyelectrolyte self-assembled thin film containing cyclo-tetrachromotropylene for chemical and bio-sensing*, Materials Science & Engineering C, Volume 8-9, pp. 123-126.

Nabok, A. V., A. K. Ray, N. F. Starodub, K. P. Dowker, 2000, *Enzyme/indicator optrodes for detection of heavy metal ions and pesticides*, Proc. SPIE, Biochemical and Biomolecular Sensing, Volume 4200, pp. 32-41.

Natale C. D., Macagnano, A., Davide, F., D'Amico, A., Legin, A., Vlasov, Y., Rudnitskaya, A., and Selezenev, B., 1997, *Multicomponent analysis on polluted waters by means of an electronic tongue*, Sensors and Actuators B: Chemical, Volume 44, pp 423-428.

Okayama, Y., Ito, T., and Shiratori, S., 2001, *Optimization of the feedback constant control for the mass-controlled layer-by-layer sequential adsorption technique for polyelectrolyte thin films*, Thin Solid Films, Volume 393, pp. 132-137.

Onda, M., K. Ariga, and T. Kunitake, 1999, *Activity and Stability of Glucose Oxidase in Molecular Films Assembled Alternately with Polyions*, Journal of Bioscience and Bioengineering, Volume 87, pp. 69-75.

Palchetti, I., Cagnini, A., Carlo, M. D., Coppi, C., Mascini, M., and Turner, A.P.F., 1997, *Determination of acetylcholinesterase pesticides in real samples using a disposal biosensor*, Analytica Chimica Acta, Volume 337, pp. 315-321.

Pearce, F., and Mackenzie, D., 1999, *It's raining pesticides*, New Scientist, Volume 162, page 23.

Philp, J. C., Balmand, S., Hajto, E., Bailey, M., J., Wiles, S., Whiteley, A. S., Lilley, A. K., Hajto, J., and Dunbar, S. A., 2003, *Whole cell immobilised biosensors for toxicity assessment of a wastewater treatment plant treating phenolics-containing waste*, Analytica Chimica Acta, Volume 487, pp. 61-74.

Plowman, T. E., Reichert, W. M., Peters, C. R., Wang, H. K., Christensen, D. A., and Herron, J. N., 1996, *Femtomolar sensitivity using a channel-etched thin film waveguide fluoroimmunosensor*, Biosensors and Bioelectronics, Volume 11, pp. 149-160.

Plowman, T. E., Saavedra, S. S., and Reichert,W. M., 1998, *Planar integrated optical methods for examining thin films and their surface adlayers*, Biomaterials, Volume19, pp. 341-355.

Plowman, T. E., Durstchi, J. D., Wang, H. K., Christensen, D. A., Herron, J. N., and Reichert, W. M., 1999, *Multiple-Analyte Fluoroimmunoassay Using an Integrated Optical Waveguide Sensor*, Analytical Chemistry, Volume 71, pp. 4344-4352.

Preininger, C., and Wolfbeis, O. S., 1996, *Disposable cuvette test with integrated sensor layer for enzymatic determination of heavy metals*, Biosensors and Bioelectronics, Volume 11, pp. 981-990.

Ray, A. K., and Nabok, A. V., 2002, *Composite polyelectrolyte self-assembled films for sensor applications*, in Handbook of Polyelectrolytes and Their Applications, Ed by Tripathy, S. K., Kumar, J., and Nalwa, H. S., Volume 3: Applications of Polyelectrolytes and Theoretical Methods.

Reder, S., Dieterle, F., Jansen H., Alcock, S., and Gauglitz, G., 2003, *Multi-analyte assay for triazines using cross-reactive antibodies and neural networks*, Biosensors and Bioelectronics, Volume 19, pp. 447-455.

Reiss, M., Heibges, A., Metzger, J., and Hartmeier, W., 1998, *Determination of BOD-values of starch-containing waste water by a BOD-biosensor*, Biosensors & Bioelectronics, Volume 13, pp. 1083–1090.

Ristori, C., Carlo, C. D., Martini, M., Barbaro, A., and Ancarani, A., 1996, Potentiometric detection of pesticides in water samples, Analytica Chimica Acta, Volume 325, pp. 151-160.

Rodriguez-Mozaz, S., Reder, S., Lopez de Alda, M., Gauglitz, G., and Barceló, D., 2004, *Simultaneous multi-analyte determination of estrone, isoproturon and atrazine in natural waters by the RIver ANAlyser (RIANA), an optical immunosensor*, Biosensors and Bioelectronics, Volume19, pp. 633-640.

Rogers, K. R., and Williams, L. R., 1995, *Biosensors for environmental monitoring: a regulatory perspective*, Trends in Analytical Chemistry, Volume 14, pp. 289-294.

Rudnitskaya, A., Ehlert, A., Legin, A., Vlasov, Yu. and Büttgenbach, S., 2001, *Multisensor system on the basis of an array of non-specific chemical sensors and artificial neural networks for determination of inorganic pollutants in a model groundwater*, Talanta, Volume 55, pp. 425-431.

Saavedra, S. S., and Reichert, W. M., 1990, *Integrated optical attenuated total reflection spectrometry of aqueous superstrates using prism-coupled polymer waveguides*, Analytical Chemistry, Volume 62, pp. 2251-2256.

Saleh, M. A., Ewane, E., Jones, J. and Wilson, B. L., 2001, *Chemical evaluation of commercial bottled drinking water from Egypt,* Journal of Food Composition and Analysis, Volume 14, pp. 127-152.

Scheller, F.W., and Schubert, F., 1992, *Biosensors*, Elseveier, Amsterdam.

Schlatter, D., Barner, R., Fattinger, Ch., Huber, W., Hübscher, J., Hurst, J., Koller, H., Mangold, C. and Müller, F., 1993, *The difference interferometer: application as a direct affinity sensor*, Biosensors and Bioelectronics, Volume 8, pp. 109-116.

Schulze, H., Scherbaum, E., Anastassiades, M., Vorlová S., Schmid, R. D., and Bachmann, T. T., 2002, *Development, validation, and application of an acetylcholinesterase-biosensor test for the direct detection of insecticide residues in infant food*, Biosensors and Bioelectronics, Volume 17, pp. 1095-1105.

Shaffer, R. E., Rose-Pehrsson, S. L. and McGill, R. A., 1999, *A comparison study of chemical sensor array pattern recognition algorithms*, Analytica Chimica Acta, Volume 384, pp. 305-317.

Shi, R. B., Stein, K., and Schwedt, G., 1997, *Determination of mercury (II) traces in drinking water by inhibition of an urease reactor in a flow injection analysis (FIA) system*, Fresenius J. Analytical Chemistry, Volume 357, pp. 752-755.

Shirshov, Y. M., Svechnikov, S. V., Kiyanovskii, A. P., Ushenin, Y. V., Venger, E. F., Samoylov, A. V., and Merker, R., 1998, *A sensor based on the planar-polarization interferometer*, Sensors and Actuators A: Physical, Volume 68, pp. 384-387.

Shirshov, Y. M., Snopok, B. A., Samoylov, A. V., Kiyanovskij, A. P., Venger, E. F., Nabok, A. V., and Ray, A. K., 2001, *Analysis of the response of planar polarization interferometer to molecular layer formation: fibrinogen adsorption on silicon nitride surface*, Biosensors and Bioelectronics, Volume 16, pp. 381-390.

Soldatkin, A. P., Volotovsky, V., El'skaya, A. V., Jaffrezic-Renault, N., and Martelet, C., 2000, *Improvement of urease based biosensor characteristics using additional layers of charged polymers*, Analytica Chimica Acta, Volume 403, pp. 25-29.

Stamm, Ch. and Lukosz ,W., 1993, *Integrated optical difference interferometer as refractometer and chemical sensor*, Sensors and Actuators B: Chemical, Volume 11, pp. 177-181.

Stamm, Ch. and Lukosz ,W., 1994, *Integrated optical difference interferometer as biochemical sensor*, Sensors and Actuators B: Chemical, Volume 18, pp. 183-187.

Stamm, Ch. and Lukosz ,W., 1996, *Integrated optical difference interferometer as immunosensor*, Sensors and Actuators B: Chemical, Volume 31, pp. 203-207.

Starodub, N. F., Kanjuk, N. I., and Kukla, A. L., 1999, *Multienzyme electrochemical sensor array for determination of heavy metal ions*, Sensors and Actuators B, Volume 57, pp. 213-218.

Steen, R. J .C. A, Freriks, I. L., Cofinoa, W. P., and Brinkmanb, U. A. Th., 1997, *Large-volume injection in gas chromatography-ion trap tandem mass spectrometry for the determination of pesticides in the marine environment at the low ng/l level*, Analytica Chimica Acta, Volume 353, pp. 153-163.

Sutherland, R. M., and Dahne, C., 1987, *IRS devices for optical immunoassays*, in Biosensors: Fundamentals and Applications, Ed. A.P.F.Turner, I. Karube, G.S.Wilson, Oxford University Press, Chapter 33, pp. 655-679.

Tanabe, A., Mitobe, H., Kawata, K., Yasuhara, A., and Shibamoto, T., 2001, *Seasonal and spatial studies on pesticide residues in surface waters of the Shinano River in Japan*, J. Agric. Food Chem., Volume 49, pp. 3847-3852.

Vaughan, A. A., and Narayanaswamy, R., 1998, *Optical fibre reflectance sensors for the detection of heavy metal ions based on immobilised Br-PADAP*, Sensors and Actuators B: Chemical, Volume 51, pp. 368-376.

Vlasov, Yu. G., Legin, A. V., Rudnitskaya, A. M., D'Amico, A., and Di Natale, C., 2000, *«Electronic tongue» -- new analytical tool for liquid analysis on the basis of non-specific sensors and methods of pattern recognition*, Sensors and Actuators B: Chemical, Volume 65, pp. 235-236.

Walker, D. S., Hellinga, H. W., Saavedra, S. S., and Reichert, W. M., 1993, *Integrated optical waveguide attenuated total reflection spectrometry and resonance Raman spectroscopy of adsorbed cytochrome c*, J. Phys. Chem., Volume 97, pp. 10217-10222.

Wu, A., Lee, J., and Rubner, M.F., 1998, *Light emitting electrochemical devices from sequentially adsorbed multilayer of a polymeric ruthenium (II) complex and various polyanions*, Thin Solid Films, Volume 327-329, pp. 663-667.

Zhang, S., Zhao, H. and John, R., 2001, *Development of a quantitative relationship between inhibition percentage and both incubation time and inhibitor concentration for inhibition biosensors-theoretical and practical considerations*, Biosensors and Bioelectronics, Volume 16, pp. 1119-1126.

Zhylyak, G. A., Dzyadevich, S. V., Korpan, Y. I., Soldatkin, A. P., and El'skaya, A. V., 1995, *Application of urease conductometric biosensor for heavy-metal ion determination*, Sensors and Actuators B: Chemical, Volume 24, pp. 145-148.

APPENDIX

The LabView program developed to control the operation of the enzyme sensor array.
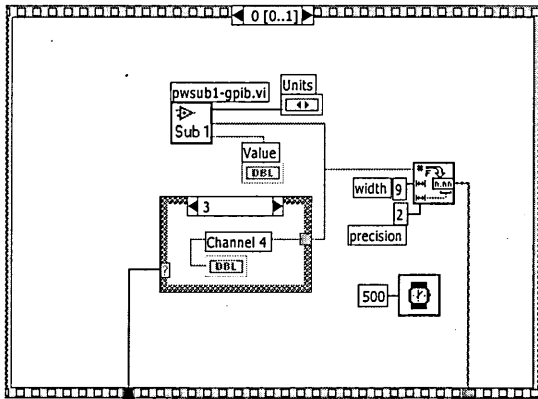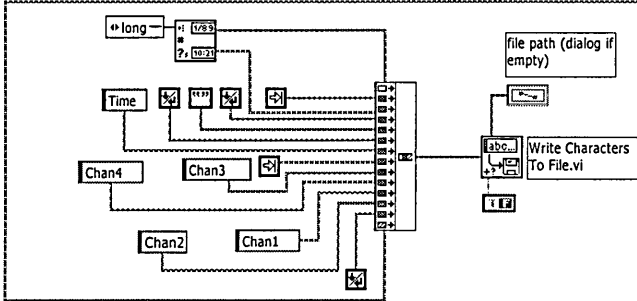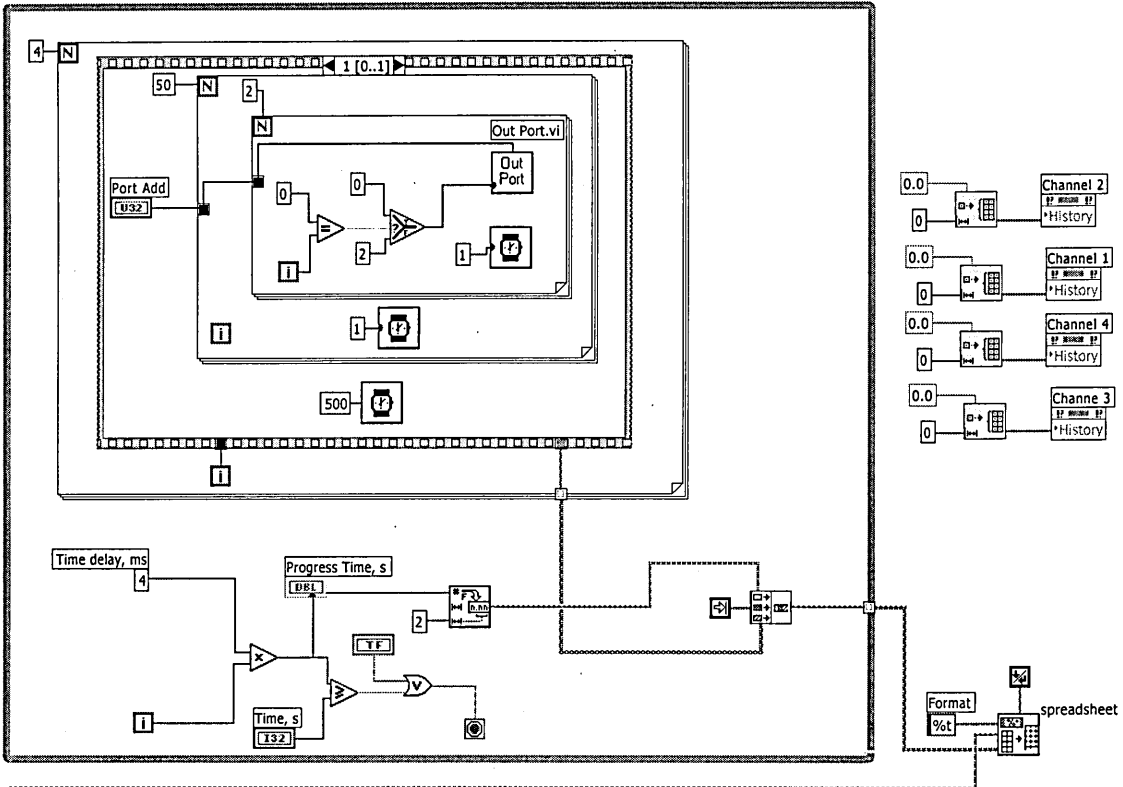
Connector Pane

pwmotor4chan4.vi
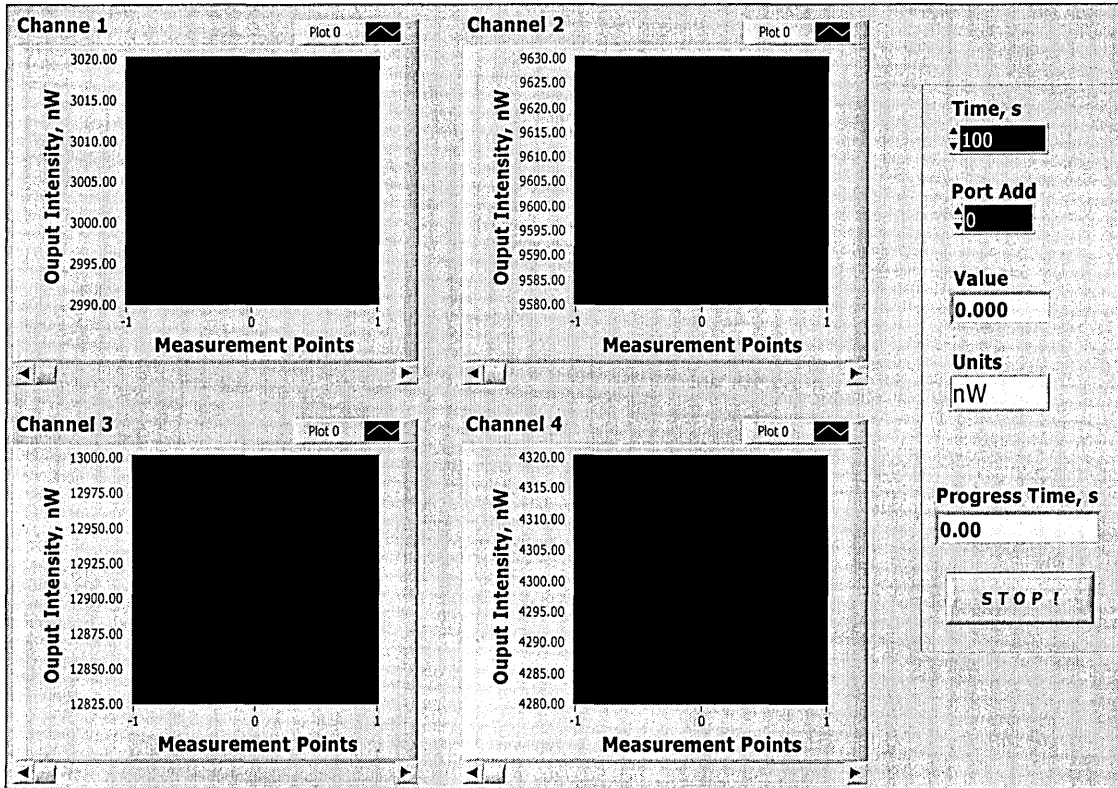
Front Panel

Block Diagram

Connector Pane
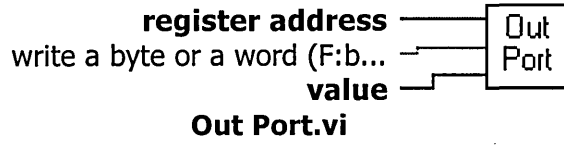
Units
Store data
Value

pwsub1-gpib.vi

Front Panel

Units

nW

Store data

0.00

Value

0.000

Block Diagram

Connector Pane

register address ———— Out
write a byte or a word (F:b... —┐ Port
value ———┘

Out Port.vi

Front Panel

register address
▲
▼ ×0

write a byte or a word (F:byte)
BYTE

value
▲
▼ ×0

Block Diagram

register address
U32

write a byte or a word (F:byte)
TF

value
U16